SOLID STATE OPTICAL CONJUGATED POLYMER AMPLIFIER; WITH ULTRAFAST GAIN SWITCHING

Vithanage Chiranthika Dimali Amarasinghe

A Thesis Submitted for the Degree of PhD
at the
University of St. Andrews

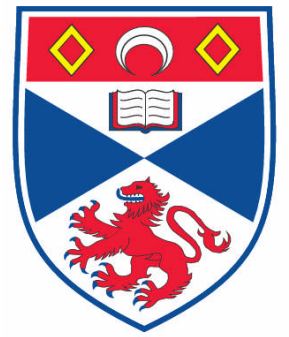

2008

Solid state optical conjugated polymer amplifier; with ultrafast gain switching

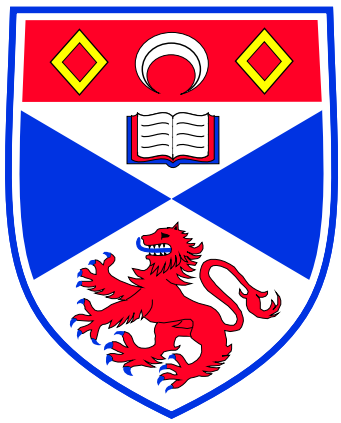

Vithanage Chiranthika Dimali Amarasinghe

February 2008

A thesis submitted to the School of Physics and Astronomy, University of St Andrews in application for the degree of Doctor of Philosophy

Declarations

I, Vithanage Chiranthika Dimali Amarasinghe, hereby certify that this thesis, which is approximately 44,000 words in length, has been written by me, that it is the record of work carried out by me, and that it has not been submitted in any previous application for a higher degree.

date _____ *signature of candidate* _____

I was admitted as a research student and as a candidate for the degree of Doctor of Philosophy in September 2004; the higher study for which this is a record was carried out in the University of St Andrews between 2004 and 2008.

date _____ *signature of candidate* _____

I hereby certify that the candidate has fulfilled the conditions of the Resolution and Regulations appropriate for the degree of Doctor of Philosophy in the University of St Andrews and that the candidate is qualified to submit this thesis in application for that degree.

date _____ *signature of supervisor* _____

In submitting this thesis to the University of St Andrews I understand that I am giving permission for it to be made available for use in accordance with the regulations of the University Library for the time being in force, subject to any copyright vested in the work not being affected thereby. I also understand that the title and abstract will be published, and that a copy of the work may be made and supplied to any *bona fide* library or research worker.

date _____ *signature of candidate* _____

Access to Printed copy and electronic publication of thesis through the University of St Andrews.

date _____ *signature of candidate* _____

date _____ *signature of supervisor* _____

Acknowledgements

I would like to start by thanking my supervisor, Professor Ifor Samuel, for giving me the opportunity to do a PhD at the University of St Andrews and for his support and guidance throughout the course of my PhD. Thank you to Dr. Graham Turnbull for always available for fruitful discussions.

Thank you to Dr. Rudoing Xia and Cora Cheung for the collaborative work on the Red-F material.

Thanks to the workshop group, particularly George Robb and the secretarial staff, particularly Mary Rodgers and Lee Staniforth, for their assistance.

Thanks to the whole 'Polyopto group'. Particularly to: Paul Shaw and Gordon, will miss you guys and our times in the lab. Paul Marsh for always taking my power meter. Ruth for being louder than me. Ying and Shu for always being lovely. Stuart, for his constant silence throughout our PhDs. Sarah, for her enthusiastic group social events. Will miss Georgios' sense of humour and those that have now left, Andreas Vasdekis (smoky the bear) and Andrew McNeil. Especially thank you to Mark Goossens for being a good friend. Thank you all for a pleasant and truly memorable experience.

The biggest thank you to Dr. Arvydas Ruseckas for all his help and discussions throughout these years. Thank you for being a good teacher. There are no words I can think of to say what an amazing mentor you have been. Thank very much.

Thank you to Liz Thomsen, Christina Larsson and Paul Cruickshank for all their support and the many good times we shared. Their combination of stubbornness, sarcasticness [1] and cynicalness [2] has kept me sane throughout these years. Stella Lam, thank you for so many memorable journeys into the past. Véro Pagé for suffering the same injustice of being an international student. Mariam Kamell for the home away from home. Many thanks to other special people in my life J-F Mercure, Andreas Rost, Meg Ramey and Dave Bolton.

Lastly, I'd like to thank my parents and my brother, without whom all this would not have been possible. Thank you for being patient with my work life all these years

and supporting me through everything I undertook. This thesis is for you.

Abstract

Conjugated polymers are organic materials which are attractive as optoelectronic devices because they have a combination of broad band emission, high gain, versatility in processing, are ductile and can be electrically pumped. This thesis describes work conducted on such conjugated polymers as amplifier devices.

The conjugated polymers used in this thesis were MEH-PPV, F8BT, GP1302 and ADS233YE. The amplifier devices used were grating coupled and end coupling waveguides. Amplification of light was demonstrated and characterised on single and multiple pulses using the grating coupled structure. Single pulse measurements obtained gains of 21 and 17 dB in a 1 mm long waveguide using the conjugated polymers MEH-PPV and F8BT. Annihilation rate was also analysed in the single pulse method with MEH-PPV, giving a value of $\gamma \approx (3 \pm 0.1)$ x 10^{-9} cm^3/s.

Amplification of a single pulse led to demonstrate amplification and the capability of the amplifier to function with multiple pulses, which resulted in F8BT being used as the gain medium. An average gain of 18 dB was obtained with F8BT in a 1 mm waveguide channel. Amplification was also investigated with end coupled waveguides. This led into investigating a suitable material or suitable combination of material for amplification with the waveguides.

Switching of an amplified pulse was attempted on F8BT and GP1302 in the amplifier device at 5 kHz. Switching of F8BT was problematic which lead to attempt switching in GP1302 which was a co-polymer of PFO and F8BT. A 70 % switching effect was obtained with GP1302. Gain recovery dynamics of F8BT, GP1302 and ADS233YE was also investigated. These measurements established a switching rate of 500 GHz for GP1302 and ADS233YE, and F8BT showed partial gain recovery indicating the presence of long lived species.

Switching was also attempted on a polymer laser. This resulted in a 100 % switched pulse with a combination of weak pump and strong switch pulse of 40 nJ and 2 μJ respectively. And a strong pump and weak switch pulse of 200 and 50 nJ respectively. Temporal delay of the switch pulse relative to the pump pulse resulted in re-timing of the laser output.

Amplification and switching of light pulses were also attempted at a higher repetition rate of 50 kHz with F8BT, GP1302, ADS233YE and MEH-PPV. This resulted in strong amplification of light in MEH-PPV and F8BT with gains of 21 and 13 dB respectively in a waveguide length of 422 μm. Weak amplification of light in ADS233YE and GP1302 was also obtained with a maximum gain of 8 and 3 dB respectively. Switching was attempted on MEH-PPV and ADS233YE.

Contents

Chapter 1

Introduction

Polymers are ubiquitous in our daily lives. Their diversity and simple processing methods have enabled them to be used for a variety of applications. Conventional polymers are electronically inert and have been used to make various items from shopping bags to liquid containers to the synthetic fibers used in clothing. Polymers can be flexible such as those used in flexible displays, or can be hard and rigid such as those used in electrical cladding tubes.

The boom in inorganic semiconducting materials has made it possible to have the modern electronic equipment we use, such as portable DVD players, mobiles phones which can connect to the internet and act as music players, and wireless internet networks. Conjugated polymers combine the simple and low cost processing techniques of insulating polymers with the conducting properties of inorganic material.

Conducting conjugated polymers were first developed in the 1970s by Heeger, McDiarmid and Shirakawa [3–5]. In 2000 they were awarded the Nobel prize in chemistry for this discovery [6]. The award recognised that conducting conjugated polymers and work towards their further development is significant for the future. In 1989, the discovery of electroluminescence in conjugated polymers by *Burroughes et al.* [7] pushed research further and brought futuristic concepts such as foldable newspapers [8] and ultrathin televisions [9] closer to our door step.

Optoelectronic devices using conjugated polymers have been demonstrated such as solar cells [10], transistors [11], photodetectors [12], optically pumped lasers [13–21] and organic light emitting diodes (OLEDs) [7, 22], with OLEDs having been the main research focus. A less developed area is optical amplifiers based on conjugated polymers.

The need for organic solid state optical amplifiers is due to the requirements of ultrafast telecommunications networks, polymer optical circuits and digital signal processing. Silica fibre networks can transmit data at a bandwidth of 2.5 Gbits/sec and higher [23]. Bandwidth to offices and homes, however, are at a rate of 4 - 10 Mbits/sec [24]. There is a reduction in the bandwidth at home because copper cables are still used to transmit data from the remote stations to the consumers. Copper cables have only a bandwidth capability of 150 Mbits/sec [23]. They have limited digital transmission capability [25] and are susceptible to electromagnetic interference [25] and result in a bottleneck at the remote stations [26]. A simple solution would be to replace the copper cables with silica fibers, opening the consumers to the full bandwidth currently possible. This however is not possible. A town would require a few hundred fibers, and a city would need up to several thousand fibers and due to the cost of silica fibers this is not viable.

An alternative to silica fibers is to use polymer optical fibers (POF). They have demonstrated high bandwidth in transmission over short distances of 200 m, and can be easily installed, spliced and connected on-site [25]. They are cheap and easy to manufacture and are very light weight. A thick bundle of POF is more flexible than the same quantity of silica glass fiber [25]. They have electromagnetic immunity and would stretch rather than break under tension [25]. All these properties make them suitable to handle the harsh inner-city environments [25]. Conjugated polymers provide amplification of light over a broad spectral range which covers the POF bandwidth and can be developed into gain based plastic optical amplifiers and switches.

Another application of conjugated polymer based devices are in personal area networks (PAN) such as those in automobiles. The automotive industry uses the red, low-loss transmission wavelength of PMMA fibers (650 nm) in their Media Oriented Systems Transport (MOST) protocols for automotive data communications systems installed in millions of cars. This can now also be used in transport, A/V networking,

security and industrial applications [27].

This thesis demonstrates the use of conjugated polymers as solid state amplifier devices. The theory of conjugated polymers is introduced in Chapter 2. This theoretical chapter includes the electronic structure, the absorption and emission of light, and gain mechanisms involved for amplification. Chapter 3 discusses the experimental techniques and equipment used. Chapter 4 describes the experimental results in amplification of light in MEH-PPV and collaborative work conducted on the conjugated polymer Red-F, with Imperial College London. Chapter 5 describes the experimental procedure in the amplification of a pulse sequence. Chapter 6 investigates switching of an amplified pulse in a sequence of pulses. Chapter 7 describes the development of the non-collinear optical parametric amplifier (NOPA), which was used as the source for the high repetition rate amplifier work described in Chapter 8. Chapter 9 details the work involved in order to get amplification in a compact waveguiding structure. The conclusions are given in Chapter 10.

Chapter 2

Theory of conjugated polymers

In this chapter the theory of conjugated polymers is reviewed. It presents an account of the electronic structure of conjugated molecules and theories relevant to the work conducted in this project.

The word 'conjugate' means to join or link, and in conjugated molecules the atoms are linked by alternating single and double bonds. The main building block of conjugated molecules is carbon. The simplest example of a double bond between two carbon atoms is ethylene, shown in Figure 2.1. Ethylene has a backbone of two carbon atoms linked by a double bond.

In order to understand how the bonding is formed one needs to start with the carbon atom. A carbon atom has the electronic configuration $1s^2 2s^2 2p^2$ in the ground state [28]. Bonding to another carbon atom would occur with the four electrons in the outer shell which are two s electrons and two p electrons [28]. It is possible for the s and p orbitals to hybridise forming three sp^2 orbitals [28]. The bond is created by the s orbitals hybridizing with two p orbitals (p_x and p_y), as shown in Figure 2.2. The p_z orbital remains unaltered. The sp^2 orbitals are all coplanar and lie at about 120^o to each other. The p_z orbital lies perpendicular to the sp^2 hybridization [28, 30]. It is the three sp^2 orbitals and the p_z orbital that form the bonding orbitals of the carbon atom [28, 30, 31].

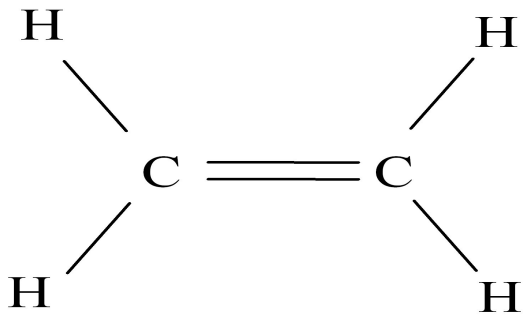

Figure 2.1: Double bond of ethene molecule C_2H_4.

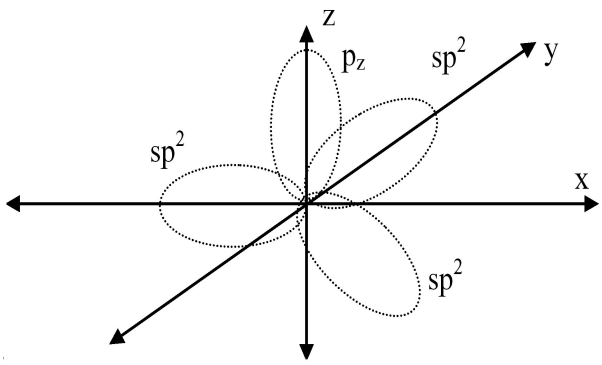

Figure 2.2: The p_z and three sp^2 orbitals of bonded carbon atoms [29].

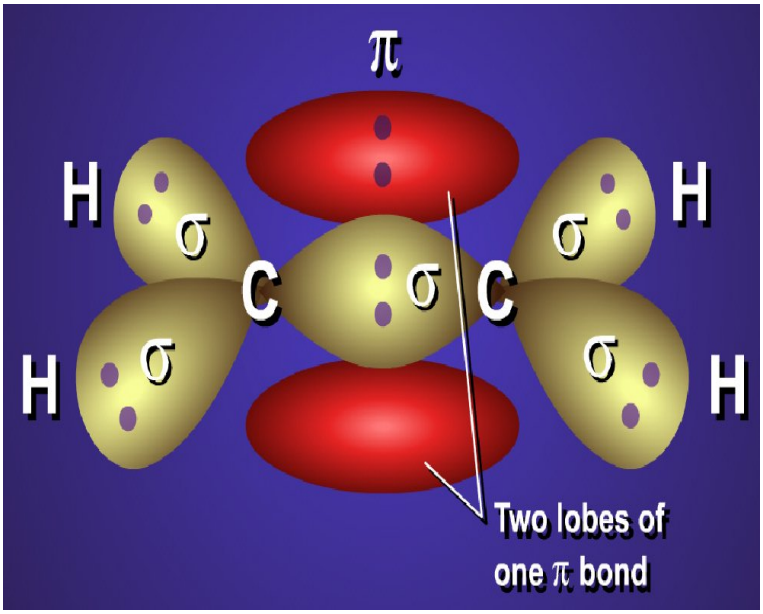

Figure 2.3: An illustration of the π-bonds and σ-bonds in ethylene, C_2H_4 [32].

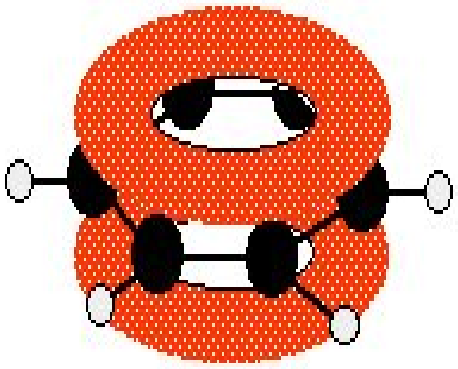

Figure 2.4: An illustration of the delocalisation of the π-bonds in benzene [33]. The π-bonds are represented by the red rings.

There are two types of bonds which form between the carbon atoms, called the σ and π bonds, shown in Figure 2.3 [28, 30]. The bonds formed from the sp^2 orbitals are called σ-bonds. Each carbon atom will bond with another carbon atom and two hydrogen atoms by a σ-bond [30]. This bond generates a highly localised electron density between the carbon and hydrogen atom [28]. The π-bond is formed when the p_z orbital in one carbon atom bonds to the p_z orbital in another carbon atom [28, 30]. The double bond is formed by the π and σ bond between the carbon atoms. The π-bond produces a delocalised electron density above and below the plane of the carbon atoms but not in the nodal plane of the molecule [28]. This can be seen in figure 2.4 where the π-bonds are formed from p-orbitals above and below the plane of the ring in a benzene molecule. The π-bond is rigid, so much so that in order to rotate the molecule, the π-bond would have to be broken [29, 34]. The electrons in the π-bond however are more weakly bound than in the σ-bond. The weakly bound electrons are responsible for the semiconducting properties as they are delocalised, i.e. they can move between carbon atoms in the π-bond along the molecule backbone and contribute to the conducting property [31]. Inert polymers do not have delocalised π-electrons and generally only have single σ-bonds, which are sp^3 hybridised [30].

The π orbitals can be divided into bonding and antibonding orbitals [28]. The bonding and antibonding orbitals form two sets of energy levels which are separated by an energy gap. Excited states are formed when an electron from the HOMO level (highest bonding π orbital) moves to the LUMO (lowest antibonding π orbital) level. HOMO stands for highest occupied molecular orbital and LUMO stands for lowest

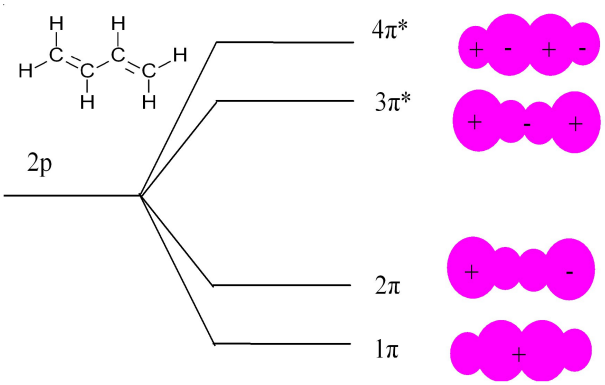

Figure 2.5: The π orbitals in 1,3-butadiene [29].

unoccupied molecular orbital. The energy change for this transition is the difference in energy between the HOMO and the LUMO level [28]. Most optical transitions occur with the π-electrons, hence the electronic transitions from the lowest energy orbital to the highest energy orbital are referred to as π-π^* transitions. The σ-bonds form a fixed potential in which the π-electrons move [28].

Consider the conjugated molecule 1,3-butadiene, the π-orbitals and their energy levels [34] relative to the p orbital and are shown in Figure 2.5. There are four electrons in the π-bonds each doubly occupying the 1π and 2π orbitals. The 2π orbital is the highest occupied molecular orbital (HOMO) and $3\pi^*$ is the lowest unoccupied molecular orbital (LUMO). The 1π and $3\pi^*$ orbitals have even parity and the 2π and $4\pi^*$ have odd parity under inversion symmetry. For transitions to occur, other elements need to be taken into account. The rules effect the probability of the molecule to be excited and are called selection rules. The initial and final electronic states have to be of opposite parity with respect to the inversion center for transitions to occur. This is the *Laporte selection rule* [34]. According to the selection rules, transitions which are not allowed may take place but will be much weaker than fully allowed transitions. In figure 2.5 the 2π orbital has even parity and $3\pi^*$ orbital has odd parity, hence a transition is allowed. However a transition is not allowed between 2π and $4\pi^*$ as they are of the same parity. If a photon of correct energy for this forbidden transition is incident on the molecule, it will have a low probability of being absorbed.

2.1 Absorption

The absorption bands in organic materials are excitonic in nature like in molecular solids, where the photoexcitation primarily results in singlet excitons [35]. When a photon impinges on a molecule and if the frequency of the photon matches the electronic transition between the HOMO and LUMO levels, then it will cause an electron to be excited to a higher state, S_1. After an electron has been excited, the charge density of the molecule changes. The molecule rearranges itself into this new electron density. This results in a shift of the wavelength peak between the absorption and fluorescence wavelength and is called the Stokes shift.

The interaction strength of the light with the material is expressed by the Beer Lambert Law equation [36]:

$$I(\lambda) = I_0(\lambda)exp^{-\alpha z} \tag{2.1}$$

Where

$$T = \frac{I}{I_0} \tag{2.2}$$

$$A = -logT \tag{2.3}$$

where λ is the wavelength of light, α is the absorption coefficient, A is the absorbance, z is the thickness of the material, T is the transmitted signal, $I(\lambda)$ is the intensity of light out at wavelength (λ) and $I_0(\lambda)$ is the incident light at wavelength (λ).

2.2 Emission

Emission occurs from electronic excited states which is shown in the Jablonski diagram in Figure 2.6. The ground state is S_0 and the S_1 and S_2 level are excited states. Each state has several vibrational levels labeled as 0, 1 and n. Absorption occurs from the lowest vibrational level in the ground state to higher states, unpopulated at thermal equilibrium. In order for the absorbing electron to transfer to the excited state, S_1, the ground state and excited state wavefunctions need to overlap. The degree of overlap will determine the rate at which this transition takes place. This transition takes about 10^{-15} s [37] and is known as the *Franck-Condon* transition.

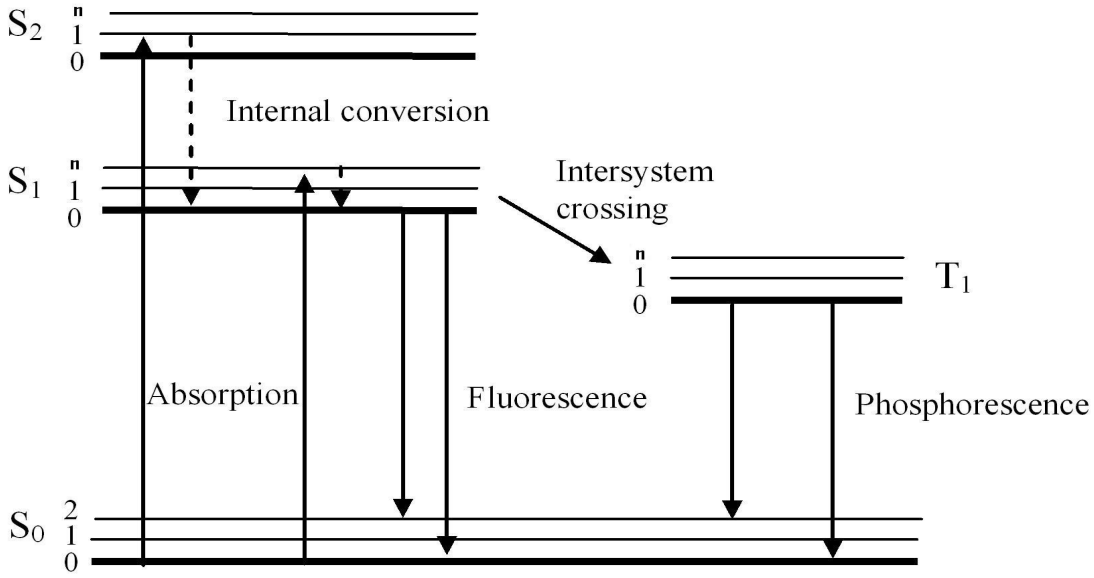

Figure 2.6: Schematic of energy levels of the molecule. The electrons are excited to an excited singlet state. Internal conversion through vibronic relaxation occurs to S_1. From there it either changes spin states and crosses to the triplet state or relaxes immediately to ground state S_0 [37].

The electrons in the S_1 state will have the same spin manifold and are called singlets. Once in the excited state, S_1, the nuclear coordinates are not in equilibrium in the new electronic configuration, hence the electron relaxes. Relaxation takes place between vibronic states on a timescale of 10^{-13} s [31]. This occurs within a given spin state and is termed internal conversion (IC). If the spin state changes manifold, the electrons are of opposite spin and are called triplets. The transfer from singlet to triplet state is termed intersystem crossing (ISC). Emission typically occurs from the lowest vibrational excited state to the highest excited vibrational ground state level, $S_1 \rightarrow S_0$, and is termed as luminescence. Emission from the lowest vibrational triplet state to the ground state, $T_0 \rightarrow S_0$, is termed phosphorescence and can have a lifetime in the order of microseconds to seconds, depending on the material [31].

The absorption and photoluminescence spectra of conjugated polymers are usually close mirror images of each other with the peaks shifted by a small Stokes shift. They are mirror images because transitions which have the highest probability of occurrence in absorption would most probably occur in emission. There are some exceptions to this which are materials that have a different geometric arrangement of the nuclei in the ground state compared to the excited state [37]. However the

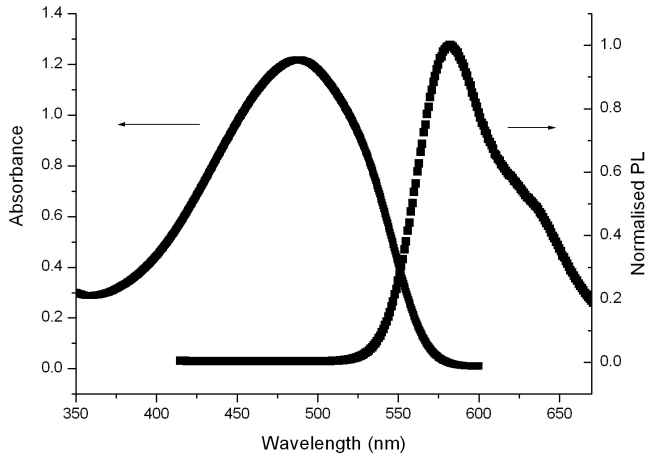

Figure 2.7: Absorption and emission spectra of MEH-PPV.

absorption spectrum is usually broader than the emission spectrum because of conformational disorder in the polymer. Conformational disorder occurs due to different conjugation lengths [1]. A material contains short and long conjugated segments and the overall absorption spectrum is determined by the inhomogeneously broadening of all the differently sized segments [38, 39]. The photoluminescence spectrum does not behave the same way because of exciton migration. An exciton created on one conjugated segment can migrate to another. This occurs from short conjugation chain lengths to long conjugation chain lengths, i.e. from points of high energy to points of low energy. Because the exciton is then at a point of minimum energy, it can no longer migrate and remains there. The trapped exciton decays radiatively from the lower energy segments. This results in a narrower emission spectrum for photoluminescence than absorption [39] and is shown in Figure 2.7 in MEH-PPV which is a conjugated polymer. Moreover, this effect will contribute to the shift between the photoluminescence peak from the absorption peak.

[1]The conjugation length is the length of the monomer units which are unperturbed

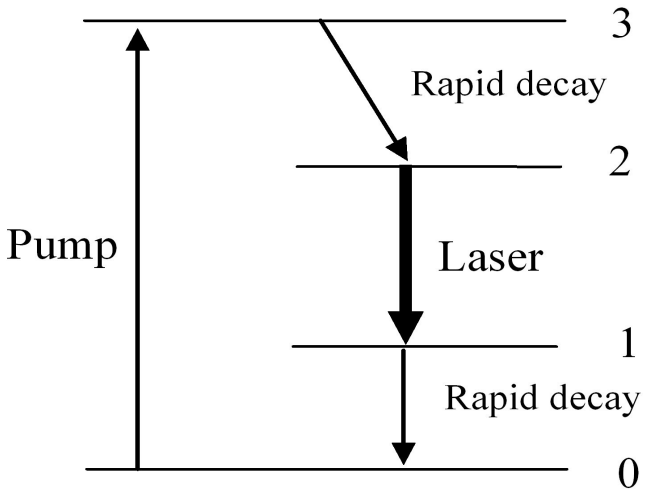

Figure 2.8: Four level system in solid state and organic dye lasers.

2.3 Optical amplifiers

Conjugated polymer optical amplifiers discussed in this thesis are solid state thin films which can exhibit optical gain. The amplification arises from stimulated emission similar to that in a four level system, as shown in Figure 2.8 [40]. The following sections describe the gain and loss mechanisms involved in amplification of light using conjugated polymer films.

2.3.1 Stimulated emission

Stimulated emission occurs from the S_1 transition to the the ground state, S_0. When the material is excited, electrons from the ground state, $S_{0,0}$, are excited to a higher vibrational level in the upper excited state, $S_{1,vib}$, which are unoccupied at room temperature. Fast vibrational cooling brings the exciton to the lowest vibrational level, $S_{1,0}$. Emission occurs from the $S_{1,0}$ state to unoccupied $S_{0,vib}$ states. The exciton reaches the $S_{0,0}$ ground state after further cooling. The ultrafast thermalization allows the gain mechanism of polymers to work as a laser medium as it follows that of a four level laser system seen in organic dye lasers [40, 41].

The emitted photons are of the same frequency and direction as the incident photon

used as a seed to *stimulate* emission at the required frequency. However, in order to get stimulated emission rather than spontaneous emission, the molecule must have population inversion. Population inversion is achieved between the $S_{1,0}$ state and the vibronic sublevels of the ground state. This leads to amplification. The intensity of the signal increases exponentially [42]:

$$I = I_0 exp[(g - \alpha)l] \tag{2.4}$$

where $g(\lambda)$ is the gain coefficient per unit length, α is the loss coefficient per unit length and l is the length of the gain medium. The gain of the material depends on the density of the excitons in the excited singlet state and on the gain cross-section. This is expressed by the equation [42, 43]:

$$g(\lambda) = N_{ex}\sigma \tag{2.5}$$

where N_{ex} is the exciton density and σ is the gain cross-section.

2.4 Loss mechanisms

In order to have high net gain, the gain produced should over come the losses in the system. Even though losses are unavoidable, they should be kept to a minimum to maximise the net gain of the system. Some loss mechanisms are discussed below.

2.4.1 Self absorption

Although the photoluminescence peak occurs at a longer wavelength than the absorption peak, if the absorption and photoluminescence spectra overlap, the emitted light may be re-absorbed. This is called self-absorption. The overlap is generally at the falling edge of the absorption spectrum with the photoluminescence spectrum. This overlap needs to be considered when deciding on the wavelength of the signal to be amplified.

2.4.2 Amplified spontaneous emission

Spontaneous emission occurs without the need for a stimulating photon. If the pumping beam intensity is sufficiently high, spontaneous emission produced can be amplified. The amplified spontaneous emission (ASE) has a large divergence and is isotropic [36]. The ASE signal generally has a broad spectral distribution and a wide divergence [36], resulting in a signal with a poor spatial and temporal coherence. The broad spectral distribution will, however, produce a narrow width due to gain narrowing [36]. The temporal coherence will also be affected by the isotropic nature of the ASE, as each component will be of different phase [36].

ASE spectra are often associated with a distinct narrowing of the peak, called gain narrowing. This can be explained by the equation [36]:

$$I(z) = I_0 exp^{\alpha_0(\omega)z} \tag{2.6}$$

Where $I(z)$ is the intensity of the signal at frequency ω, z is the propagation distance and $\alpha_0(\omega)$ is the small signal gain. The intensity of the beam increases exponentially as a function of z. This results in signals with frequencies close to the line center to be amplified more than those at the wings [36]. At high pump densities it produces sharp spectral narrowing of the signal [36].

In amplifiers ASE is an unwanted effect and adds to the noise figure, which is the amount of excess noise the amplifier adds to the output signal. It can extract energy by stimulated emission [36] and hence limit the gain by transferring energy to this emission signal rather than to the probe beam. In optical amplifiers, alongside back ground radiation and photo-luminescence, amplified spontaneous emission is one of the main noise factors.

2.4.3 Excited state absorption

Another source of loss is excited state absorption (ESA). If the stimulated emission spectrum overlaps with the spectrum of the excited state absorption, then there will be no stimulated emission generated and so no lasing [42]. If stimulated emission and

ESA are at different wavelengths, then there is stimulated emission.

For a certain probe wavelength, if the ESA cross-section is larger than the stimulated emission cross-section, then the probe signal would be absorbed by the material. This absorbed energy would push the excitons to higher excited states, S_n. The excitons would relax to the S_1 through internal conversion, however this would occur in the order of 10^{-12} s. Without the presence of the probe signal, there would be no *stimulated* emission. The excitons would eventually relax from the S_1 state to the ground state, emitting photons which are not in frequency to the probe signal and hence there would be no amplification of the probe signal.

Excited state absorption is a problem for polymers and prevented observing lasing in polymers until 1996 [42].

2.4.4 Charges

Upon excitation at high pump energy densities, the excitons can separate into oppositely charged carriers. These carriers or charges, can be either within the same polymer chain (called *intra-chain charge pairs*) or between polymer chains (called *inter-chain charge separation*). The intra-chain charge pairs formed are geminate charge pairs which have a charge separation lifetime in the order of $\sim 10^{-13}$ s [44]. The formation of geminate charge pairs can lead to more ESA bands which could compete with stimulated emission [40]; whereas the inter-chain charges are long lived species [44], which would depopulate the S_1 state and thus reduce the gain.

2.4.5 Exciton exciton annihilation

High pump energy densities will produce a large density of excitons. If these excitons are within the annihilation radius, they will combine to form an exciton of higher energy and reduce the population at S1, thus reducing the gain.

2.4.6 Triplets

Triplets are long lived states at wavelengths longer than the S_1 to S_0 transition. Singlets can cross from the S_1 state to the T_1 state, this is termed as 'inter-system crossing.'

2.4.7 Photoluminescence traps

Energy accumulated by excitons can be transferred to traps located in the polymer chains. Traps are defects or sections of the polymer which quench the photoluminescence and will reduce the gain. For this reason, the polymer needs to be as close to defect free as possible. But defects can occur during the production of the compound in industry and during experiment. Industrially produced polymers can contain a number of light absorbing impurities which are produced in side reactions during polymerization, processing and storage [45]. These impurities are generally not part of the polymer chain.

During experiments, photodegredation occurs due to exposure of the sample to oxygen and water vapour. The photo-oxidation reaction forms a carbonyl group, which is a carbon atom sharing a double bond with an oxygen atom. The oxygen molecule is an electron accepter leading to charge separation of the exciton and a reduction in the PL yield [46]. The experiments are conducted under vacuum to minimise any photo-oxidation.

Chapter 3

Experimental Methods

This chapter describes the laser system, the streak camera, the key experimental technique and sample preparation. The laser system is a femto-second Ti:sapphire oscillator which was used to seed two regenerative amplifiers, an optical parametric amplifier (OPA) and a noncollinear optical parametric amplifier called TOPAS-white. These amplifiers were used to probe the photo-physics of the polymer. The gain dynamics were recorded by either lock-in amplifiers or a streak camera.

3.1 The laser system

A femtosecond laser system is needed in order to study electronic processes occurring at 10^{-15} seconds in organic and inorganic materials. At the University of St Andrews, a femto-second laser-amplifier system was used. This system was based around a femtosecond Spectra Physics Mai Tai laser. The Mai Tai laser is a laser oscillator producing pulse widths of 100 fs with a tuning range of 750 to 850 nm at a repetition rate of 80 MHz. A simple layout is shown in Figure 3.1 [47]. The output from the Mai Tai was used to seed two regenerative amplifiers (at 5 and 50 kHz) and an optical parametric amplifier (OPA) at 5 kHz.

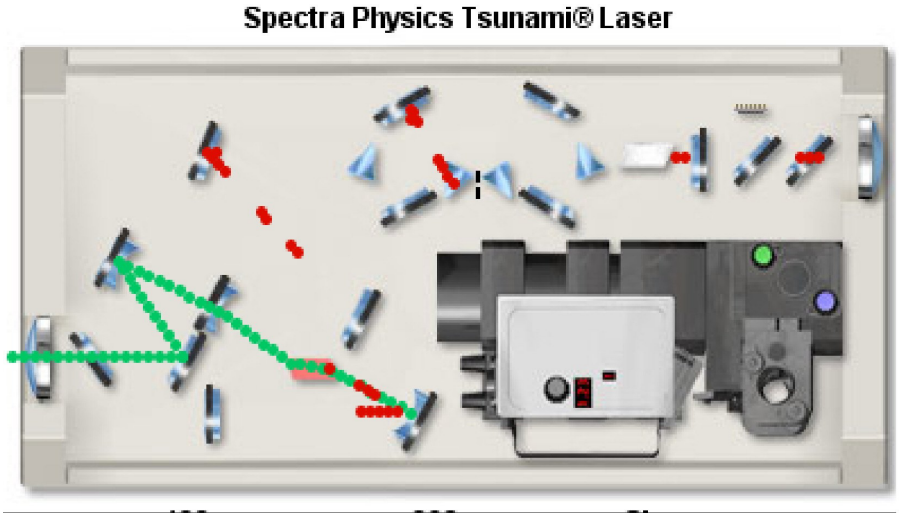

Figure 3.1: Image of the inside of a Spectra-Physics Ti:sapphire laser [47].

3.1.1 Laser oscillator: Mai Tai

The Mai Tai laser system is comprised of two lasers; the cw (continuous wave) diode pumped Nd:YVO_4 laser and a modelocked Ti:sapphire laser (pulsed output). The diode laser, ND:YVO_4, generates a signal at 532 nm which is used to pump the Ti:sapphire laser cavity. This is tunable from 280 nm to $\sim$ 1 μm, providing sub 100 femtosecond pulse widths with an average output power of $\geq$ 700 mW [48].

3.1.2 The cw pump laser

The pump chamber contains a solid state, high powered cw laser. The output is produced in a pump chamber with a Nd:YVO_4 crystal at 1064 nm and has an output power $\geq$ 10 W. This output is frequency doubled by a lithium triborate (LBO) crystal within the chamber to produce a 532 nm signal with an output power of $\geq$ 5W.

The Nd:YVO_4 crystal consists of ND^{3+} ions doped in a yttirum vanadate crystalline matrix. The crystal is pumped in the red (or infrared) region by fiber coupled laser diode bars which are placed in the power unit. The excited electrons quickly decay to the $F^4_{3/2}$ level, which is the upper level of the lasing transition and remain here for $\sim$ 60 μs. Its most favorable lasing transition is from $I^4_{1/2}$ to the ground state, with

emission of a photon at 1064 nm. Because electrons in this state relax quickly the population remains low allowing for the population inversion to be achieved quickly. At room temperature the emission cross-section will be high allowing for a low lasing threshold. There are other transitions which compete with the $I^4_{1/2}$ transition, notably at 1319, 1338 and 946 nm, but all these have lower gain and a high lasing threshold. The Quiet Multi-Axial Mode Doubling (QMAD) technique, designed by Spectra-Physics, allows for a low-noise conversion to the second harmonic. This is possible by using a very large number of axial modes to average the nonlinear coupling effects. By having many oscillating modes it reduces the relative power in each mode. This avoids having modes with a peak power high enough to induce nonlinear effects and hence reduce the noise level and provides a highly stable output. Figure 3.2 illustrates this concept.

3.1.3 The pulsed output chamber

The pulsed output is generated by a mode-locked Ti:sapphire cavity. The Ti:sapphire rod is a crystalline material which is made by combining Ti_2O_3 in a melt of Al_2O_3. The Ti^{3+} ions replace a small amount of the Al^{3+} ions, doping the sapphire. The lasing is a result of the Ti^{3+} titanium ions in the Ti:sapphire rod. As seen in Figure 3.3 the absorption band of the Ti:sapphire rod ranges from 400 to 600 nm. The fluorescence band ranges from 600 nm to 1000 nm. Lasing action is from the lower vibronic level of the excited state, to the upper vibronic level of the ground state. The lasing wavelength occurs at > 670 nm to reduce self absorption effects and occurs in cw, but is modelocked to give a pulsed output at a repetition rate of ~ 80 MHz.

Mode locking is the technique used to produce light pulses of short duration, either picosecond (ps) or femtosecond (fs). The output of the laser would be of many modes, light of different frequencies and phase, oscillating independently and separated by a frequency of :

$$\Delta v = \frac{c}{2L} \tag{3.1}$$

where Δv is the frequency of separation, c is the speed of light in a vacuum and L is the resonator length. The modes would compete with each other resulting in a low

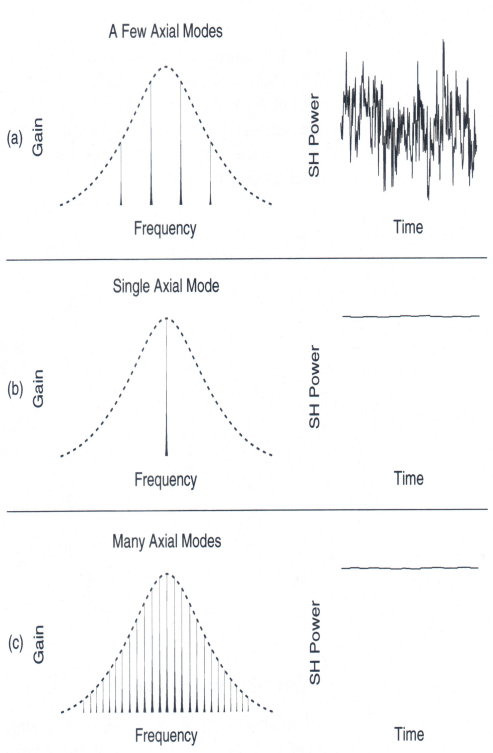

Figure 3.2: (a) Second harmonic output from a few axial modes. (b) Second harmonic output from a single mode. (c) The QMAD approach uses many axial modes which produces a highly stable second harmonic output [47].

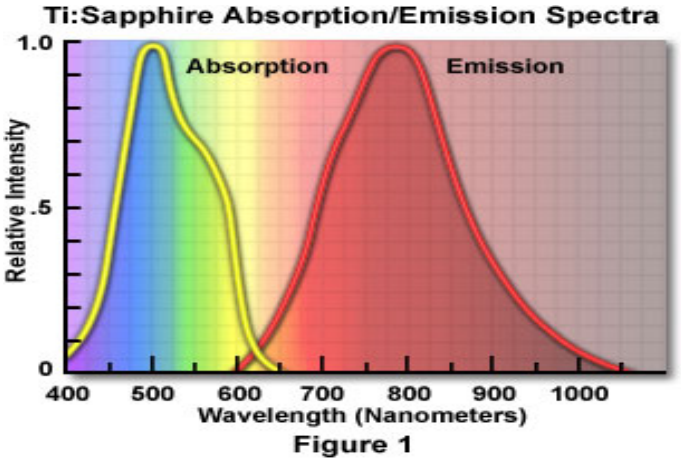

Figure 3.3: Absorption and emission spectra of Ti:sapphire rod [47].

and random output power. If the modes were oscillating together with a fixed phase, the mode will periodically constructively interfere with each other and produce an intense burst of light. This is a mode-lock laser. The pulses are separated by the time taken for one round trip in the resonator, τ, which can be calculated by:

$$\tau = \frac{2L}{c} \tag{3.2}$$

$$\Delta v = \frac{1}{\tau} \tag{3.3}$$

An acousto-optic modulator (AOM) is used to mode lock the laser and allows the laser to operate for long periods without dropout or shut downs due to pure Kerr lens mode locking [1]. The AOM is driven by a radio frequency (rf) signal (the rf signal is place in the laser head) and works on the acousto-optic effect. The acousto-optic effect is a change in the refractive index caused by the mechanical strain of a sound wave propagating in a dielectric. The sound wave is an rf signal which is generated by an piezoelectric transducer. The modulated refractive index acts as a grating, hence

[1]Kerr lens modelocking uses the Kerr effect to mode lock the laser. The Kerr effect is due to the intensity dependent refractive index arising from a nonlinear material with a third order nonlinearity, $\chi^(3)$. [49]. As the pulse travels through a nonlinear material, the higher refractive index seen at the centre of the beam retards the wavefront more than at the edges, resulting in self focusing. Thus a weak positive lens is induced in the material and the beam is focussed [50, 51].

why AOMs are sometimes called Bragg cells. Light impinging on the grating will scatter and the angle of scatter and frequency of scattered light can be controlled by the frequency of the rf signal. The period of the modulator is matched to the round trip of the resonator. If the mode arrives at the correct time, which should be set to the point of minimum loss, it can pass through the modulator. Synchronization of the modulator with the cavity round trip is essential and is ensured with a feed back circuit which automatically adjusts the modulator frequency to the cavity length.

The femtosecond pulse widths are produced by exploiting self phase modulation (SFM). SFM occurs due to the interaction of light with the nonlinear refractive index:

$$n = n_0 + n_2 I \tag{3.4}$$

SFM is explained further in chapter 7. However other optical components in the laser cavity will also cause the spectrum of the pulse to spread with a positive group velocity dispersion (GVD) and will continue to broaden as it oscillates within the cavity unless negative GVD is introduced to obtain near transform limited pulses. In the Mai Tai, this is done by using prism pairs which introduce negative GVD over a large bandwidth.

3.1.4 Regenerative amplifiers

The regenerative amplifiers take the high energy laser pulses and amplify them to produce pulses of higher energy. There are two regenerative amplifiers called the Spitfire and Hurricane. The Spitfire was used in experiments with the non-collinear optical parametric amplifier (NOPA). Regenerative amplifiers use *Chirped Pulse Amplification* [52] to avoid nonlinear effects, such as constructive self focusing. Such nonlinear effects would damage the gain medium and limit the amplification, thus short pulses would not be easily amplified. The workings of both the regenerative amplifiers are the same and are collectively described in detail below.

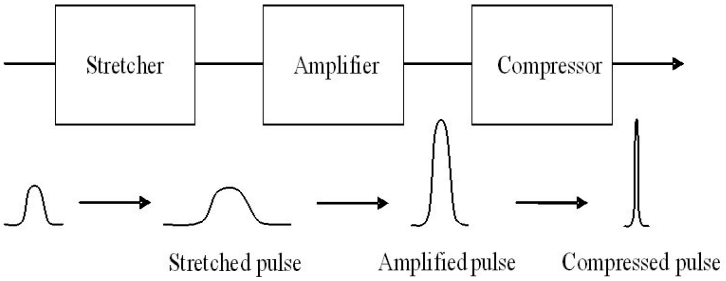

Figure 3.4: Chirp pulse amplification [52–54].

3.1.4.1 Chirped pulse Amplification

The input pulse is stretched giving a pulse of significantly lower power [53, 54]. This is amplified and compressed to its original pulse width. Figure 3.4 shows the general principle of this method. The pulse would be transform limited, for a Gaussian pulse this would be:

$$\Delta v \Delta t > 0.441 \tag{3.5}$$

where Δv is the bandwidth and Δt is the pulse width. The pulse is stretched and compressed by diffraction gratings. The diffraction grating would disperse the different frequencies present in the input pulse. The pulse stretching, shown in Figure 3.5, is set up such that the redder components travel less than the blue and exit the stretching region first, thus resulting in a stretched pulse. In compressing the pulse, also shown in Figure 3.5, the compression set up is arranged so that the bluer components travel less than the red, hence 'catching up' with the red components resulting in a compressed pulse.

3.1.4.2 Spitfire and Hurricane

The Spitfire is a 50 kHz regenerative amplifier and the Hurricane is a 5 kHz regenerative amplifier. The schematic for the Spitfire is shown in Figure 3.6. The Hurricane

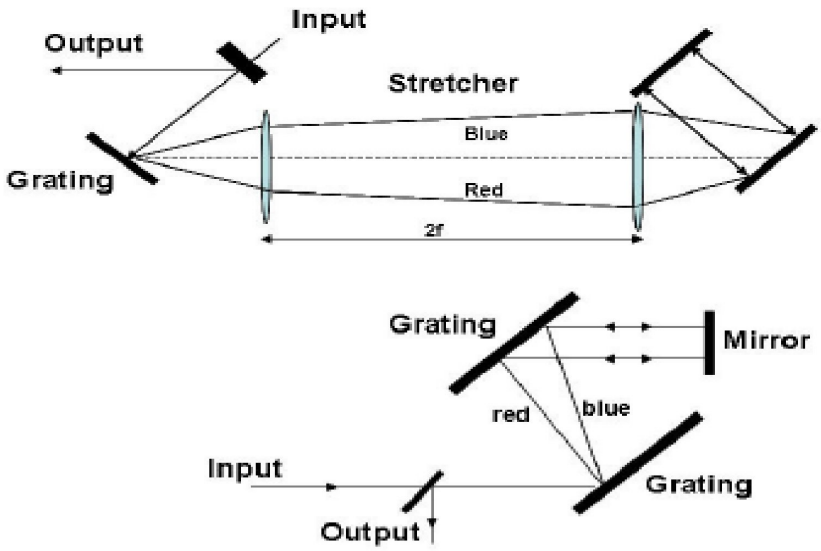

Figure 3.5: Principle of pulse stretcher (top) and compressor (bottom) [53, 54].

has a similar layout but is pumped by a diode pumped laser called Evolution. Input from the Mai Tai oscillator passes through a Faraday isolator and stretcher before impinging on the Ti:sapphire material. The amplifying medium in the Spitfire is a Ti:sapphire rod and it is pumped by a Nd:YLF diode laser at 532 nm called the Merlin. The light entering is rotated by 45^0 by the Faraday rotator. If the light travels back, it will be rotated by a further 45^0, turning the polarization to the horizontal plane. As the polarizer at the entrance is vertically aligned, the light will be stopped from exiting [53, 54].

The 800 nm signal is amplified within the Ti:sapphire rod which has been excited by the Nd:YLF diode laser. Amplification in a Ti:sapphire rod in a single pass is 10^6 times the input and with a multiple pass system the light is amplified to $> 10^6$. A Pockels cell unit is used to trap the light in the resonator which will allow it to amplify several times over before exiting.

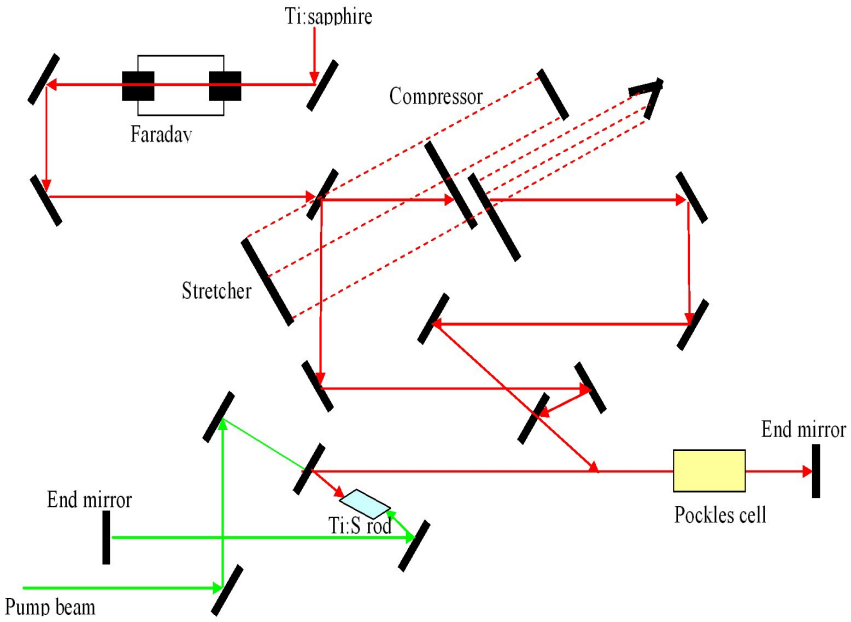

Figure 3.6: Schematic of the Spitfire [53].

3.1.5 Optical parametric amplifier

The OPA amplifies light using a nonlinear process rather than using population inversion used in lasers. The Hurricane is used to pump the Spectra-Physics optical parametric amplifier (OPA) producing 100 fs pulses, tunable from 200 nm to 10 μm at a repetition rate of 5 kHz. This wide tunable range made it an ideal source for transient absorption on materials where the absorption and emission spectra are within the range of the OPA [55]. As seen in Figure 3.7, the input from the Hurricane is split into two beams. Of this, 4% is used to generate a white light continuum. The continuum ranges from $\sim$ 450 to 750 nm and is produced by tight focusing of the 800 nm signal on a sapphire plate, Al_2O_3. The remaining 800 nm signal is used to pump a Beta Barium Borate (BBO) crystal. The amplification occurs in two stages or two passes. The pump beam is split into two beams for each stage. Fifteen percent of the light is used to pump the first pass of the OPA, called the pre-amplifier stage. The remaining light is used for the second pass called the power amplification stage.

In the pre-amplified stage, the continuum and first pump beam are overlapped temporally and spatially on the parametric crystal BBO at the phase match angle to

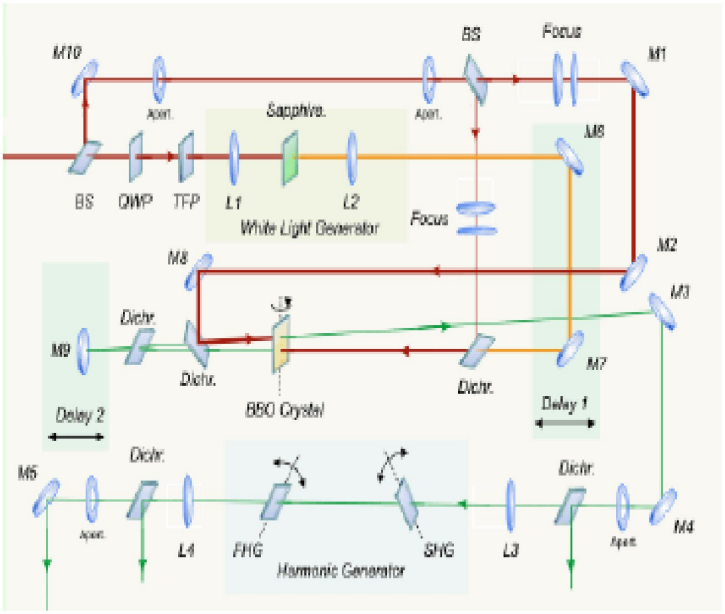

Figure 3.7: Schematic of the OPA [55].

generate the signal and idler wave. These beams are reflected back to the crystal to act as the seed pulse for the power amplifier stage. They are overlapped temporally and spatially with the pump beam of the power amplifier stage. Any residual 800 nm beam is separated from the amplified signal and idler. The wavelength of the OPA can be selected by changing the distance traveled by the pump, which changes the temporal overlap of the pump with the continuum. Sum frequency and difference frequency mixing are possible and the wavelength range can be extended to the harmonics by using more nonlinear crystals.

3.2 Noncollinear optical parametric amplifier

The Topas-white is a noncollinear optical parametric amplifier. The white light continuum is produced by a thin sapphire plate using $\sim$ 2 % of the input energy. The white light continuum generated is a single filament with a spectral range of 450 - 1200 nm and divergent. This divergence is controlled using a chromatic aberration free, low astigmatism collimator which directs the collimated beam to the pulse

shaper [56].

The pulse shaper is a double pass negative dispersion pulse stretcher. It is used to modify the phase characteristics of the white light continuum in a way that enabled the fused silica compressor to cancel the phase modulation induced on the amplified signal.

The pumping wavelength is at 400 nm which is the second harmonic (SH) of the 800 nm input signal. The pulse generator produces two beams of the 400 nm signal which is used to pump the first and second stage of the parametric amplifier. Both the pre-amplified and power amplification stages use the same BBO crystal. The geometry allows an extremely broad spectral amplification bandwidth that allows for a compression of the amplified pulse down to 10 - 20 fs pulse width. The output from the power amplifier stage is highly divergent. This divergent beam is collimated and compressed using fused silica prism plates [56].

3.3 The Streak camera

The streak camera is a device used to measure light as functions of time, intensity, position and wavelength. For example, it can be used for time-resolved spectroscopy, which is the temporal variation of a signal with respect to the wavelength. Or in time and space-resolved measurement, which is temporal variation of incident light at particular wavelengths with respect to its position. The streak camera has a temporal resolution of $\sim$ 2 ps and a wavelength range from X-rays to near infrared [57].

The light from the sample comes out at a sharp downward angle. This is guided towards the streak camera by mirrors and lenses and focused into the slit of the streak camera. The image of the slit is formed by the optics on the photocathode of the streak tube. It is converted into a number of electrons which is proportional to the intensity of the light. The electrons pass through a pair of accelerating electrodes and bombard a phosphorous screen, producing light at the point where the electrons impinge. Before reaching the phosphor screen, the photoelectrons pass through a pair of sweep electrodes. A high voltage is applied to these electrodes at a timing

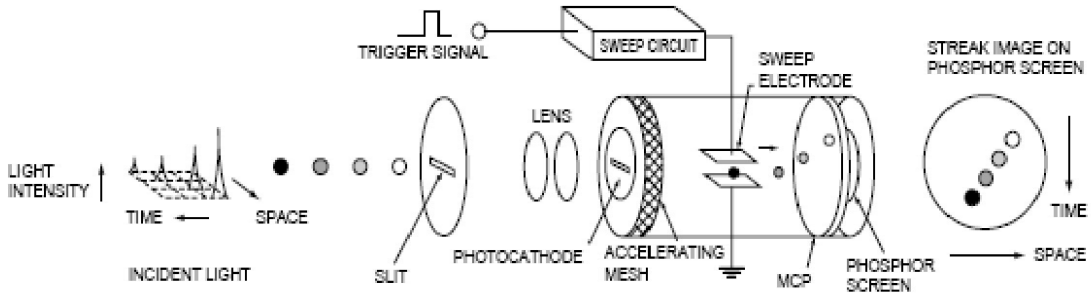

Figure 3.8: Operating principle of streak tube [57].

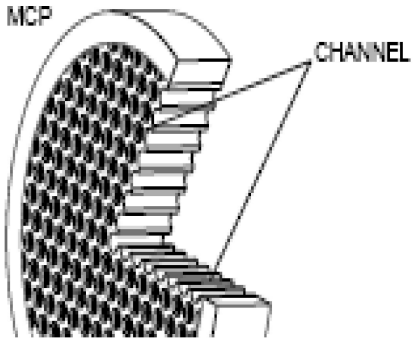

Figure 3.9: Schematic of a micro-channel plate [57].

synchronized to the incident light. This initiates a high speed sweep so that the electrons which arrive at slightly different times are deflected at different angles in the vertical direction allowing to determine the temporal position. They then enter the micro-channel plate (MCP) (shown in Figure 3.9) which is an electron multiplier consisting of many thin glass capillaries (with internal diameters of 10 - 20 μm) bundled together to form a plate with a thickness of 0.5 - 1 mm. The internal walls are coated with another electron emitting material so that when the electrons bombard the walls, they multiply in number, allowing the streak camera to measure even weak signals. A single electron can be multiplied up to 10^4 times. The multiplied electrons impinge the phosphor screen and are recorded by a CCD camera [57].

The recorded image was refreshed every 12.5 ns because the streak camera was synchronized to and triggered by the Mai Tai operating at 80 MHz. Any input into the streak camera was always less than this refresh rate and the temporal resolution of the image depended on the stability of the Mai Tai. The laser excitation repetition rates used were always lower (50 kHz and 5 kHz) than the repetition rate used to trigger the streak camera. This meant that the image would refresh faster than the repetition rate of the signal input to the camera. Ordinarily the same repetition rate as the input is used for the triggering, however the 5 kHz and 50 kHz repetition rates did not have a significant effect on the refreshed image.

The streak camera allowed measurement of the temporal and spectral profile of the amplified signals at different wavelengths simultaneously. This was particularly useful as it not only made temporal alignment of the pump and probe simpler, but also allowed the alignment of the switch pulse to any peak of the three probe pulses. Fast image procuring and high temporal resolution allowed multiple probe signals to be distinctly distinguished. The images in Figure 3.10 show how the temporal and spectral profiles would appear on the streak camera. The image is the photoluminescence from the material GP1302, and the two plots show the spectra and the luminescence decay with time.

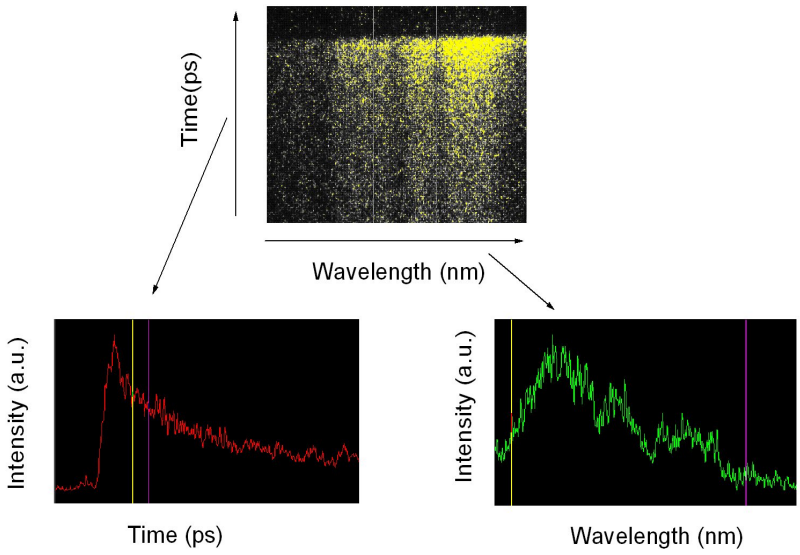

Figure 3.10: Streak camera image of photoluminescence. The y axis of the image shows the temporal position and the x axis of the image shows the wavelength of the signal. The time decay and spectral profiles of the signal can be obtained from this image.

3.4 Transient absorption

Transient absorption, also known as pump-probe measurement, is a process used to examine the ultrafast dynamics of photo physical processes [58] present in organic materials. Various molecular processes occur with the absorption of light; for example, emission, energy transfer and molecule orientation. Transient absorption experiments can be used to look at these molecular processes. Through the study of these molecular processes, one can understand the physics of the organic materials and hence design materials better suited to the experimental operation. This is highly necessary as one of the requirements to produce better devices are good materials.

Transient absorption is a tool used to 'probe' materials and to intricately examine the molecular processes occurring and hence allow to characterise the electronic states and structural properties of a given material. In my case, such information is necessary in order to determine the switching wavelength for the different materials attempted for switching. To examine the amplifying capabilities of the various materials, the process used was stimulated emission and this was demonstrated in a

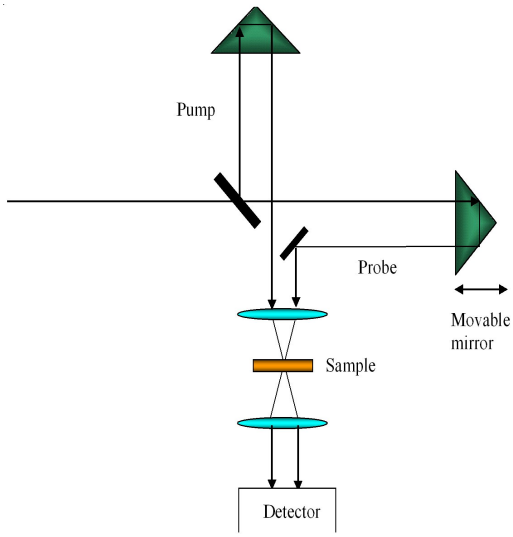

Figure 3.11: Schematic of transient absorption set up with grating amplifier [58].

transient absorption/pump-probe experiment.

Figure 3.11 shows the schematic of a typical transient absorption set up. The input beam is split in two by the beam splitter. One beam is directed to the sample and the second arrives after a delay of τ. Both beams enter the sample at the same region.

The magnitude of absorption is measured by the ratio of the affected probe beam to the unaffected probe beam. The decay dynamics are monitored by measuring the transmission or reflectance of the probe beam as a function of the time delay. The change in the transmission of the probe pulse is calculated using the equation[59]:

$$\frac{\Delta T}{T} = \frac{T_{ON} - T_{OFF}}{T_{OFF}} \tag{3.6}$$

where T_{ON} and T_{OFF} are the transmission through the sample with the pump on and off respectively. If there are no photo induced changes in reflectivity, then the change in transmission will be [59]:

$$\frac{\Delta T}{T} = -\Delta\alpha d \tag{3.7}$$

where $\Delta\alpha$ is the change in induced absorption and d is the sample thickness. As $\Delta\alpha(t,\lambda) = \delta N(t)\sigma(\lambda)$ [59], where δN is the excited state population and σ is the

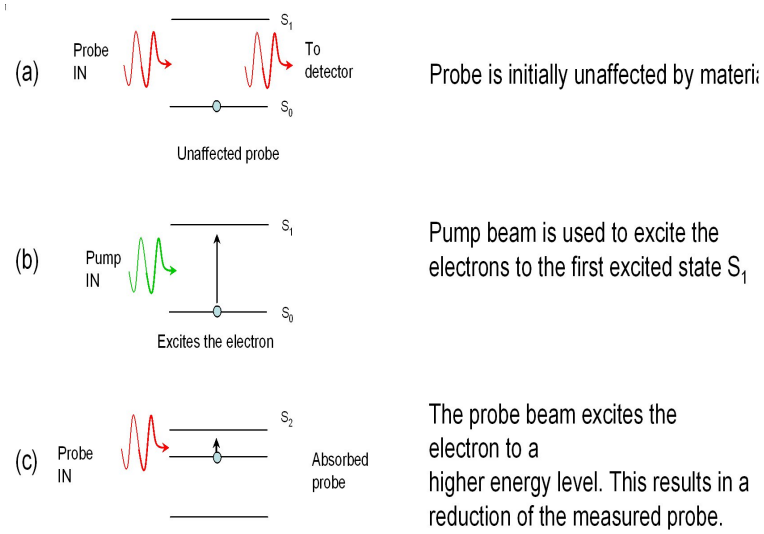

Figure 3.12: Step-by-step view of excited state characterisation in a transient absorption set up.

absorption cross-section. By measuring the change in the transmission, the time dependence of the excitons and the wavelength dependence on the absorption cross-section can be measured. A positive $\frac{\Delta T}{T}$ would be due to stimulated emission or photo bleaching. Stimulated emission will occur if the emission wavelength has negligible absorption at the ground state. If the wavelength has significant absorption, i.e. it has very little photoluminescence, then it is due to ground state bleaching [60]. A negative $\frac{\Delta T}{T}$ would be due to excited electrons being excited to higher energy levels.

Figure 3.12 shows the molecular processes involved when characterising the electronic/energy levels of a material. A pump beam is used to excite the electrons from the ground state to the first excited state called S_1. If the probe beam, at a certain wavelength, is absorbed by the material, this is an indication that there is a higher electronic state present.

For stimulated emission, the probe wavelength is within the emission spectrum of the material and stimulates relaxation of the excitons, as shown in Figure 3.13. The excitons emit photons upon relaxing down to the ground state. The emitted photons are of the same frequency and wavelength as the probe beam, thus amplifying the probe signal. By varying the time between the pump and probe beams it is possible to measure the amplified probe signal in the temporal domain.

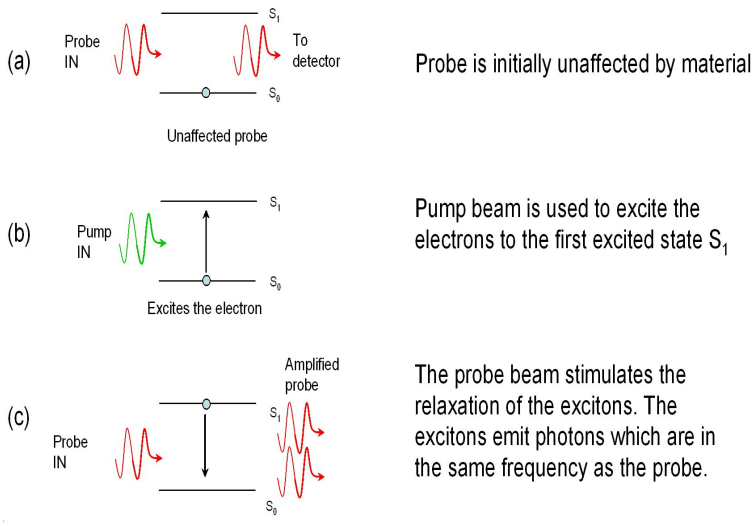

Figure 3.13: Step-by-step view of obtaining amplified probe from stimulated emission in a transient absorption experiment.

3.5 Preparation of material

Materials were purchased in powder form from different sources. MEH-PPV was supplied by American Dye Source (ADS); Covian, F8BT and ADS233YE were supplied by ADS, and GP1302 was supplied by Cambridge Display Technologies. These were made into solutions using particular solvents in which the polymer was soluble. Once the solvent has been added to the solute, a magnetic stirrer is added and the solution is left overnight on a stirrer in a sample bottle. This method ensures that all the solute has been dissolved by the next morning.

The polymer was processed into a film by spinning the solution at high speeds on a spinner. A few drops of the solution were placed on a substrate and this was spun for 40 seconds at a spin speed that would give the required thickness. The solvents used were volatile, resulting in a film of the solute. Film thickness was calculated from the measured absorbance using an absorption coefficient derived through spectroscopic ellipsometry performed by another member of the group, Paul Shaw.

Chapter 4

Gratings based Amplifier

Optical amplifiers are important devices for data communications. They compensate for losses associated with the transmission or splitting of signals. Inorganic semiconducting optical amplifiers and Erbium Doped Fiber Amplifiers (EDFA) are commonly used in silica fiber networks to regenerate attenuated signals, for wavelength selection and for all-optical switching. However the existing technology does not allow for high bandwidth at low costs in consumer networks [25]. With the rapid advancement in technology, there is a high demand by consumers for high speed digital services in the home and in the office areas. Polymer technology is seen as a suitable low-cost alternative to replace the twisted pair cables at remote stations and reduce the bottle neck in local area networks [26]. Their simple processing techniques allow them to be fabricated on any surface, which is suitable for integrated circuits and combined with suitable low cost materials such as polymethylmethacrylate (PMMA), can be used to fabricate polymer based fibers. Polymer optical fibers are suitable transmission medium to provide broad bandwidth, low cost telecommunications services to the consumer homes, i.e. for short haul data transmission. Moreover they are flexible, ductile under strain, versatile, have low manufacturing costs, are easy to install and have the advantage of being able to be installed on-site [25, 26]. They would require, just as in silica networks, organic semiconducting lasers and amplifiers to generate signals and boost the signal at certain stages along the fiber.

Organic semiconducting polymers are attractive gain media [40, 61–66] for such amplifiers [43, 67–69] and lasers [13–20, 42] due to their high optical gain, broad spectral ranges, low manufacturing costs, capability to be electrically pumped [62, 70, 71], and their versatility in being able to be fabricated into a variety of optical devices. The potential for high optical gain in semiconducting polymers was first shown in solution by *Lawrence et al.* and *Heliotis et al.* [67, 72] with amplification up to 40 dB in OC_1C_{10}-PPV and F8BT. However, for practical applications, a solid state polymer amplifier would be much more convenient. Such an amplifier had been demonstrated by *Goossens et al.* giving 18 dB gain in a waveguide length of 300 μm [68].

Dye doped polymer amplifiers have been demonstrated to achieve high gains of 26 and 14 dB [73, 74]. However conjugated polymers have several advantages over dye films. Unlike dye doped films and rare earth ions, conjugated polymers exhibit less concentration quenching of the luminescence [42, 70]. This is because the molecular structure in polymers is large, disordered and contains side chains. These result in the molecules showing less aggregation at high concentrations, which allow for photoluminescence efficiencies of > 60 % to be obtained in neat films [42]. This contrasts with the situation in dyes and rare earth ions, in which the efficiency drops significantly at high concentrations [42].

A major challenge with solid state amplifiers is the fabrication of efficient waveguides and coupling light in and out. Amplification is observed when the pump and probe beams overlap temporally and spatially. In solution based amplifiers, the solution is placed in a 1 cm wide quartz cuvette. In solid state amplifiers the solution is spin coated on a quartz substrate to form a thin film. Overlapping the two beams is easier in solution than in film as there is a larger volume in which to overlap the beams than in the film. Thin polymer films are also amorphous. Cleaving them does not produce smooth clean edges required for edge coupling. For the first solid state amplifier in this work, gratings were used to couple the light into the polymer.

The solid-state polymer amplifier produced in this project was based on the conjugated polymer poly[2-methoxy-5-(2'-ethylhexyloxy)-*p*-phenylene vinylene](MEH-PPV). This polymer was purchased from the company, American Dye Source (ADS). Further work was conducted on MEH-PPV from Covion (for comparison) and Red F from the Dow Chemical Company. The latter was collaborative work conducted with Imperial College London.

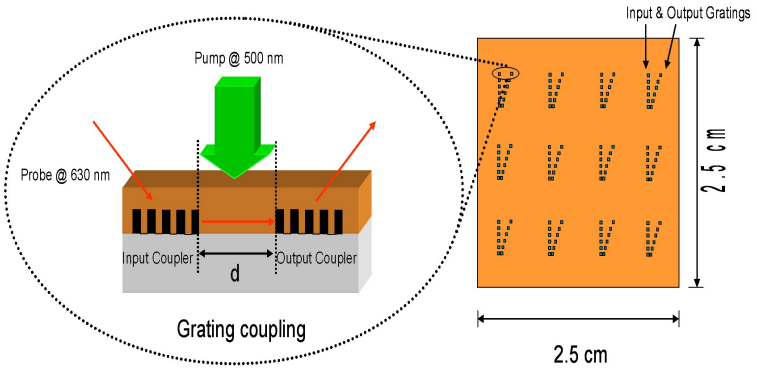

Figure 4.1: On the left hand side: The signal beam is coupled into the polymer film, waveguided through the pumped region and coupled out. On the right hand side: Silica substrate (orange) with grating couplers (white squares). All the output couplers are at fixed distances from the input. The input coupler is on the left. From column left to right, the grating periods were 420, 440, 460 and 480 nm.

4.1 Grating Structure

The amplifier structure uses a grating architecture, shown in Figure 4.1. The gratings were etched by Dr. Andreas Vadeskis onto a 5 cm^2 piece of silica using reactive ion etching. To avoid optical feedback the axis of the output coupler was rotated by 20°, as shown in Figure 4.2. This also ensured that the amplified output was spatially separated from any surface reflections. Gratings of four different periods were etched; Λ = 420 nm, 440 nm, 460 nm and 480 nm. The polymer was spin coated on top of the gratings. Light was coupled into the film, waveguided through a photo-excited region and coupled out. Output couplers were placed at different distances from the input coupler to create a number of waveguide lengths. The length of the different waveguides were 1022, 822, 622, 422, 322, 222 and 122 μm. The grating period used for the experiments with MEH-PPV was Λ = 440 nm and the length of waveguides used were 1022 μm, 822 μm, 622 μm and 422 μm.

Signal transmission was measured using a He-Ne laser at 630 nm for three channels. Figure 4.3 shows the measured input and output powers for waveguides of length 322 μm, 222 μm and 122 μm. The coupling efficiency was calculated using the relationship:

$$T = C^2 \exp^{-\alpha d} \tag{4.1}$$

Where T is the transmission $\frac{\text{outputpower}}{\text{inputpower}}$; α is the absorption co-efficient, d is the length

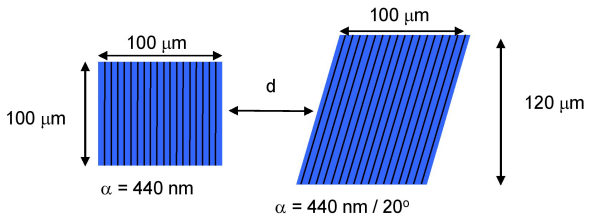

Figure 4.2: Schematic of a grating pair. On the left is the input coupler and on the right is the output coupler. The output coupler is rotated by 20°.

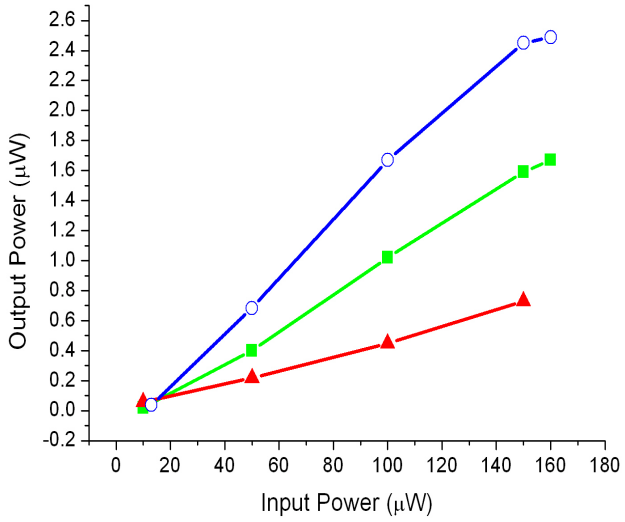

Figure 4.3: Measurements of input and corresponding output powers taken with 322 μm (*red line*), 222 μm (*green line*) and 122 μm (*blue line*) wave guide lengths.

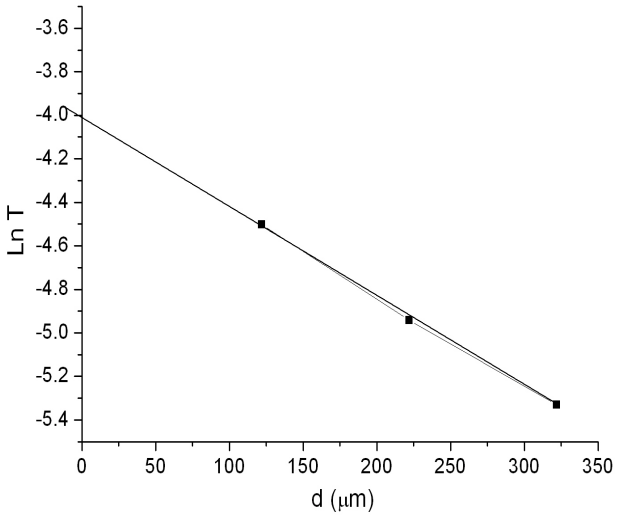

Figure 4.4: Plot of lnT against the waveguide length, d

of the waveguide and C is the coupling constant. Equation 4.1 can be re-written as:

$$\text{lnT} = 2\text{ln}C - \alpha d \tag{4.2}$$

By plotting lnT against distance, d, (figure 4.4), from equation 4.2, values for α and C can be obtained from the gradient and ($d = 0$) intersection point respectively. The values were $C = 18.2$ % and $\alpha = 32.5$ cm^{-1}. When calculating the probe energy, the 20 % coupling was taken into consideration.

4.2 Setup

Transient absorption was used to demonstrate amplification. Transient absorption experiments have been shown to be suitable to demonstrate gain, giving optical gains of $\sim$ 50 cm^{-1} through very thin ($\sim$ 100 nm) conjugated polymer films [63, 75, 76]. The pump wavelength was kept at 500 nm, which is within the absorption band of the material. The signal wavelength was tuned within the fluorescence band from 615

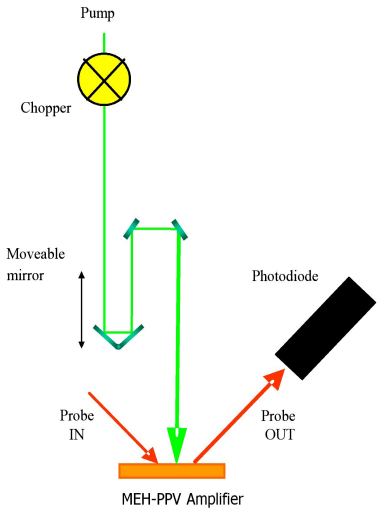

Figure 4.5: Schematic of transient absorption setup with grating amplifier

to 650 nm. The pump beam had a repetition rate of 2.5 kHz and the signal beam had a repetition rate of 5 kHz; both beams had a pulse duration of 100 fs. A time delay was applied to the pump beam to observe the temporal change of the amplified signal. The setup is shown in Figure 4.5.

Gain measurements were taken for different waveguide lengths. The gain was calculated from the intensity ratio of the amplified to the unamplified signal energy, after subtraction of the photoluminescence background (measured with the signal beam blocked).

$$G(\mathrm{dB}) = 10\log\frac{P_{\mathrm{ON}} - P_{\mathrm{B}}}{P_{\mathrm{OFF}}} \tag{4.3}$$

where P_{ON} is the amplified signal, P_{OFF} is the unamplified signal (probe) energy and P_{B} is the background. (Under typical conditions; $\mathrm{P_B} < 0.01$ of $\mathrm{P_{ON}}$). The pump energy density was then varied with the signal pulse energy fixed at $\sim$ 2 nJ inside the waveguide, just after the input coupler.

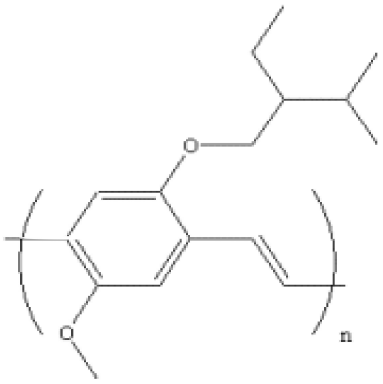

Figure 4.6: Molecular structure of the conjugated polymer MEH-PPV

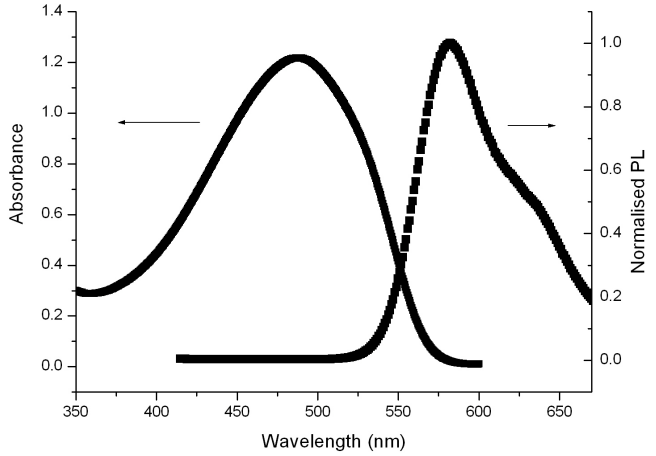

Figure 4.7: Absorption and Emission spectra of MEH-PPV

4.3 MEH-PPV; absorption and photoluminescence

MEH-PPV is an orange coloured conjugated polymer. The molecular structure is shown in Figure 4.6. Figure 4.7 shows the absorption and photoluminescence spectra. The emission peak is at 580 nm and the absorption peak is at 500 nm. The edge of the absorption band overlaps a portion of the emission spectrum. This causes re-absorption of emitted light, increasing losses. To reduce losses, pump dependency measurements were taken at a wavelength as far away as possible from this absorption shoulder without compromising the emission strength.

4.3.1 Preparation of MEH-PPV

The polymer was first made into a solution using chlorobenzene at a concentration of 6 mg/ml. Chlorobenzene was used because it did not restrict PL emission as other solvents. *Nguyen et al.* [77] found that some solvents, such as THF, caused the polymer chains to coil up, hence reducing inter-chain interaction and suppressing photo luminescence. In contrast chlorobenzene caused polymer chains to lie open and flat, resulting in higher PL output. The solution was spin coated onto the amplifier structure at 1250 rpm for 40 seconds to form a 100 nm thin film. According to work conducted by *Sheridan et al* [78], for a film thickness of 100 nm the cutoff wavelength for waveguiding is > 680 nm in MEH-PPV. The probing wavelengths were below this value.

4.3.2 ASE measurements

ASE measurements were taken with a film of MEH-PPV spun on a quartz disk to show that there is net gain in the material. The beam was focussed into a 1D stripe of 1 cm length and the excitation wavelength was at 500 nm and the ASE threshold and wavelength were ~ 0.4 μJ/cm^2 and 630 nm respectively. The 1 cm stripe length allows for a larger build up of ASE over the 2D spot size used in the amplifier experiments. Hence the ASE threshold value obtained here would not be the same as in the amplifier measurements. The aim of conducting this ASE experiment was to obtain the ASE wavelength and to ensure that the material has net gain, indicating that the amplification is due to stimulated emission.

Figure 4.8 shows the ASE peak intensity variation with pump energy.

4.3.3 Results using MEH-PPV

The effects of probe wavelength, pump and probe energy were explored for different waveguide lengths to understand the operation of the amplifier.

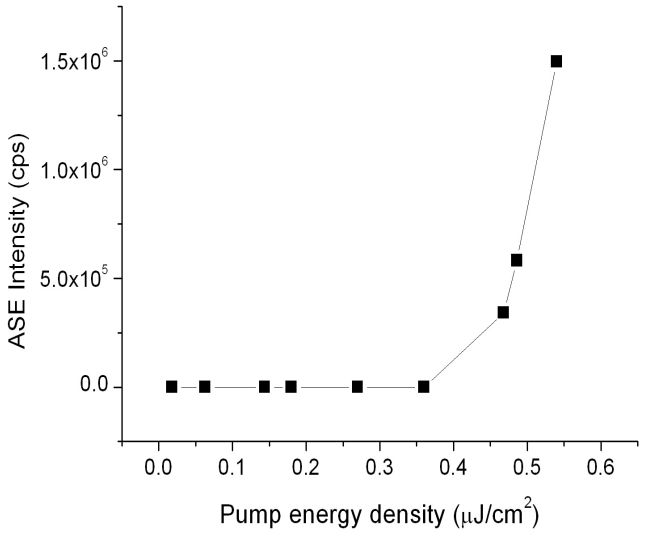

Figure 4.8: Variation of the peak intensity with the pump energy.

4.3.3.1 Gain dependence on Pump energy density

The pump wavelength was kept at 500 nm and the probe wavelength was kept at 630 nm, with a small signal/probe energy of 2 nJ just after the input coupler. The aim of this experiment was to determine the gain for different pump energy densities and the highest achievable gain. Three lengths of waveguides were used: 1022, 622 and 422 μm. The pump spot was circular and its size was altered to fit within each waveguide length by varying the position of the focusing lens. The fixed distances of the waveguides provided a scaling reference for the spot size. Higher gains would be achievable with a lower probe energy, however coupling into the polymer would have been harder. A gain of 21 dB was obtained for the longest waveguide of length 1022 μm (shown in Figure 4.9). Channels of length 622 and 422 μm gave gains of 18 and 14 dB respectively (Figures 4.9 and 4.10). All the channels showed the same increase of signal power with the increasing pump energy.

Amplification in conjugated polymers arise from stimulated emission in a four level system as in organic laser dyes [40, 43, 67, 69]:

$$\sigma = \frac{1}{Nl} ln \frac{P_{\mathrm{ON}} - P_{\mathrm{B}}}{P_{\mathrm{OFF}}} \tag{4.4}$$

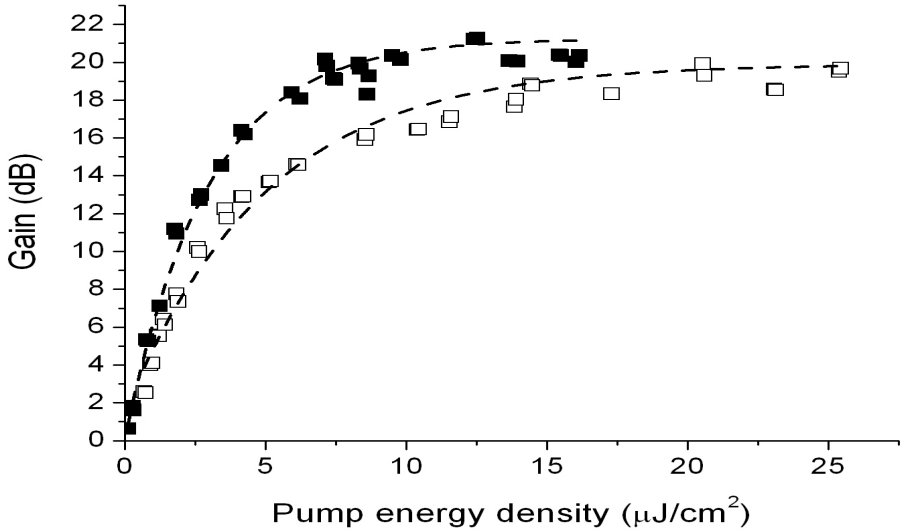

Figure 4.9: Gain vs pump energy density for waveguides of length 1022 μm (*closed squares*) and 622 μm (*open squares*) The *dashed line* is a guide for the eye.

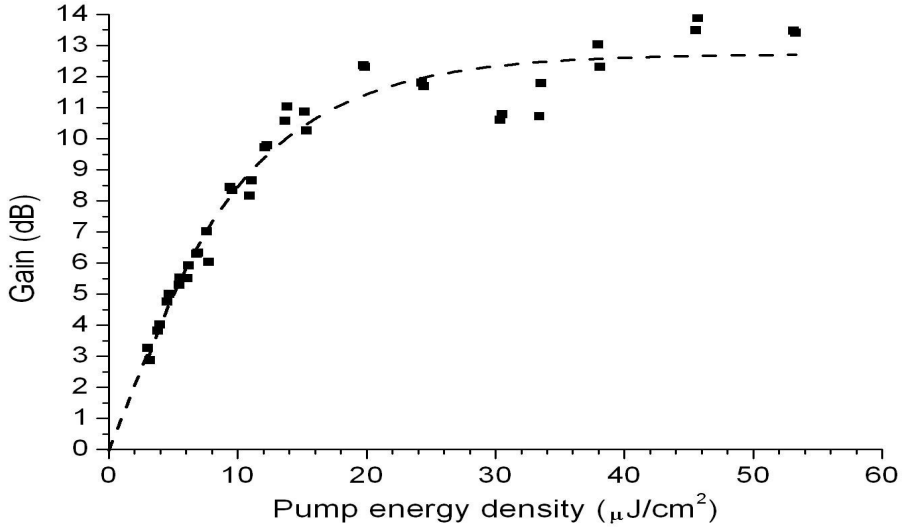

Figure 4.10: Gain vs pump energy density for waveguide of length 422 μm. The *dashed line* is a guide for the eye.

where N is the exciton density and l is the length of the polymer guide and σ is the gain cross-section.

$$N = \frac{Pumppower * P}{AR\hbar vd} \tag{4.5}$$

where P is the percentage of pump wavelength absorbed, A is the area of the excited region, R is the repetition rate, $\hbar$ is Planck's constant, v is the frequency of the pump light, d is the thickness of the material. The optical gain is dependent on the gain cross section, σ, which is a property of the material. By plotting $ln\frac{P_{\mathrm{ON}}-P_{\mathrm{B}}}{P_{\mathrm{OFF}}}$ against Nl, the value of σ can be calculated using Equation 4.4. *Note that it is only calculated on the the linear portion of the excitation density dependence, which is at the low pump energy densities.* The averaged value for waveguides of length 622, 422 and 1022 μm, with a probe wavelength of 630 nm, was (4 $\pm$ 1) x 10^{-17}cm^2. This agrees with a value reported for a similar polymer, polyparaphenylenevinylene, which was in the order of 10^{-17} cm^2 [67].

For each waveguide, the highest achieved gain is different because of the different waveguide lengths. As expressed in Equation 4.4, the gain is directly proportional to the length of the waveguide. A longer waveguide would result in higher gain. The number of excitons generated increases with the increase in the pump energy. A limit is reached where further pumping does not lead to an increase in the gain and could lead to subsequent degradation of the polymer. This point is called *gain saturation* and is caused by amplified spontaneous emission (ASE) and exciton exciton annihilation [75, 76].

4.3.3.2 Broadband amplification

To test the tunability spectra of the amplified light in the amplifier device, gain dependency on the pump energy was measured for two different probe wavelengths of 650 and 615 nm.

These wavelengths were chosen because they come under the broad emission spectra of MEH-PPV. A gain of 15 dB was obtained for probe wavelengths of 650 and 615 nm as shown in Figures 4.11 and 4.12. This indicated that the MEH-PPV grating amplifier can give high gain over a large bandwidth of 35 nm. At a probe wavelength of 650 nm, the 15 dB gain was obtained in a 1022 μm long waveguide. This gain

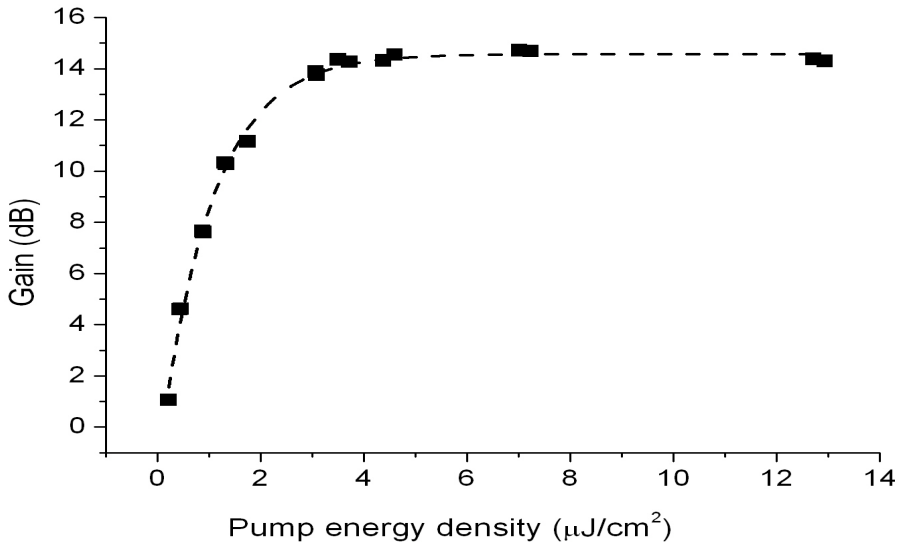

Figure 4.11: Gain vs pump energy density for a probe wavelength of 650 nm in a waveguide of length 1022 μm. The *dashed line* is a guide for the eye.

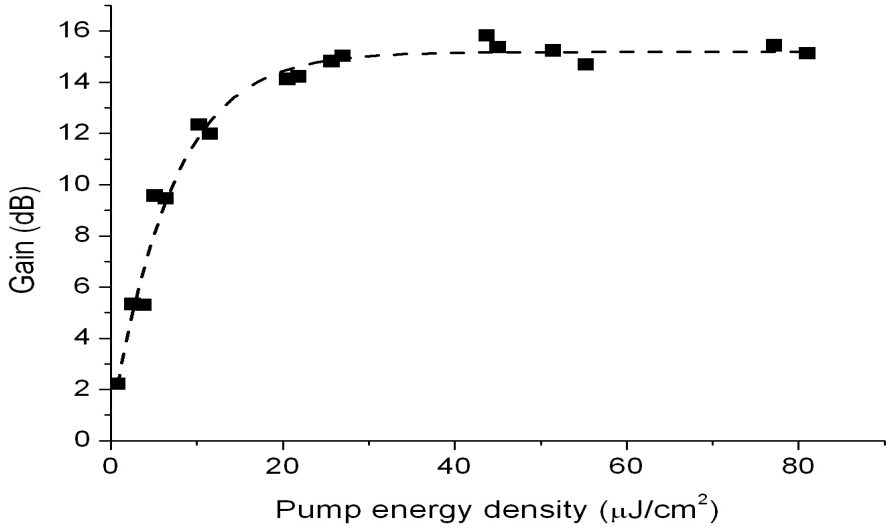

Figure 4.12: Gain vs pump energy density for a probe wavelength of 615 nm in a waveguide of length 422 μm. The *dashed line* is a guide for the eye.

value is lower than the value of 21 dB obtained at 630 nm. It is due to excited state absorption, where the spectrum of the excited state absorption overlaps with the stimulated emission spectrum. At the probe wavelength of 615 nm a gain of 15 dB was also obtained. A waveguide of length 422 μm was used because there was no probe light output using the longer channels (> 422 μm), this was because the probe light was being absorbed within the longer waveguides.

4.3.3.3 Exciton-exciton annihilation

A major contributor to gain saturation is *exciton-exciton annihilation*. At high pump densities, the gain decays faster with the build up of excitons. Increasing the pump energy produces more excitons. When the density of excitons reaches a sufficient level, two excitons within the annihilation radius combine to form a single exciton of higher energy. The excess energy is rapidly lost and the net effect is the loss of one exciton. As the gain is proportional to the exciton density, the optical gain decreases. At very high pump energies, the gain lifetime can be < 2 ps. Exciton-exciton annihilation can be modeled using the rate equation [76, 79–81]:

$$\frac{dN}{dt} = -kN - \gamma N^2 \tag{4.6}$$

where $N(t)$ is the exciton density at time t, $k = 1/140$ ps is the decay rate with no annihilation and γ is the annihilation rate. This equation can be solved mathematically for constant γ as:

$$N(t) = \frac{N(0)exp(-kt)}{1 + \frac{\gamma}{k}N(0)[1 - exp(-kt)]} \tag{4.7}$$

A plot of 1/N(t) vs exp(kt) gives $\gamma \approx (3 \pm 0.1)$ x 10^{-9} cm^3/s. The spot sizes were measured using a beam profiler to ensure accuracy of the annihilation rate value. This annihilation rate value is similar to reported values in other conjugated polymers, which were in the range of 10^{-8} to 10^{-9} cm^3/s [75, 76]. However, it is an order of magnitude lower than that calculated for MEH-PPV reported by *Lewis et al* [81].

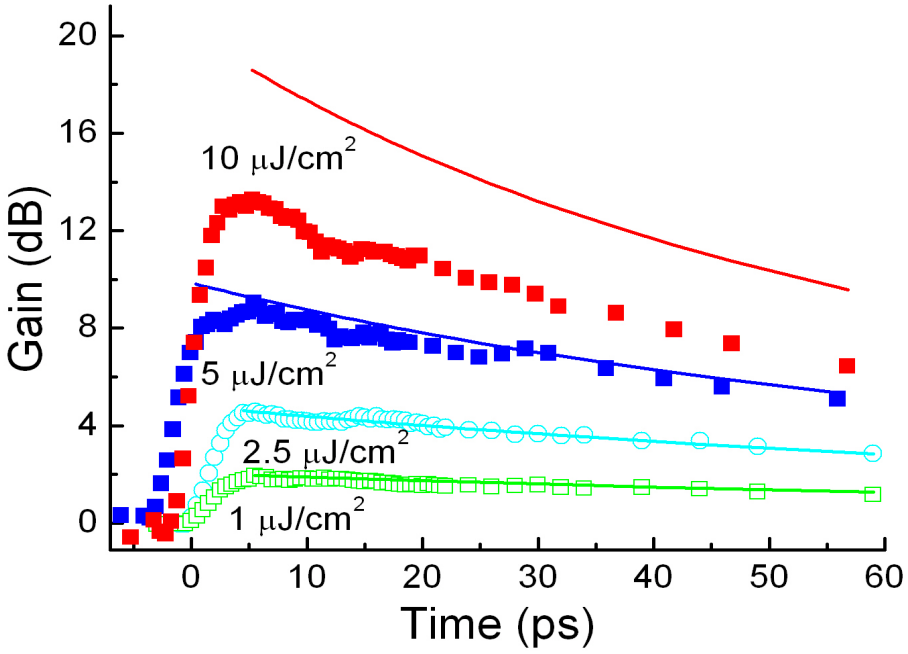

Figure 4.13: Gain vs time delay between pump and probe pulses (symbols) in a 622 μm long wave guide. The decay as predicted by equation 4.7 is shown by the *solid lines*.

The annihilation rate is lower possibly because initially there is rapid annihilation occurring on a time scale shorter than the instrumental response function which reduces the excited state population leading to an over estimation of the population and a reduction in the annihilation rate.

The calculated and experimental gain dynamics are in good agreement for pump energy densities of up to 5 μJ/cm^2, as shown in Figure 4.13. At the highest energy density, the experimental gain is lower than the calculated gain by a constant fraction. This is possibly due to other photo-induced effects, such as ASE, taking place. Pump energy densities greater than 10 μJ/cm^2 showed line narrowing, which is a signature of ASE as shown in Figure 4.14. In addition the generation of higher energy carriers would absorb in the gain region and reduce the gain [43].

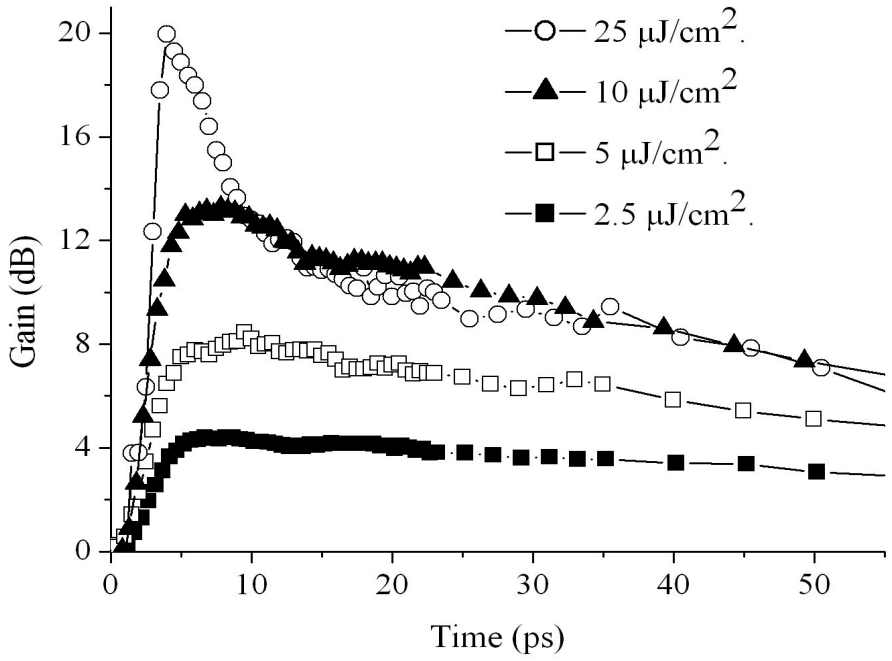

Figure 4.14: Gain vs time delay between pump and probe pulses (symbols) in a 622 μm long wave guide. With the increase in pump energy density, the gain life time reduces and distinct line narrowing is observed at high pump energy densities.

4.3.3.4 Gain dependence on probe energy

Measurements were taken with a waveguide of length 822 μm and the results are shown in Figure 4.15. The pump energy density was maintained at 2 μJ/cm^2. Optical gain decreases when the probe energy is high enough to deplete the excited state population. The experimental data was fitted to the theoretical dependence for a homogeneously saturated optical pulsed amplifier [72, 74, 82] :

$$G = \frac{A}{C_3} ln[1 + G_0[exp(\frac{C_3}{A}) - 1] \tag{4.8}$$

where

$$C_3 = \frac{E_{\mathrm{IN}}(\sigma_{\mathrm{abs}} + \sigma_{\mathrm{se}})}{h v_{\mathrm{in}}} \tag{4.9}$$

E_{IN} is the signal energy input, G_o is the small signal (probe) gain, $\sigma_{\mathrm{abs,se}}$ are the absorption (abs) and stimulated emission (se) cross sections, h is Planck's constant, $v_{\in}$ is the probe frequency and A is cross sectional area of the probe. From this fit a small signal/probe gain coefficient of 11 dB was obtained, which is the gain obtained for an input signal that is very weak. Assuming that absorption at this wavelength, 630 nm, is negligible ($\sigma_{abs} = 0$), the stimulated emission cross section was calculated to be σ = (5 $\pm$ 2) x 10^{-16} cm^2. This value is slightly higher than that calculated from Equation 4.4. The saturation signal energy density, $\frac{E_s}{A}$, was calculated to be 853 μJ/cm^2 using the relationship [67, 83]:

$$E_s = \frac{Ahv}{\sigma_{\mathrm{abs}} + \sigma_{\mathrm{se}}} \tag{4.10}$$

Therefore:

$$\frac{E_{in}}{C_3} = \frac{E_s}{A} \tag{4.11}$$

The saturation signal energy density is the amount of probe energy density which leads to a 50 % reduction of the gain [49]. The maximum probe energy density used in this thesis was 25 μJ/cm^2, this value was below the calculated saturated signal energy density.

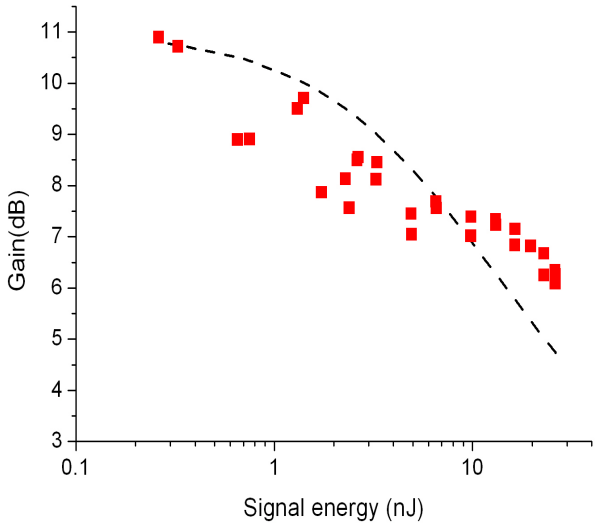

Figure 4.15: Gain dependence on probe energy. The waveguide length used was 822 μm shown by the *red symbols* and the theoretical fit to equation 4.8 is shown with a *dashed line*. The probe wavelength was 630 nm.

4.3.3.5 Gain dependence on pump energy density using MEH-PPV provided by Covion

A second supply of MEH-PPV became available after the experiments described above. A pump probe experiment was conducted with this material using waveguides of length 1022 μm, 822 μm and 622 μm. The gains obtained were 21.4 dB, 18 dB and 16.5 dB respectively. Comparing this with the material provided by ADS showed no large difference in gain. The results are shown in Figures 4.16, 4.17 and 4.18. This shows that substantial gain can be obtained in MEH-PPV obtained from more than one source.

4.4 Grating amplifier using the polymer Red-F.

Amplification, using the same pair of gratings, was also obtained with a polymer called Red-F, provided by Dow Chemical Company. Red-F was analysed because as a laser material it has given a low laser threshold of 1.1 μJ/cm^2 [84]. The work was

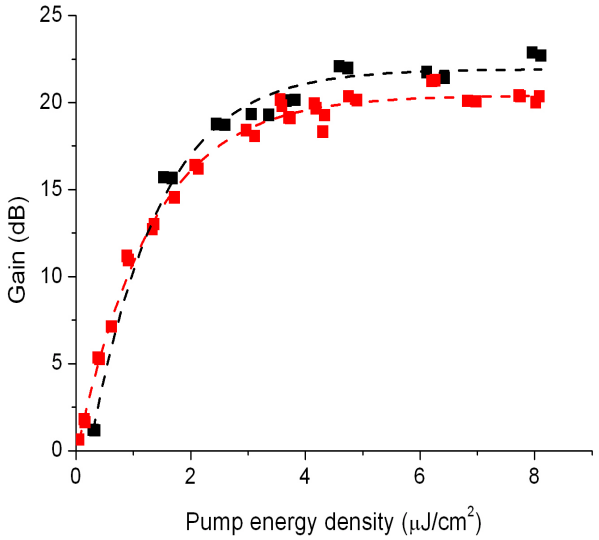

Figure 4.16: Gain dependence on pump energy. The waveguide length was 1022 μm and the probe wavelength was 630 nm. The Covion material is the *black symbols*, and the ADS material is the *red symbols*. The *dashed black* and *red lines* are a guide for the eye.

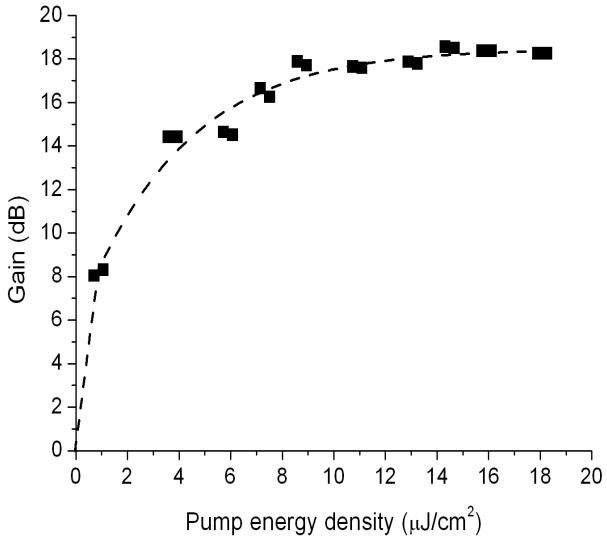

Figure 4.17: Gain dependence on pump energy for MEH-PPV provided by Covion. The waveguide length was 822 μm and the probe wavelength was 630 nm. The *dashed line* is a guide for the eye.

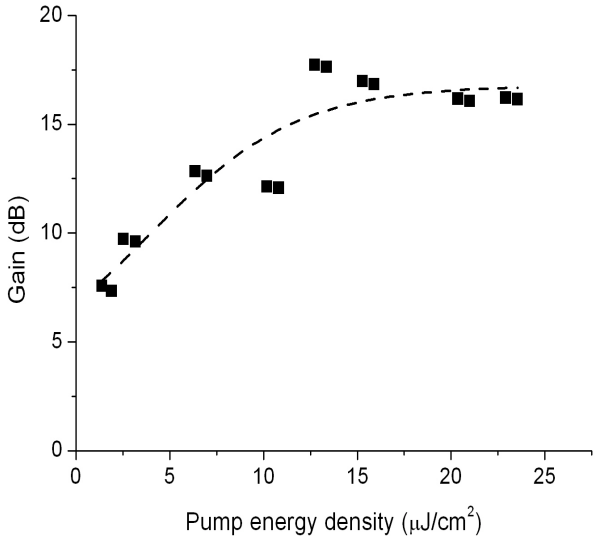

Figure 4.18: Gain dependence on pump energy for MEH-PPV provided by Covion. The waveguide length was 622 μm and the probe wavelength was 630 nm. The *dashed line* is a guide for the eye.

a collaboration between Imperial College London and the University of St Andrews conducted by myself and Cora Cheung. Previous work has been conducted between both universities on a blend of the same material with F8BT [68]. This demonstrated amplification of Red-F blended with F8BT on waveguide of lengths 300 μm, 200 μm and 100 μm. A maximum gain of 18 dB was obtained. The emission wavelength was at 650 nm, which was specifically tuned to the centre low loss window of polymethylmethacrylate (PMMA) widely used in polymer optical fibres and polymer integrated circuits [85].

4.4.1 Red-F: absorption and photoluminescence

The Red-F material is from the polyfluorene family and consists of four main parts: a red chromophore, the conjugated polymer F8BT and two other parts which are not disclosed by Dow Chemical Company.

Figure 4.19 shows the absorption and emission spectra of Red-F and F8BT [1] [86].

[1] Ignore F8DP, it is not relevant to this work

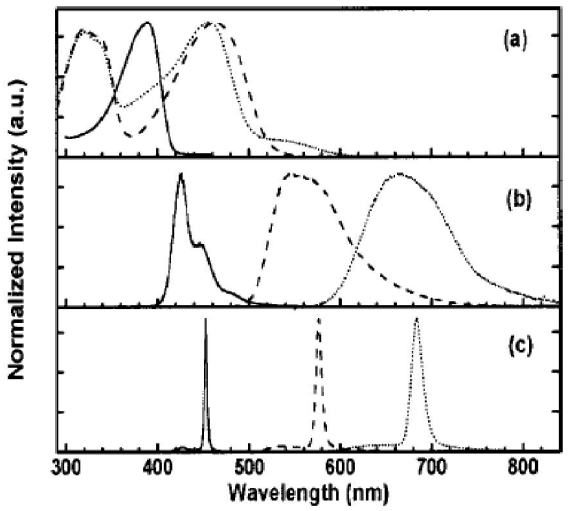

Figure 4.19: (a)Absorption, (b) emission and (c) ASE spectra of Red-F *dotted lines*, F8BT *dashed lines* and F8DP *solid lines* [86].

The absorption spectrum of Red-F follows F8BT very closely except for a shoulder at > 500 nm.

4.4.2 Preparation of Red-F

The Red-F material was spin coated at 2500 rpm for 40 seconds from a toluene solution to produce a 250 nm neat film, and 1000 rpm for a 150 nm film blended with F8BT. Work was first carried out with neat films of Red-F. This led on to the use of blended films in order to reduce photoinduced effects because the chromophores would be spaced further apart.

4.4.3 Results with neat Red-F

Experiments were initially conducted with neat Red-F films. The pump wavelength was 515 nm and the probe wavelength was 675 nm. Gains of 18 dB, 17 dB and 16.4 dB were obtained for waveguides of length 1022, 822 and 622 μm respectively and are

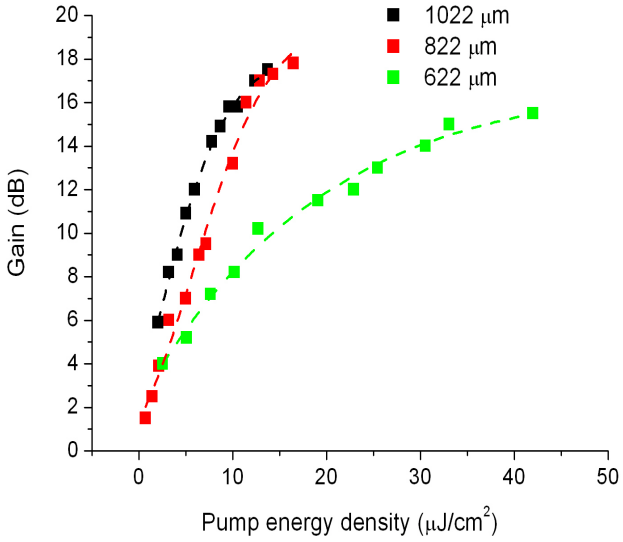

Figure 4.20: Gain dependence on pump energy for neat Red-F amplifier in different waveguide channel lengths. The *dashed lines* are a guide for the eye.

shown in Figure 4.20. Figures 4.21, 4.22 and 4.23 are the temporal spectra for the three channels. If no additional losses were present, then the gain for a 1022 μm long waveguide would be expected to be greater because the gain of a 300 μm waveguide with a Red-F blend had been reported to be 18 dB [68, 85]. This indicated that in this case, the shorter waveguide lengths with the neat film of Red-F would give gains of $<$ 18 dB. The next option was to try a blended film of Red-F with F8BT.

4.4.4 Results with blended Red-F

The Red-F was blended with F8BT. They were mixed in a ratio of 1:1 by weight. The blended film would space the Red-F chromophores further apart thus reducing any photoinduced effects. The material was pumped at 450 nm which would transfer energy to the red chromophore and emit in the PL region of Red-F.

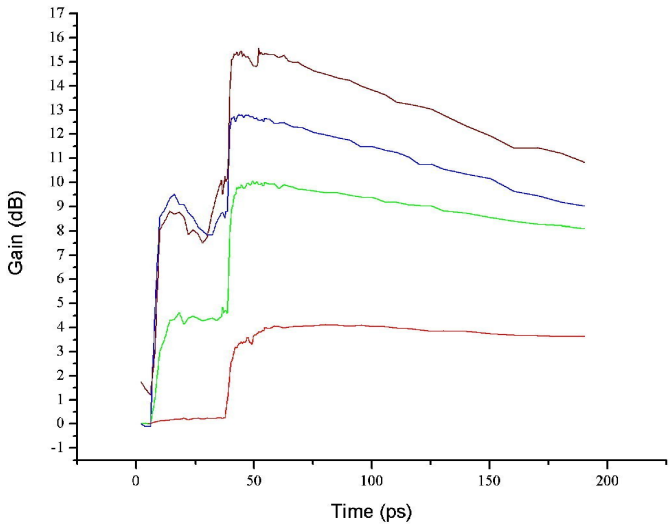

Figure 4.21: Gain lifetime for a neat film of Red-F in a 622 μm long waveguide. The pump energy densities are 2.5, 12.0, 28 and 33 μJ/cm^2 for the *red, green, blue* and *brown lines* respectively.

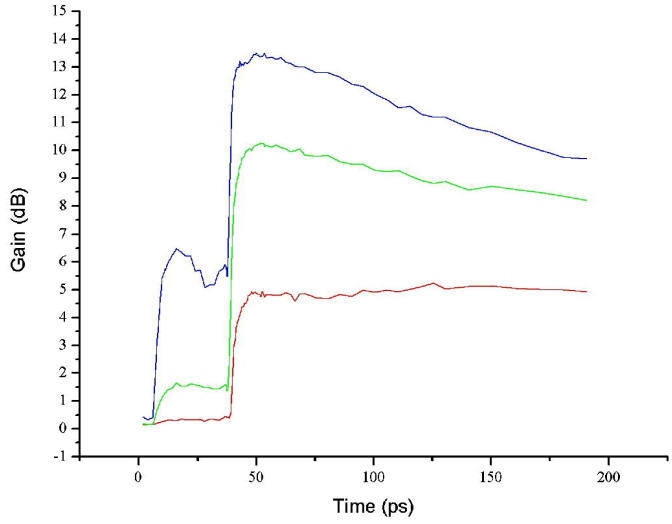

Figure 4.22: Gain lifetime for a neat film of Red-F in a 822 μm long waveguide. The pump energy densities are 1.4, 5.0 and 10.7 μJ/cm^2 for the *red, green* and *blue lines* respectively.

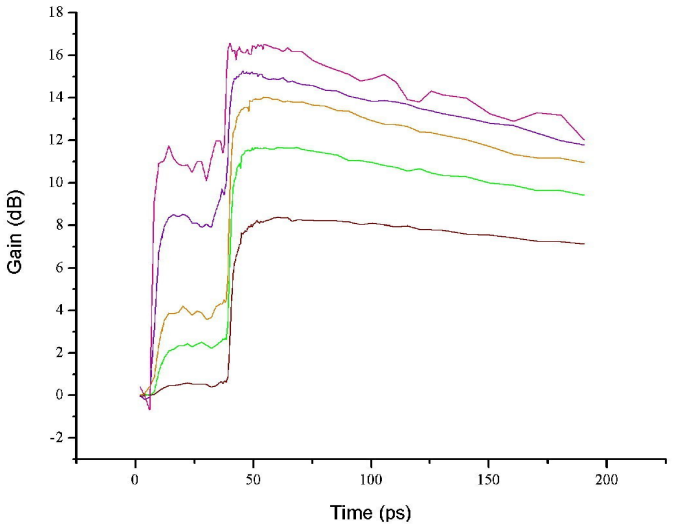

Figure 4.23: Gain lifetime for a neat film of Red-F in a 1022 μm long waveguide. The pump energy densities are 3.2, 6.0, 7.8, 9.6 and 13.7 μJ/cm^2 for the *brown, green, yellow, purple* and *pink lines* respectively.

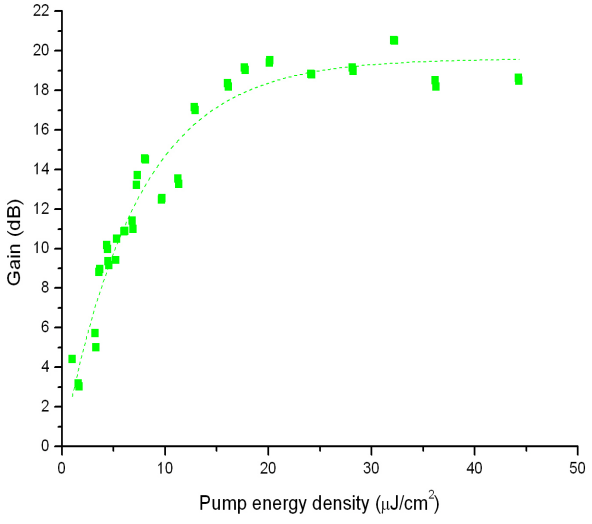

Figure 4.24: Gain dependence on pump density for 1022 μm long waveguide with a probe wavelength of 660 nm in a blended film of Red-F. The *dashed line* is a guide to the eye.

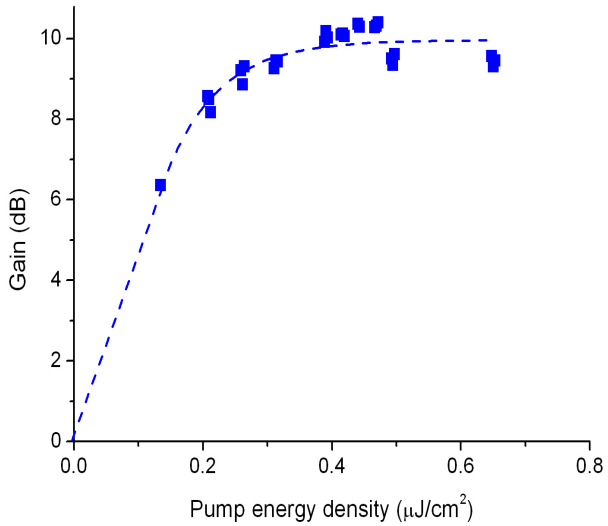

Figure 4.25: Gain dependence on pump density for 422 μm long waveguide with a probe wavelength of 660 nm in a blended film of Red-F. The *dashed line* is a guide to the eye.

4.4.4.1 Gain dependence on pump energy density.

Measurements were taken to observe the gain dependence on pump energy density. The probe energy was kept constant at 2 nJ. The length of the waveguides were 1022 μm and 422 μm. The probe wavelength used was 660 nm and the pump wavelength was kept at 450 nm. Gains of 19.5 and 9 dB were achieved for the 1022 and 422 μm waveguide lengths respectively and the results are shown in Figures 4.24 and 4.25.

4.4.4.2 Broadband amplification.

The probe wavelength was changed to a lower and higher value of 640 and 680 nm respectively. Measurements at 640 nm used a waveguide of length 622 μm and gave a gain of 15.2 dB, shown in Figure 4.26. For the probe wavelength of 680 nm, a channel length of 1022 μm was used and a gain of 7.8 dB was measured, shown in Figure 4.27.

Again the lower gain maximum with the high probe wavelength is associated with excited state absorption. The large difference between the gain maximums for a probe wavelength at 660 nm and 680 nm indicate there is a large ESA cross-section present

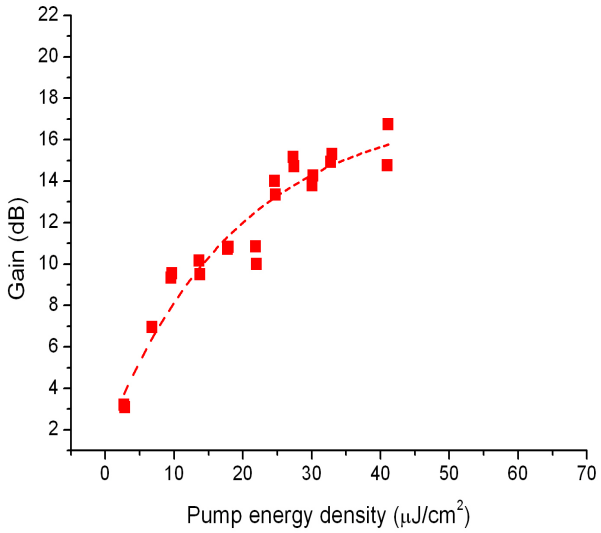

Figure 4.26: Gain dependence on pump density for 622 μm long waveguide with a probe wavelength of 640 nm in a blended film of Red-F. The *dashed line* is a guide to the eye.

at this wavelength. However the gain obtained for the lower probe wavelength of 640 nm, does not appear to have been heavily affected by ground state losses.

4.4.4.3 Gain dependence on probe energy density

The gain dependence on the probe energy was measured by keeping the pump energy constant at 2 μJ/cm^2. The probe wavelength was kept at 660 nm. The small signal gain coefficient, G_o was measured from the plot, Figure 4.28, to be 4.7 dB. Using these values the gain cross-section can be calculated from Equation 4.8 to be (1.3 $\pm$ 0.5) x 10^{-16} cm^2. Using Equation 4.4, the gain cross-section was calculated to be (0.9 $\pm$ 1.2) x 10^{-16} cm^2. These values are comparable to previously reported values of Red-F, which were to the order of 10^{-16} cm^2 [61]. The saturation signal energy density was calculated using the relationship in Equation 4.11 to be 2.3 mJ/cm^2. The probe energy density used, $\sim$ 25 μJ/cm^2, which was below the saturation signal energy density.

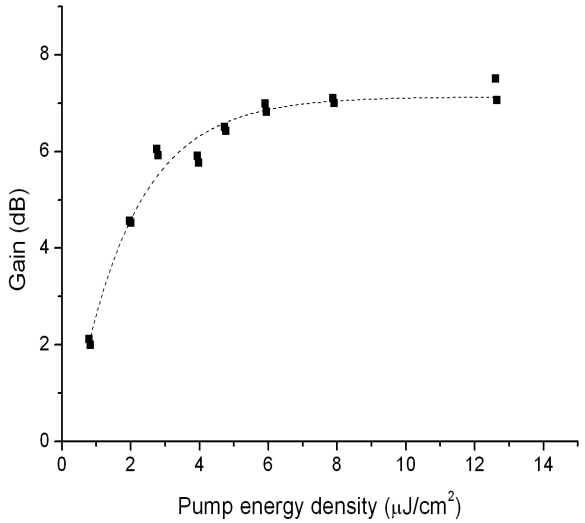

Figure 4.27: Gain dependence on pump density for 1022 μm long waveguide with a probe wavelength of 680 nm in a blended film of Red-F. The *dashed line* is a guide to the eye.

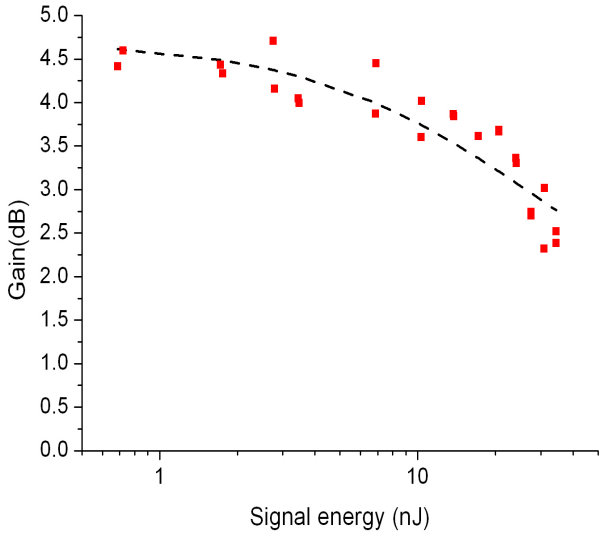

Figure 4.28: Gain dependence on probe energy on a channel length of 622 μm in a blended film of Red-F. The probe wavelength was set at 660 nm. The experimental plot is shown by the *red symbols* and the theoretical fit is the *dashed line*.

4.5 Conclusion

Optical amplification in solid films of conjugated polymers has been demonstrated. In MEH-PPV a maximum gain of 21 dB was achieved in a 1 mm long waveguide at a wavelength of 630 nm. Gains of greater than 13 dB were obtained for a gain bandwidth of 26 THz. The polymer Red-F gave a gain of 18 dB in the neat form at 675 nm and 20 dB in the blend with F8BT at 660 nm. Gains of > 6 dB was observed in a bandwidth of 27 THz.

Solid state conjugated polymer amplifier devices have shown to have gain per mm of 21 dB/mm, 18 dB/mm and 60 dB/mm [68]. Many of the other solid state organic amplifier devices are either optical fiber or end coupled waveguide amplifiers operating in the visible or IR regime. They mostly consist of an active material doped in an inactive polymer matrix. The active material could be a dye or rare earth ions. Examples of such devices have shown gains per mm of:

Dye doped (dB/mm)
0.037 [87]
0.054 [88]
0.06 [89]
0.23 [90]
2 [73]
0.9 [74]

in the visible range of about 500 to 650 nm. For wavelengths operating at > 1 μm, (in the silica fiber regime) polymers have been used to produce novel gain media with gains per mm of:

Rare earth ions (dB/mm)
0.16 [91]
0.084 [92]
0.72 [93]

The visible range amplifiers can be used in the low loss window of PMMA for short haul data transmission. The rare earth doped amplifiers were produced to improve the existing EDFAs as they allow higher concentrations of the metal to be used [94]. Figure 4.29 gives a visual representation of the overall net gain obtained in conjugated polymer amplifiers, dye doped fibre amplifiers and EDFAs. The net gain obtained in conjugated polymers is higher than that obtained in dye doped and rare earth doped polymer optical fibers which are researched for the same purpose. The plot shows

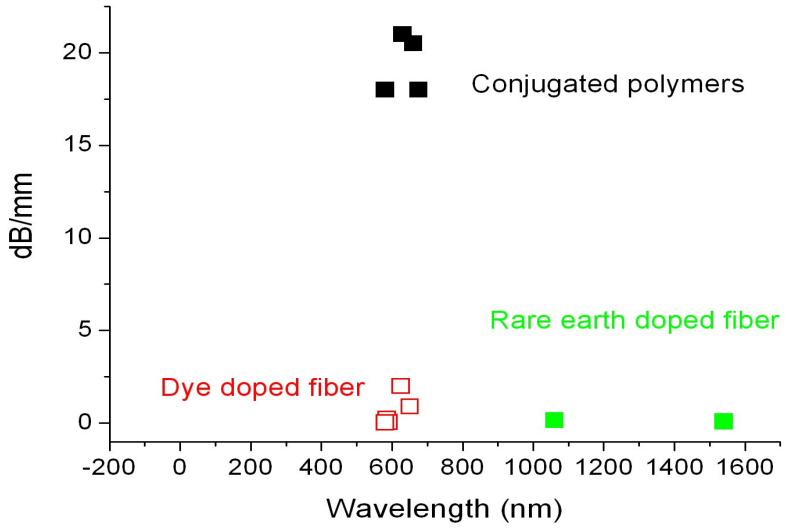

Figure 4.29: Variation of the net gain in different polymer optical amplifiers.

the potential of conjugated polymers over dyes and rare earth ions. Blending the conjugated polymers in an inert matrix would reduce the gain, however conjugated polymers exhibit low concentration quenching. Hence more active polymer can be present in the inert matrix than possible with dyes or rare earth ions, providing a higher net gain.

All the experiments were conducted under vacuum. Under this condition, the amplifier allowed amplification of 12 million pulses. For practical applications the device would have to be encapsulated, as is done in organic light emitting diodes [95], to ensure there is no contact with oxygen and water vapour which would photodegrade the material and reduce the emission [96]. Further studies would need to be conducted on encapsulation of the amplifier. However these results show promise that conjugated polymers can lead to high performance and low cost devices for short haul data transmission.

Chapter 5

Data Amplifier

Polymer optical amplifiers are designed to be used with graded index polymer optical fibers and polymer integrated circuits, primarily for telecommunications networks. The work in the previous chapter details the performance of an operating polymer amplifier using a single signal. However data is not a single pulse but streams of pulses. The purpose of the work presented in this chapter was to investigate the feasibility of amplifying multiple pulses in a polymer amplifier. This requires substantial gain lifetime in order to amplify multiple pulses equally at high pump energy densities.

5.1 F8BT single pulse amplifier

Although MEH-PPV gave a high gain value of 21 dB, it had a very short gain lifetime at pump densities of > 9 μJ/cm^2. For multiple pulses, this was a problem because pulses in a sequence would all amplify at extremely different rates. In order to amplify a pulse sequence equally, a polymer which gave high gain and a good gain lifetime at high pump energy densities was required. Poly 9,9-dioctylfluorene-co-benzothiadiazole (F8BT) had been demonstrated as a good polymer gain medium [61, 66]. F8BT is a yellow powder (molecular structure is shown in Figure 5.1), with an absorption peak at 470 nm and photoluminescence peak at 550 nm, shown

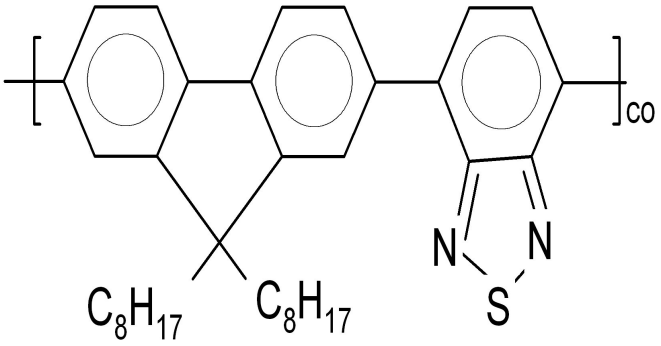

Figure 5.1: Molecular structure of the conjugated polymer F8BT.

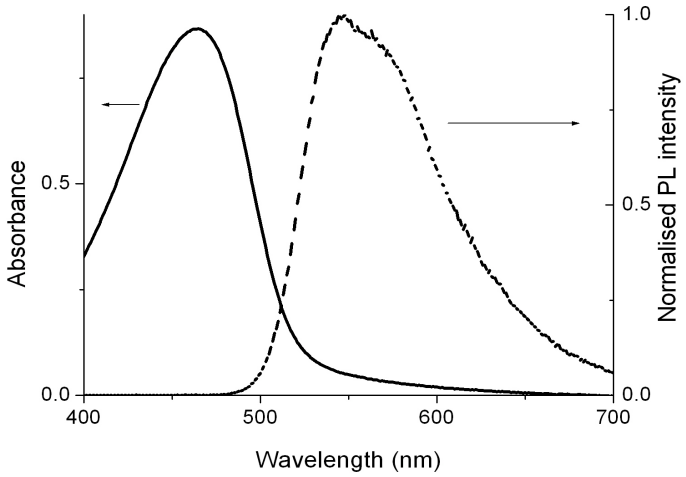

Figure 5.2: Absorption and emission spectra of F8BT.

in Figure 5.2. It is a co-polymer of the polymers poly 9,9-dioctylfluorene (F8) and benzothiadiazole (BT) to the ratio of 0.2:1, and has already been demonstrated as a solution based amplifier by *Heliotis et al* [72] and as a laser [18–20, 66]. The first task was to establish the gain and gain lifetime of F8BT as an amplifying medium using the gratings in the previous chapter.

5.1.1 F8BT: absorption and photoluminescence

Excitation and signal wavelengths were 497 and 580 nm respectively. These wavelengths were obtained from an optical parametric amplifier (OPA) pumped by a Ti:sapphire oscillator. The reason the signal wavelength was not at the peak of the emission spectrum was because the absorption tail was present in this region. To reduce any absorption losses, the signal wavelength was chosen to be in a region of weak absorption. Once the signal wavelength was tuned on the OPA, the corresponding beam for the pump would be tuned automatically to 497 nm, which still showed an absorbance of 0.5 for a 250 nm thick film.

5.1.2 Preparation of F8BT

F8BT was spin coated on to the gratings from solution. The solution was made using toluene and had a concentration of 30 mg/ml to give a polymer thickness of 250 nm when using a spin speed of 1000 rpm. These parameters were taken from work conducted using the same polymer in previous publications [20].

5.1.3 Amplified spontaneous emission

ASE measurements were conducted on films of F8BT before running device tests. Three films of different thicknesses; 127, 250 and 630 nm, were used. They were excited at 497 nm at 5 kHz from the OPA. Figures 5.3, 5.4 and 5.5 show the emission spectra for the film thicknesses of 127, 250 and 600 nm respectively. The resulting emission is a broad PL with the ASE at 582 nm. The ASE threshold appears to be slightly higher for thicker films; 0.3, 0.3 and 0.6 μJ/cm^2 for film thicknesses of 127, 250 and 600 nm respectively. Strong line narrowing begins to occur (FWHM of 5 nm) at pump powers > 0.8 μJ/cm^2.

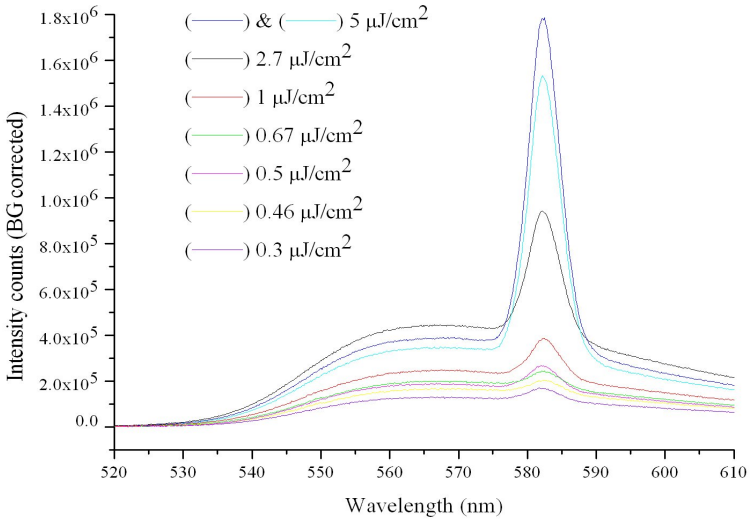

Figure 5.3: PL and ASE spectra of a 127 nm thin film of F8BT spin coated on quartz. The excitation wavelength was 497 nm at 5 kHz. The ASE peaks at 582 nm.

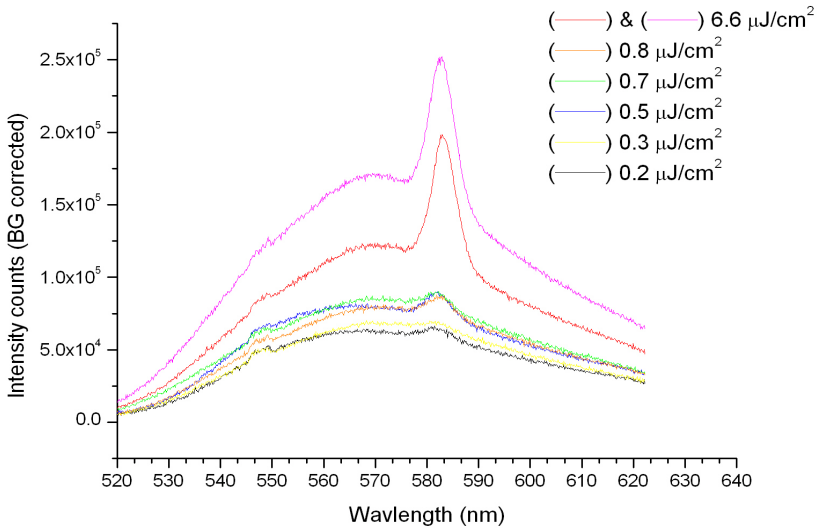

Figure 5.4: PL and ASE spectra of a 250 nm thin film of F8BT spin coated on quartz. The ASE peaks at 582 nm.

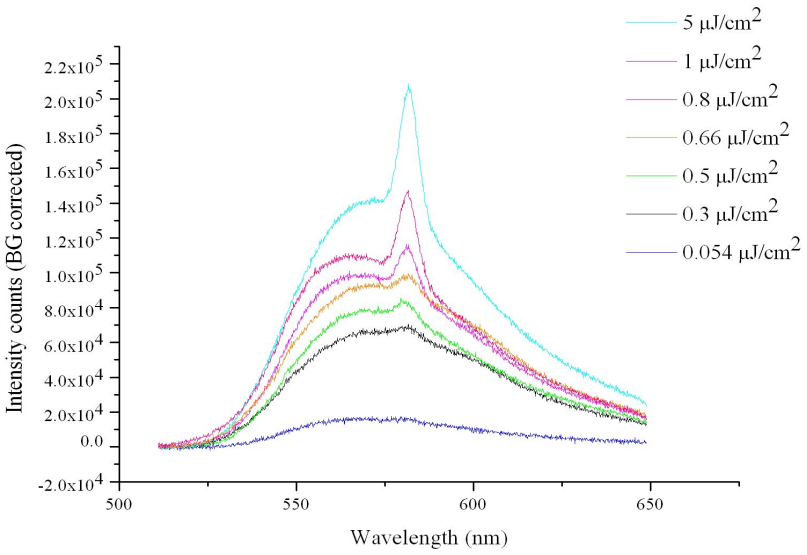

Figure 5.5: PL and ASE spectra of a 600 nm thin film of F8BT spin coated on quartz. The ASE peaks at 582 nm.

5.1.4 Experiment: Amplification with a single signal pulse

Experiments were conducted to obtain the gain for different waveguide lengths. Gain was calculated from the intensity ratio of the amplified to the unamplified signal energy, after subtraction of the photo luminescence background (measured with the signal beam blocked) using Equation 4.3 [43, 67, 69]. The signal energy was kept constant at $\sim$ 1 nJ just inside the waveguide.

5.1.5 Gain dependence on pump energy

Gains were measured in waveguides of lengths 1022, 822 and 622 μm. These gave maximum gains of 17, 13 and 10 dB respectively. The plots are shown in Figure 5.6. They show that the gain increased with increasing length of the gain material and that the polymer is able to give a high gain of 17 dB for a short waveguide of length 1022 μm. The gain cross section was calculated from the linear region of the plots (at low pump density) using Equation 4.4. The gain cross section was calculated to be (1.45 $\pm$ 0.174) x 10^{-17} cm^2. This value is comparable to values previously reported, which were in the range of 10^{-16} to 10^{-17} cm^2 [19, 61, 72].

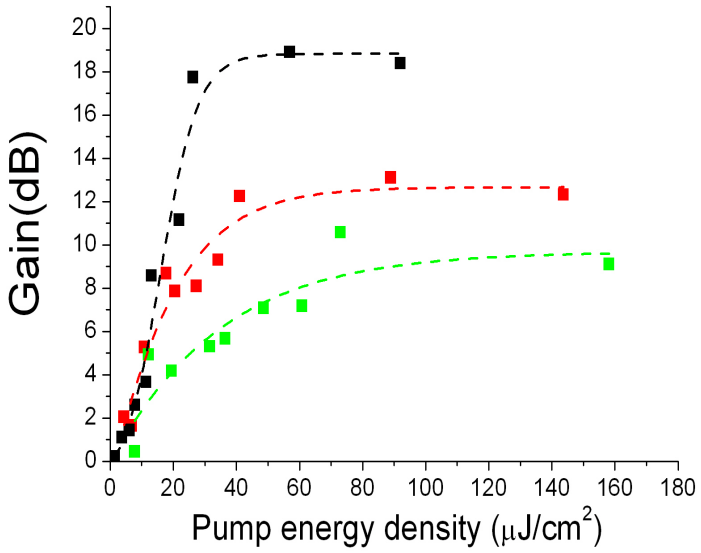

Figure 5.6: Gain dependence on waveguide length, 1022 μm *black symbols*, 822 μm *red symbols* and 622 μm *green symbols*. The *dashed lines* are a guide to the eye.

5.1.6 Gain lifetime

The gain dynamics of the material was compared with results using MEH-PPV on the 1022 μm long waveguide at a high pump density of 20 μJ/cm^2. MEH-PPV showed strong ASE with a fast gain lifetime of 5 ps, and F8BT had a slow lifetime decay of 209 ps. The signal energy used with MEH-PPV was $\sim$ 2 nJ (just after the input coupler) and with F8BT was $\sim$ 1 nJ (just after the input coupler). Figure 5.7 shows the time dynamics of both MEH-PPV and F8BT.

A higher signal energy was used with MEH-PPV (2 nJ) than with F8BT (1 nJ) due to coupling difficulty at the time of the experiment. The lower signal energy used on F8BT should result in F8BT experiencing a higher gain than MEH-PPV if the two materials had the same optical and chemical properties. However, even with a higher signal energy, MEH-PPV shows stronger gain. It also shows sharp line narrowing, indicating ASE at lower pump energies compared with F8BT. Figure 5.7 shows this effect. For the pump density comparisons between the two materials, the percentage of the excitation beam absorbed has been taken into consideration.

Even though MEH-PPV showed stronger gain, the long gain lifetime of F8BT was

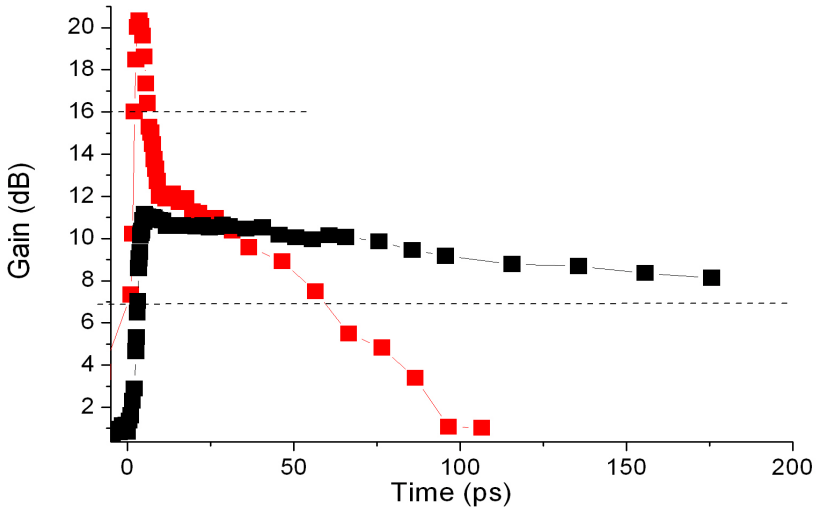

Figure 5.7: Time dynamics of MEH-PPV (*red line*) and F8BT (*black line*) in a 1022 μm long waveguide. Both traces are for the same pump energy density of 20 μJ/cm^2. The signal energy was higher in the case of MEH-PPV (2 nJ), than for F8BT (1 nJ). The dashed line is the $\frac{1}{e}$ position on the dB scale.

more suitable for amplification of multiple pulses. Further work into the gain lifetime of other conjugated polymers was not carried out in order to test F8BT with multiple pulses.

5.2 F8BT multiple pulses amplifier

F8BT was chosen as the material to investigate optical amplification of a pulse sequences. The gain measurements were taken using the streak camera [57]. In order to produce multiple pulses, the setup was modified from the single signal pulse experiment.

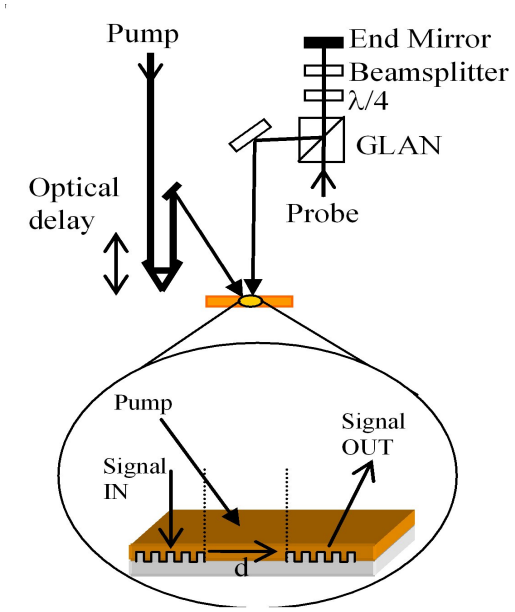

Figure 5.8: Schematic of setup.

5.2.1 Experimental setup

Figure 5.8 shows the setup for this experiment. The pump and signal beams were at 497 and 580 nm at 5 kHz. The pump beam passes through a delay line, which is set at time zero, the point of temporal intersection of signal and pump beams. The signal was coupled into the F8BT amplifier and the output was measured with the streak camera instead of the lock-in amplifier to obtain temporal resolution of the pulses. Due to the resolution of the streak camera, the signal and pump beams had to be stretched from 100 fs to 10 ps using a TF-10 glass block. The multiple pulses were generated using a partially reflecting mirror. A quarter waveplate was used to rotate the polarisation of light reflected from the mirror. This was directed towards the F8BT amplifier using a GLAN polariser, this is shown in detail in Figure 5.9.

5.2.2 Experiment: Amplification of multiple signal pulses.

Experiments were conducted to obtain the gain for different waveguide lengths. The signal energy was kept constant at 0.04 nJ just after the input coupler. Figure 5.10 shows amplification of three probe pulses in a 622 μm long waveguide. As the figure

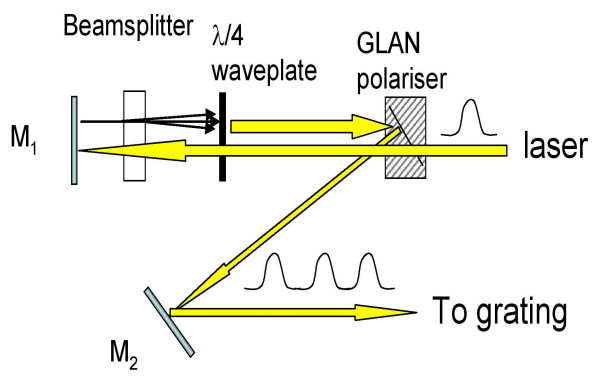

Figure 5.9: Schematic of setup showing the generation of the pulse sequence.

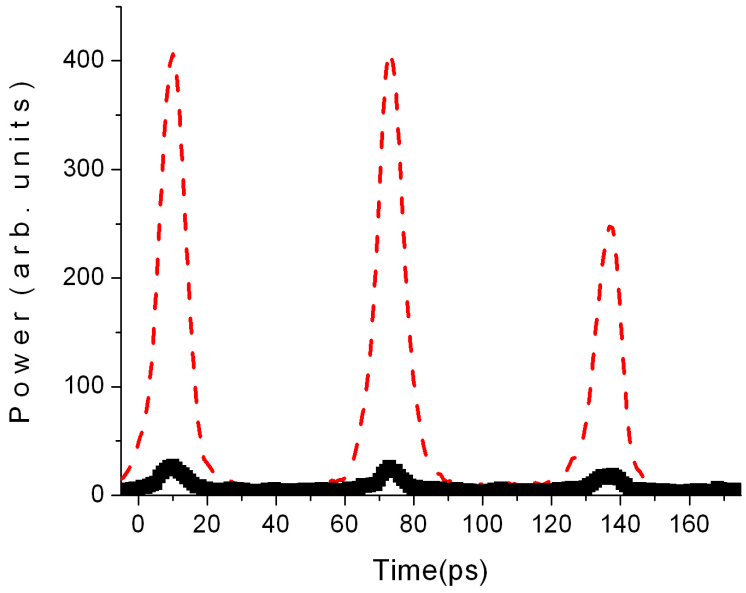

Figure 5.10: Amplification of three probe pulses in a 622 μm waveguide. The *black symbols* are the three unamplified probe pulses. The *red line* shows the amplified pulses.

shows, the peak of the probe pulse arrives at 10 ps from the zero point. This peak was aligned to the rising edge of the pump beam to obtain maximum amplification. Hence the subsequent timings of the three peaks have been labeled from the peak positions, i.e. t = 10 ps, t = 70 ps and t = 140 ps. The figure also shows how the gain lifetime affects the quality of amplification. The first two pulses are equally amplified, but the third pulse, being 130 ps away from the peak of the pump pulse, experiences a smaller amplification factor.

5.2.3 Gain dependence on pump energy density

Gain measurements were taken for several waveguide lengths. The gain was calculated for each pulse using the equation [43, 67]:

$$G(dB) = 10\log\frac{P_{\text{out}}}{P_{\text{in}}} \tag{5.1}$$

Where P_{out} and P_{in} are the amplified and non amplified probe signal powers after background subtraction.

The gains for each peak followed each other well. The maximum gain from the average of the three peaks were 18, 17, 11 dB for waveguides of length 1022, 822 and 622 μm respectively. The shorter waveguide of length 322 μm gave a 8 dB gain. The gains for each peak increased with increase in the pump energy until saturation took place. The longest waveguide gave the highest gain. The gain cross-section was calculated from Equation 4.4 to be σ = (5.8 $\pm$ 3.6) x 10^{-17} cm^2. The value determined is comparable to previously reported values, which were in the range of 10^{-16} to 10^{-17} cm^2 [19, 61, 72] and within the value calculated in the single pulse method.

5.2.4 Probe energy dependence

The gain dependence on the probe energy was measured for a waveguide of length 1022 μm. Figure 5.15 shows the variation for each pulse. The *symbols* are the experimental data. At a probe energy of 0.04 nJ, the gains for the three peaks were

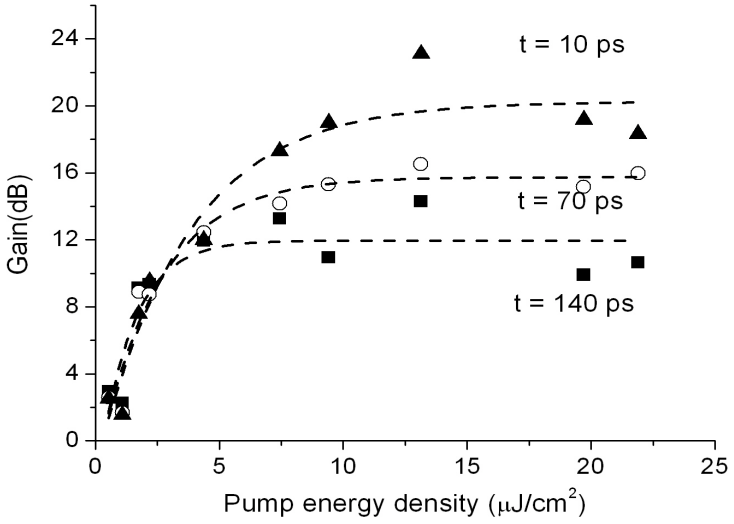

Figure 5.11: Gain measurements for waveguide length of 1022 μm. Each plot shows the gain dependence on pump energy for each pulse at t = 10 (*triangular symbols*), t = 70 ps (*circular symbols*) and t = 140 ps (*square symbols*). The *dashed lines* are a guide to the eye.

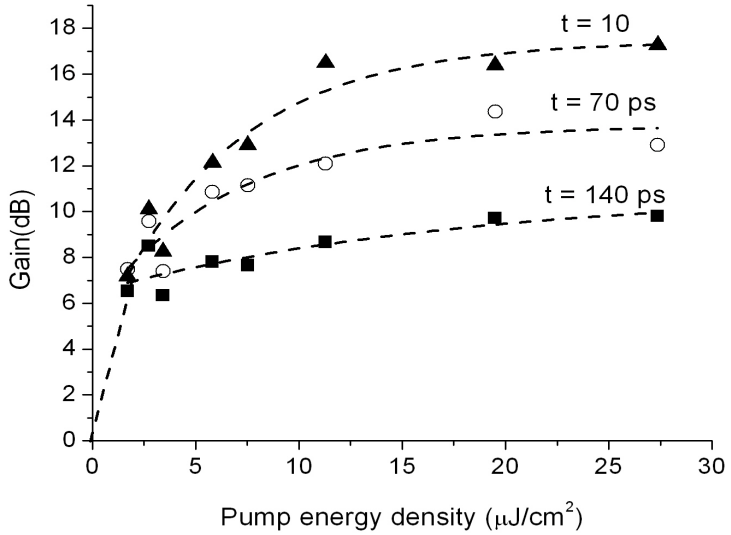

Figure 5.12: Gain measurements for waveguide length of 822 μm. Each plot shows the gain dependence on pump energy for each pulse at t = 10 (*triangular symbols*), t = 70 ps (*circular symbols*) and t = 140 ps (*square symbols*). The *dashed lines* are a guide to the eye.

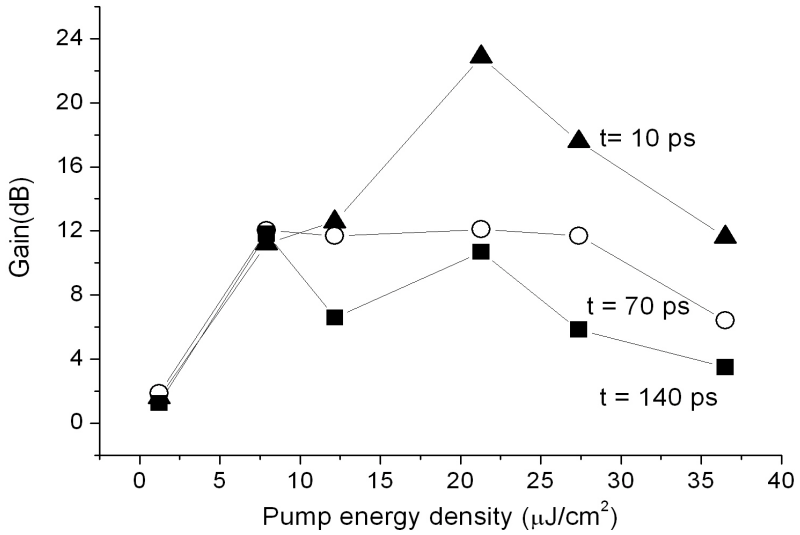

Figure 5.13: Gain measurements for waveguide length of 622 μm. Each plot shows the gain dependence on pump energy for each pulse at t = 10 (*triangular symbols*), t = 70 ps (*circular symbols*) and t = 140 ps (*square symbols*).

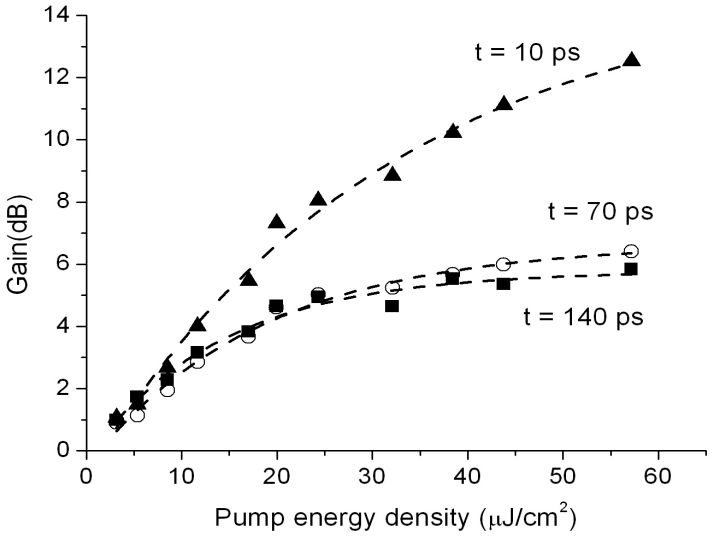

Figure 5.14: Gain measurements for waveguide length of 322 μm. Each plot shows the gain dependence on pump energy for each pulse at t = 10 (*triangular symbols*), t = 70 ps (*circular symbols*) and t = 140 ps (*square symbols*). The *dashed lines* are a guide to the eye.

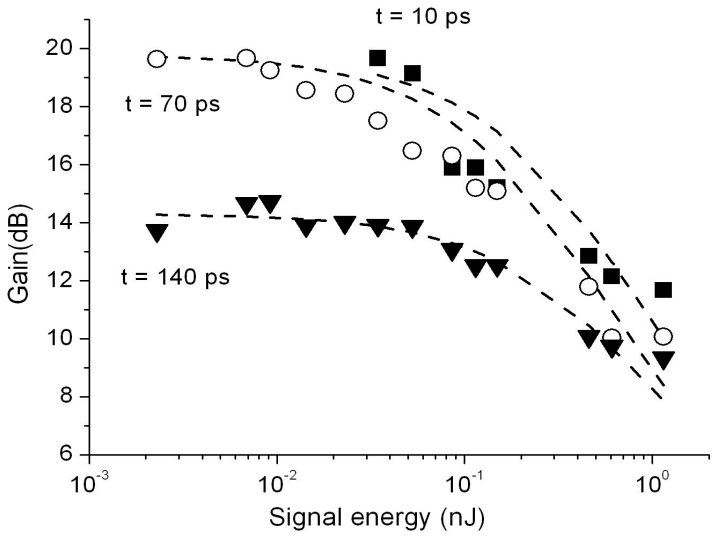

Figure 5.15: Gain dependence on signal energy for signal pulses delayed by 10, 70 and 140 ps with respect to the pump pulse in a 1022 μm long waveguide (*symbols*) and the theoretical fit (*dash lines*). The pump energy density was kept constant at 10 μJ/cm^2.

19, 16 and 14 dB. This corresponds to the values obtained for the same pump energy density (10 μJ/cm^2) in Figure 5.11 which were 19, 16 and 12 dB. The theoretical curve (dashed lines) was fitted to the experimental results using Equations 4.8 and 4.9 [72, 74, 82]. Fitting Equation 4.8 to the data, gives $G_o = 20$ dB for the first two pulses and $G_o = 14$ dB for the third pulse. This is the gain obtained for a very weak input signal. The saturation energy density was calculated to be 680, 859 and 853 $\mu J/cm^2$ for peaks 1, 2 and 3, all of which are higher than the probe energy density of 0.5 μJ/cm^2. Assuming that absorption at this wavelength is negligible ($\sigma_{\text{abs}} = 0$), the stimulated emission cross section was calculated to be (4 $\pm$ 1) x 10^{-16} cm^2 for all three curves and is in agreement with previously reported values, which were in the range of 10^{-16} to 10^{-17} cm^2 [19, 61, 72] and is comparable to the values calculated using Equation 4.4.

5.2.5 Time dynamics

Figure 5.16 compares the time dynamics of the three pulse method with the single pulse method for a pump energy density of 12 μJ/cm^2. The figure shows that the

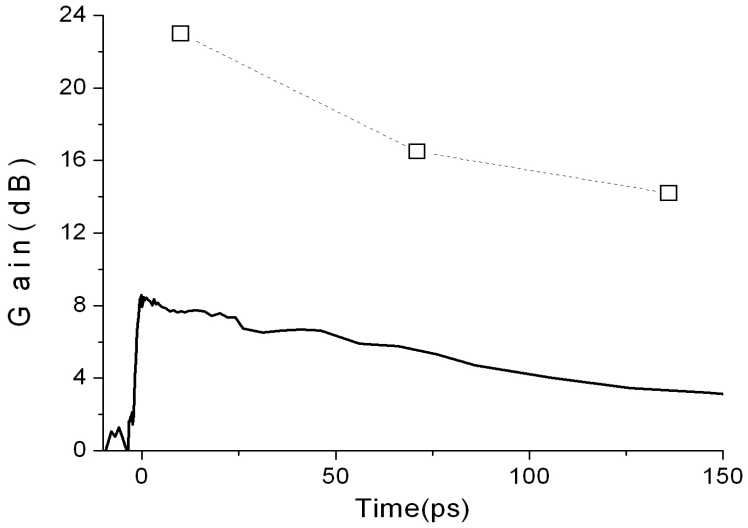

Figure 5.16: Gain obtained for signal pulses at different time delays for a waveguide length of 1022 μm. The *symbols* show time dependence for three signal pulses and the *solid line* is for a single pulse experiment. Probe energy is 0.04 nJ and 1 nJ for the three pulse and single pulse experiment respectively.

three pulse method follows the same decrease in gain with increase of time delay between the pump and probe pulses, as in the single pulse method. The maximum gain obtained in the single pulse method is low due to the higher probe value.

5.3 Conclusion

In conclusion, an experiment was built to test the amplification of multiple pulses using an organic amplifier. This led to a search for a high gain conjugated polymer with a longer gain lifetime than previously used.

The material, F8BT, was shown to amplify three pulses consecutively with a maximum gain of 23 dB (gain of peak 1) in a waveguide length of 1 mm for a probe energy of 0.04 nJ. After averaging over all three peaks this gain was 18 dB. At a lower probe energy of 1 nJ, a maximum gain of 17 dB was obtained with a single pulse. The gain indicated by Figure 5.15 at a probe and pump energy density of 1 nJ and 10 μJ/cm^2 respectively, is $\sim$ 8.5 dB. This is $\sim$ 3.5 dB higher than that obtained in Figure 5.6

because it is possible in the probe variation measurements that the probe energy in the waveguide is slightly less than the calculated value.

It would be possible to amplify larger pulse sequences if the gain lifetime at high pump energy densities was longer. Alternatively it would be possible to have more signal pulses within the gain lifetime of the pump by stretching the pump pulse relative to the signal pulses. Another alternative would be to have a higher repetition rate on the pump beam relative to the signal beams. Both of these ideas would allow more signal pulses to overlap with the pump pulse and hence amplify equally.

Chapter 6

All-optical switching of an amplifier

All-optical switches are essential for future high speed optical telecommunications networks, integrated circuits and signal processing. An all-optical switch which is cheap to manufacture and capable of amplification as well as switching either single or multiple pulses would have many applications. It would be easy to process and could be fabricated on any surface. In addition, it would be compatible with other polymer based devices and would eliminate the need for a separate switching device, thus allowing for better utilisation of circuit board space. This chapter discusses the steps taken towards such a device.

Considerable work has been conducted in organic material using both resonant and non-resonant switching techniques. The former modulates the gain or transmission of the probe by a switch pulse resonant to the excited or upper excited state [97–100]. Much research has been conducted on using resonant switching on organic materials to produce optical storage devices [101–103]. Such devices have long recovery times and would not be suitable for ultrafast telecommunications networks. Non-resonant switching exploits the third order nonlinearity, $\chi^{(3)}$, of the material [104, 105]. With this method, however, in both organic and inorganic materials there is an issue of ab-

sorption. If the absorption of the material is high, then there would not be sufficient intensity to produce a nonlinear phase shift. This has been analyzed by *Stegeman et al.*, to produce a figure of merit (FOM) [106]:

$$FOM = \frac{n_2 I}{\lambda_{vac} \sum \alpha_n I^{n-1}} \tag{6.1}$$

$$L = \frac{1}{\alpha} \tag{6.2}$$

where n_2 is the intensity dependent refractive index, L is the effective length and $\sum \alpha_n I^{n-1}$ is the total absorption. The figure of merit has to be greater than one in order for the material to be able to provide the required nonlinear phase shift [106]. However, satisfying the figure of merit in organic material has been challenging [106–109]. The issue is that most material have a high absorption coefficient and low nonlinear refractive index. Hence the light is absorbed by the material and there is insufficient intensity to produce the required nonlinear phase shift.

A great deal of investigation has already been conducted on inorganic semiconducting optical amplifiers (SOA) for optical switching. Switching occurs through the interaction of finite carriers with a highly intense switch pulse which depletes the gain. The ultrafast depletion raises the average energy of the remaining carriers leading to carrier heating [110, 111] which aids in the gain depletion. The switching effect can be measured by either the change in the absorption/gain or the refractive index of the device [111]. For the refractive index case; the change in gain changes the refractive index of the material according to Kramer's-Kronig relations [111, 112]:

$$n(\omega) = 1 + c/\pi P \int \frac{g(\Omega)}{\Omega - \omega} \tag{6.3}$$

Where $n(\omega)$ is the linear refractive index, $g(\Omega)$ is the absorption and gain and P is the Cauchy principal value of the integral [111]. The change in the refractive index will subsequently change the phase and the power of the propagating waves and modify their interference [111, 113]. The switching effect in SOAs have been demonstrated through gain [114–117], polarisation [115, 118] and phase modulation [110, 114, 116, 119].

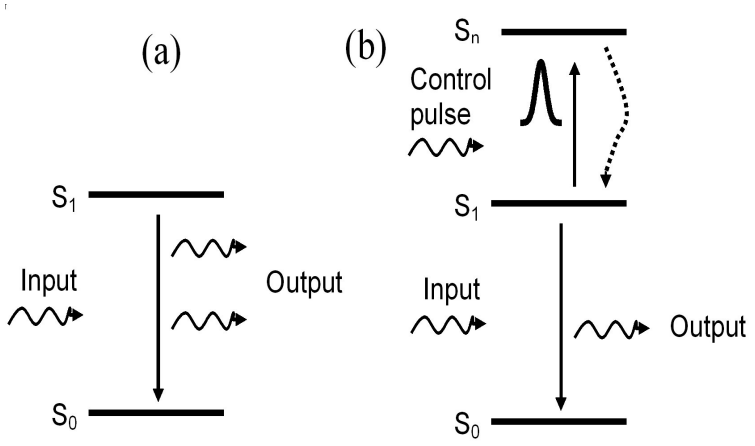

Figure 6.1: Principle of switching. The energy level diagram shows how the input and switch pulses affect the probe pulse. (a) Amplification of probe light. (b) The switch pulse pushes excitons to a higher excited state and the resulting probe signal is not amplified. [128].

To briefly mention other inorganic switches (which are not amplifiers) are photonic crystals [120–123] and thermo-optic switches [124–126]. These also exploit the optical nonlinearity of the material and have demonstrated switching through transmission and reflection modulation. The photonic crystals in particular have demonstrated ultrafast recovery rates of $\geq$ 30 fs [121, 122] and low pump energies of 520 fJ [123]. In order to obtain high efficiencies, low crosstalk or low switching power (low switch pulse power), some of the device structures are made of polymers [127] or organic/inorganic hybrids [123–125]. The polymers are optically inert but provide an advantage over inorganic materials because they are easy to structure and tailor, have suitable thermooptic coefficients (for thermo-optic switches [124]) and have a large third order nonlinearity [127].

Switching in this chapter was conducted by using a switch pulse resonant to a higher excited state, S_n. The amplification of the pulse is switched off because the switch pulse excites the excitons to an upper excited state, thereby removing the gain, illustrated in Figure 6.1. The number of excitons available to relax from S_1 to the ground state, S_0, are reduced and the probe beam is not amplified. Figure 6.2 shows how a pulse can be switched off from a stream of pulses. When the switch is applied or the beam unblocked, it will terminate the amplification of the probe pulse allowing the probe pulse to pass through unaffected. In this thesis, the switch pulse would be called either 'switch' or 'control' pulse.

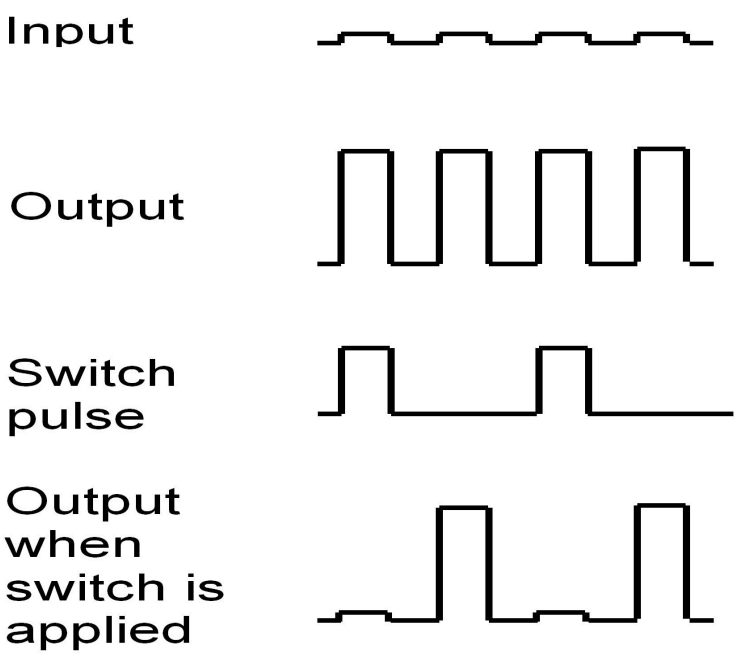

Figure 6.2: Switching of a data stream shown in a pulse sequence. The output pulse sequence of the amplifier is modulated by a highly intense switch pulse.

6.1 F8BT amplifier switch

Switching was initially attempted on F8BT as it was constructive to move the project forward from the end of the previous project described in the chapter 'Data Amplifier'. Switching of amplified light with F8BT was unsuccessful. The following section describes attempts to switch off the amplification of light in F8BT and work involved in characterisation of the temporal position of the switch pulse and the effect of the switch pulse on the remaining pulses.

Some changes were made to the existing set up used for the data amplifier to incorporate the switch pulse. The switch beam has a pulse duration of 10 ps and the wavelength was chosen to be 800 nm because work had been demonstrated showing that there was excited state absorption at this wavelength [129, 130]. The rest of the set up remained the same as that in the data amplifier chapter. Figure 6.3 shows the setup with the addition of the switch delay. The pump and probe wavelengths were at 497 and 580 nm respectively and the output was recorded with the streak camera. The switching energy was determined by varying the switch power and recording the effect on the amplified pulse sequence. This is shown in Figure 6.4 and resulted in 1

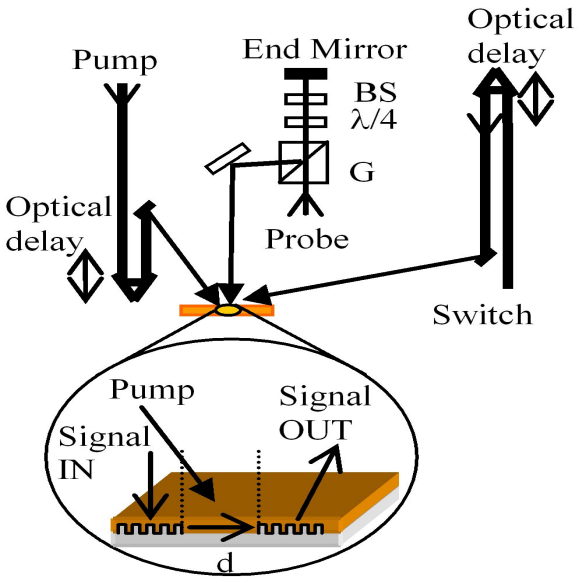

Figure 6.3: Schematic of setup.

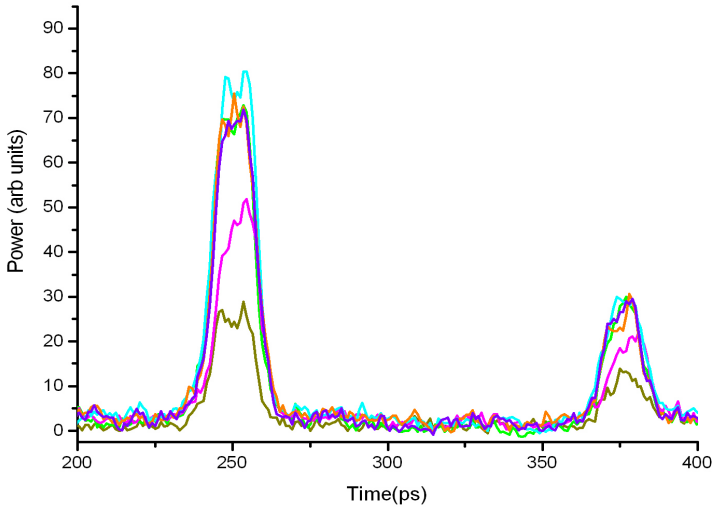

Figure 6.4: Results from using different switch powers. The unamplified probe is the *dark yellow line* and amplified probe with the switch pulse blocked is the *green line*. The remaining traces are the amplified probe with the switch pulse unblocked. The switch energies were 0.36 (*orange line*), 0.46 (*blue line*), 0.84 (*purple line*) and 1 μJ (*pink line*).

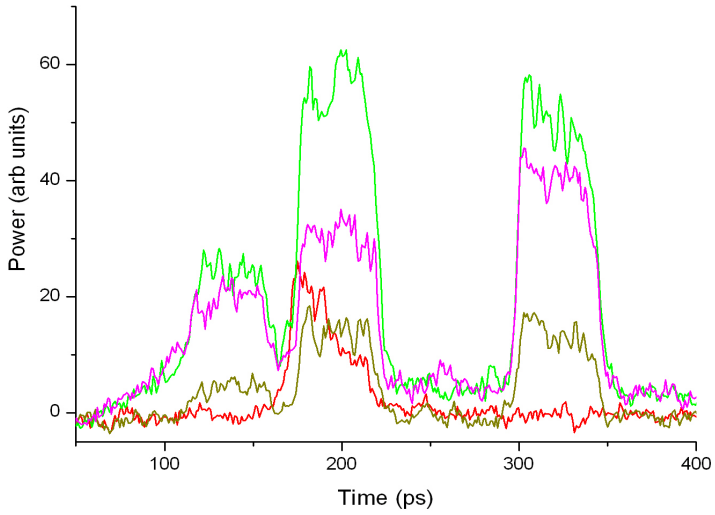

Figure 6.5: Traces showing unamplified probe (*dark yellow line*), amplified probe with switch pulse blocked (*green line*), amplified probe with switch pulse unblocked (*pink line*) and switch pulse aligned to the centre pulse (*red line*).

μJ being used for the switch and resulted in short waveguide lengths of 100 - 400 μm being used for the experiment.
Attempts at switching F8BT resulted in either:

(i) 50% of the amplified pulse turned off.

(ii) All the pulses had been slightly affected.

(iii) No switching effect.

Case (ii) was because if the switch pulse was too strong or applied for too long, it would affect the material which resulted in the amplified output of all three pulses being affected. Figure 6.5 represents case (i) and (ii). The pulses are broad because the slit to the streak camera was opened wider than previously used, to collect more light. The first peak is not well amplified because it is not precisely on the time zero of the pump pulse indicating how precision is required. However, the switching was demonstrated on a strongly amplified pulse, which was the middle pulse. The switch pulse was temporally aligned to the this pulse. The pump, probe and switch pulse energies were 0.083 μJ, 0.026 nJ and 1 μJ respectively. Moreover, the recovery of the

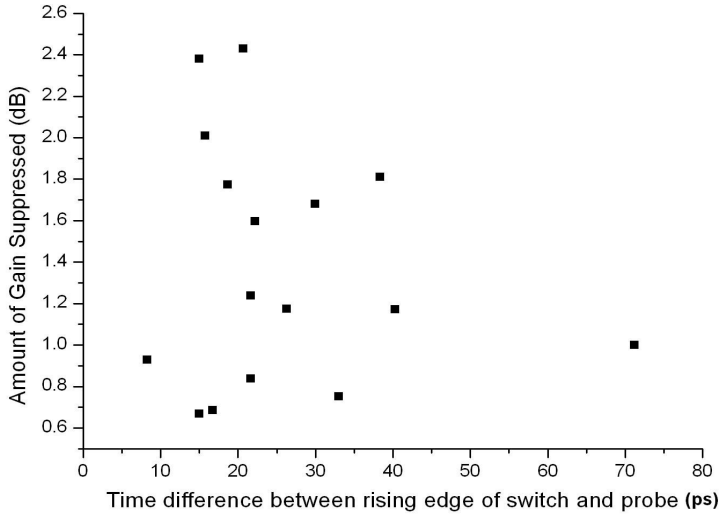

Figure 6.6: Plot showing the amount of gain reduced in dB against the position of the switch pulse relative to the amplified probe pulse to be switched.

amplified pulse was not immediate. The pulse would recover fully ~ 3 seconds after the switch pulse was blocked. An unrecovered pulse would be attributed to damage in the polymer, but there was no visible damage.

The switch pulse was recorded on the streak camera from scatter from the polymer film. Hence it is not a guarantee that the temporal position of the switch pulse is the same as that recorded. In order to determine the correct temporal delay for the switch pulse, measurements were taken of the effect of the switch pulse on the amplified probe, for different timings of the switch pulse. The results are shown in Figure 6.6 and show a plot of the amount of gain suppressed against the temporal spacing between the probe pulse to be switched and the switch pulse. The distance between the switch and amplified probe pulse to be switched was calculated from the rising edge of both pulses. The result is fairly scattered. The suppressed gain seems to fluctuate at all temporal positions. However it does show highest values at 15 - 20 ps which is equivalent to a 1.5 mm spacing, and the switch pulse was kept at this point.

The setup was built to allow freedom of movement of the third pulse relative to the remaining. The position of the first and second pulses could not be altered because they were produced by the front face and inner face of the partial reflector

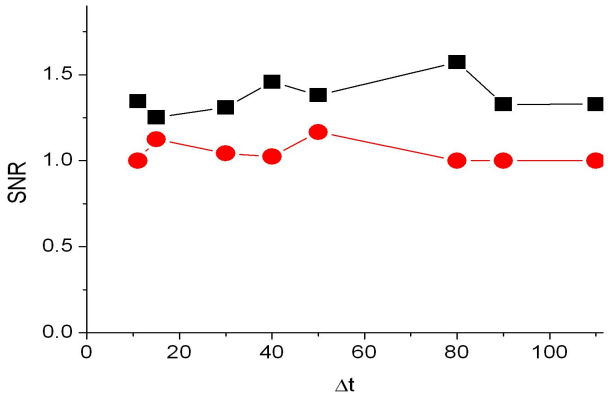

Figure 6.7: Variation of the ratio of amplified pulse with switch blocked to unblocked for B2 (*square symbols*) and B3 (*circular symbols*) against position of B3 from B2.

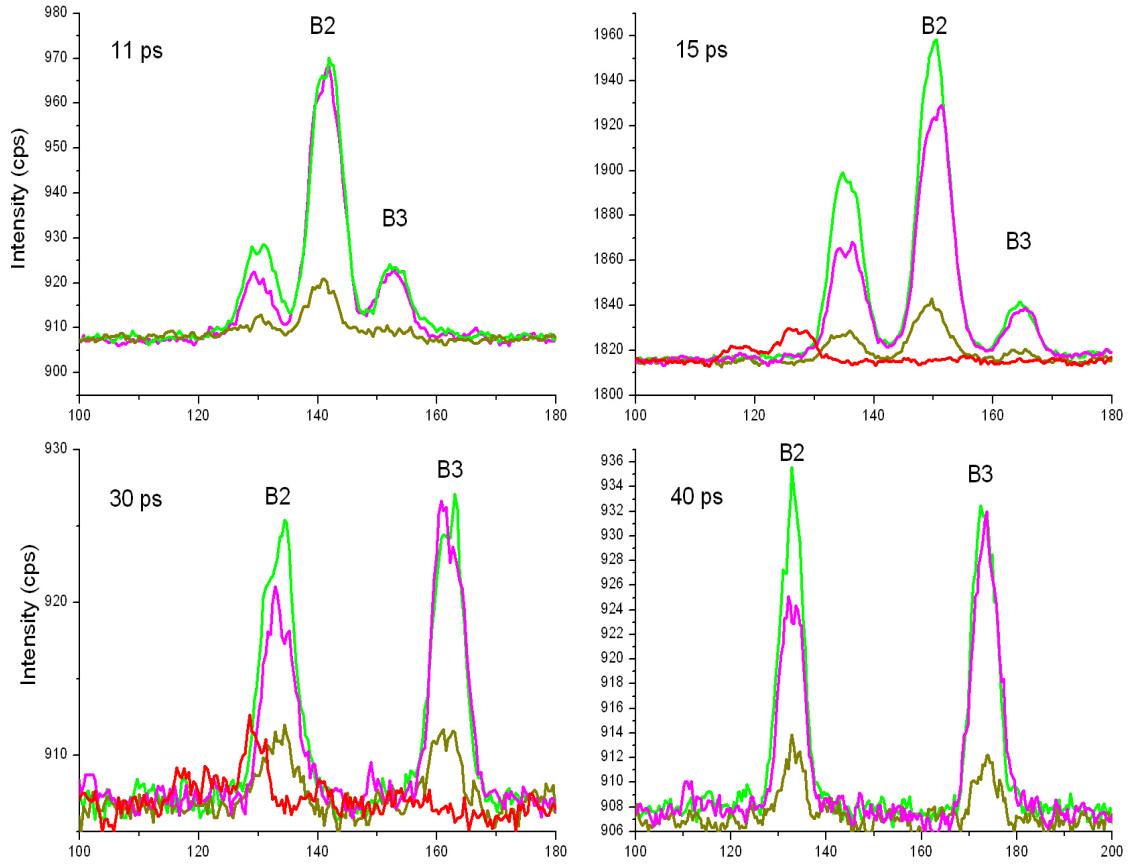

Figure 6.8: Data showing pulse to be switched and third pulse at temporal delays of 11, 15, 30 and 40 ps. Unamplified probe (*dark yellow line*), amplified probe with switch pulse blocked (*green line*), amplified probe with switch pulse unblocked (*pink line*) and switch pulse aligned to the centre pulse (*red line*).

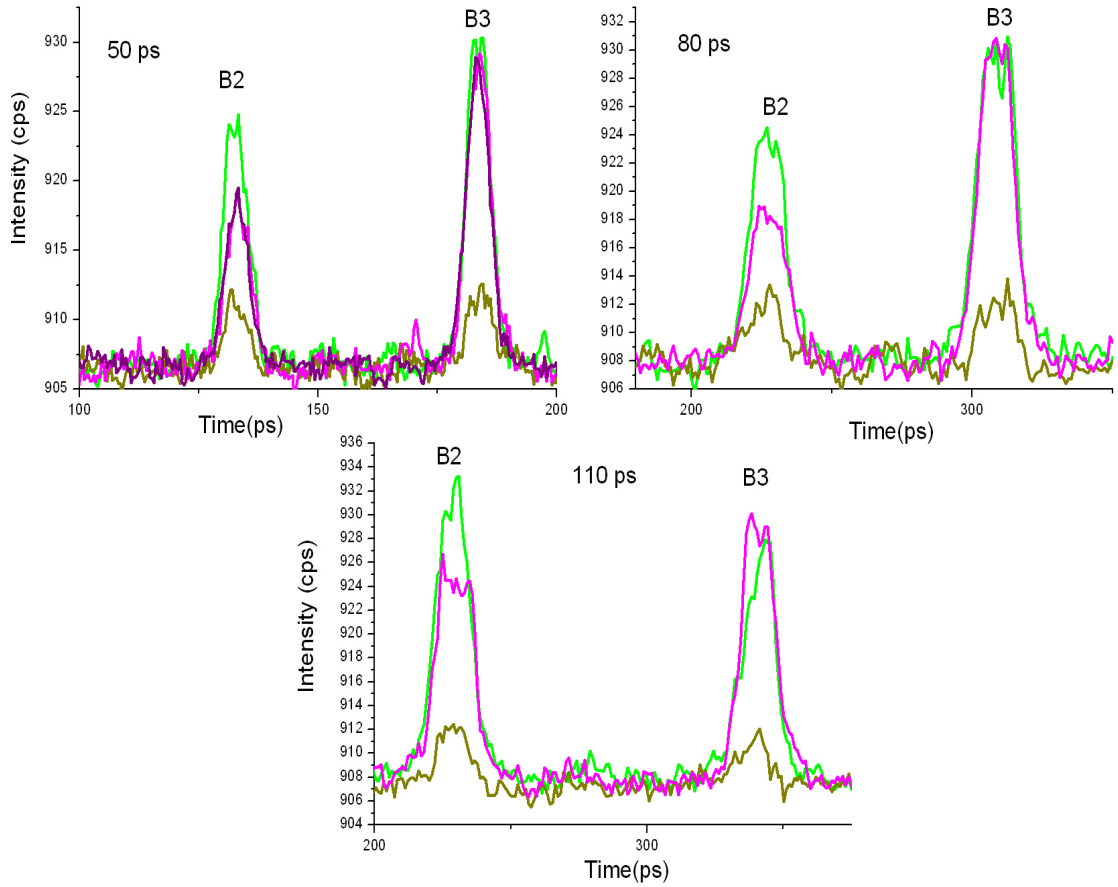

Figure 6.9: Data showing B2 and B3 at temporal delays of 50, 80 and 110 ps. Unamplified probe (*dark yellow line*), amplified probe with switch pulse blocked (*green line*), amplified probe with switch pulse unblocked (*pink line*) and switch pulse aligned to the centre pulse (*red line*).

(labeled as 'BS' in Figure 6.3). Whereas the third pulse was produced by a mirror (labeled as 'end mirror' in Figure 6.3). For the remaining paragraph I will call the first and second pulses produced by the partial reflector and the pulse produced by the end mirror as B1, B2 and B3 respectively. A number of measurements were taken at different positions of the end mirror. The aim of the test was to observe any effect of the switch on B3 as it was moved closer to B2. The switch pulse was applied to B2. The reason only B2 and B3 were considered was because the switch pulse should not affect B1 as it was arriving after. Several measurements were taken of the ratio of the switching effect for each temporal position of B3. The ratio of the amplified pulse with the switch blocked to unblocked was calculated for each measurement. These were averaged and plotted in Figure 6.7. It shows that the ratio of the amplification with the switch pulse blocked to unblocked is nearly 1 for all temporal positions of B3 indicating that it is unaffected. Both peaks were unaffected by each other. Figures 6.8 and 6.9 show measurements taken at each temporal position of B3.

The material did not switch at each attempt and any switching obtained was partial, indicating the switch pulse was not fully effective and was not being fully absorbed by the F8BT chromophores. Experiments into the photo-physical processes of F8BT would have to be conducted in order to understand why full switching was not possible with F8BT. An alternative was to use a blend of F8BT. The second material could act as a spacer. The blend would push the emission wavelength further form the absorption edge aid in reducing re-absorption effects. A copolymer was used as it would avoid possible phase separation and time was an issue. Such a copolymer was obtained from Cambridge Display Technologies (CDT), and consisted of fluorene and benzothiadiazole units. Scans from the absorption and emission spectra confirmed presence of F8BT and PFO. This material was named as GP1302 by CDT, and will be called this during the rest of the chapter.

6.2 GP1302 amplifier switch

GP1302 was a yellow material comprising of benzothiadiazole and fluorene units to the ratio of 1:10.

Figure 6.10 shows the absorption and emission spectra. At the time of measurement,

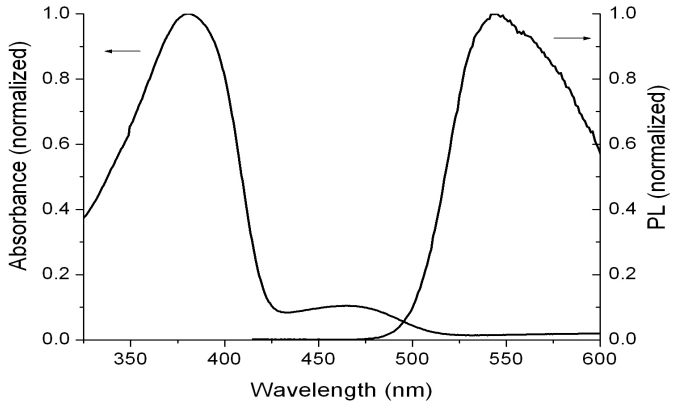

Figure 6.10: Absorption and emission spectra of GP1302.

from the emission spectra, the ASE peak was taken to be similar to that of F8BT; 580 nm. ASE measurements taken later with an excitation wavelength of 400 nm, indicate that the ASE peak would have been at 570 nm, which was reasonable as it was $\sim$ 30 nm away from the PL peak. This particular measurement is further mentioned in the discussion section in chapter 8 due to its relevance to that topic.

The aim was to excite the F8BT and use the PFO as a spacer to reduce potential quenching of the switch pulse in the material. This is discussed further in the conclusion section of this chapter. Experiments were first conducted with a drop cast film and then a spin coated film. As there was no literature on this material, a material concentration of 20 mg/ml was used after discussions with students testing other optical properties of the same material. Pump and probe wavelengths used were 497 (which had a 37 % absorption) and 580 nm. The PL peak and ASE wavelengths were 530 and 570 nm.

A drop cast film was initially used because a thick polymer would be required as the material would have had less of the active chromophore. Drop casting affected the surface morphology. In spite of this, attempts were made to couple light in and out. Some switching was observed in a 200 μm waveguide, shown in Figure 6.11. As the film was quite thick (thickness was not measured), it was possible that the pump energy was absorbed in the first few nano meters. The waveguided mode of the probe light was closer to the silica substrate. Figure 6.12 shows the position of the TE_0 relative to the substrate for a film thickness of 600 nm in F8BT. Hence

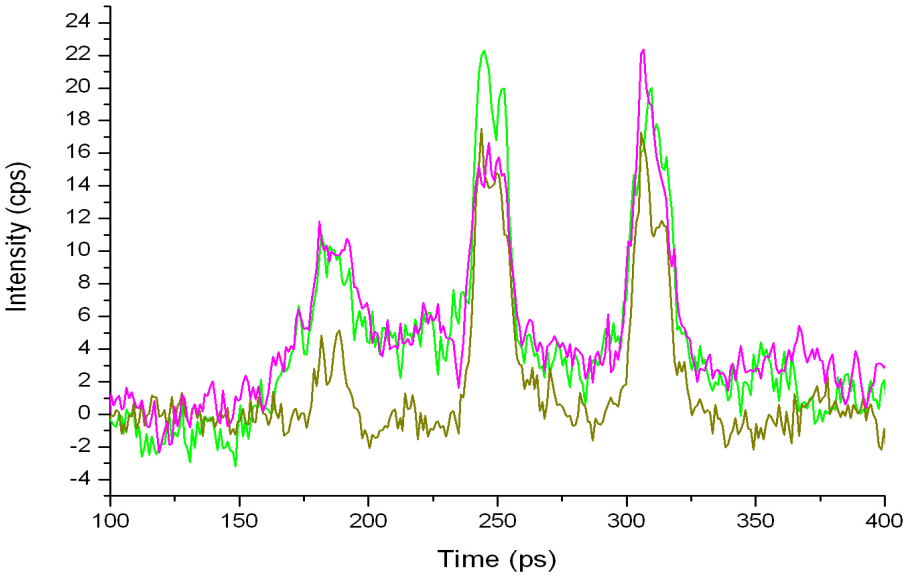

Figure 6.11: Switching in a drop cast film of GP1302. The *yellow line* is the unamplified probe, the *green line* is the amplified probe with the switch blocked and the *pink line* is the amplified probe with the switch unblocked. The amplified probes sit above the PL luminescence which has not been subtracted in this case.

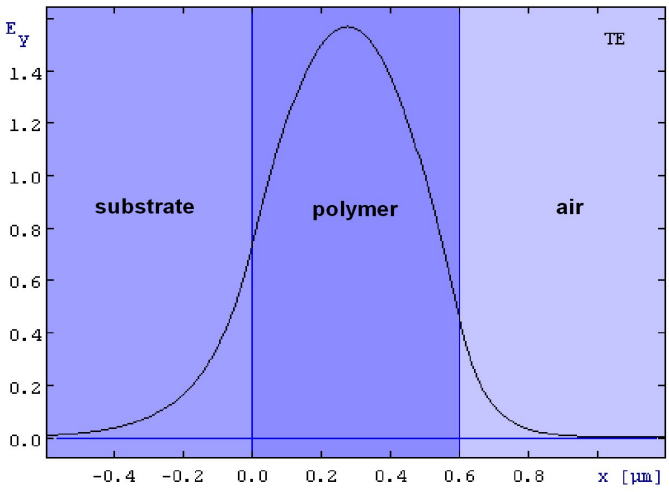

Figure 6.12: TE_0 mode in a 600 nm thick polymer film of F8BT to demonstrate the position of the waveguiding mode with respect to the polymer film and the substrate.

the waveguided mode may not overlap with the excited polymer region for a thick polymer where absorbtion occurs within the first few nanometers. For this reason the excitation and coupling was done through the substrate, which ensured that the probe was propagating through the excited region of the polymer.

The film was also spin coated, spun at 600 rpm from a 20 mg/ml solution to form a $\sim$ 600 nm thick layer [1], which was coupled into, from the substrate side. In this case, the amplified pulse was switched off by 70 % in short waveguide lengths of 300 and 400 μm. Energies of the signal and switch pulses, and the pump energy density were 0.13 nJ, 1 μJ and 176 μJ/cm^2 respectively. Longer waveguide lengths of 500 and 600 μm showed 50% $<$ x $<$ 70% switching. This is probably because with the increase in waveguide length, the energy of the switching pulse needed to be increased to keep the energy density the same. However, the maximum available switch power at the time gave insufficient energy density to fully switch the amplified peak in longer waveguide lengths. Figure 6.13 shows the switching effect in a waveguide length of 400 μm. Figure 6.14 shows switching in waveguide lengths of 300, 500 and 600 μm.

6.3 Recovery time

The recovery time of GP1302 was measured with a transient absorption set up, shown in Figure 6.15. The input was from the TOPAS-white light source. The probe, pump and switch wavelengths were 550, 400 and 800 nm respectively and the energies used were 40 nJ, 0.24 μJ and 5.6 μJ respectively. The pulse width was 100 fs. The output was measured with lock-in amplifiers via photodiodes. The polymer was spin coated at 800 rpm from a solution of 20 mg/ml on a quartz disk. The measurement was conducted by performing a normal pump probe scan of the material.

Figure 6.16(a) shows the gain dynamics of GP1302 as a function of time. The pump scan was halted 3 ps before the probe pulse. Note that the switch beam was blocked during the pump scan. The fast 5 ps decay was due to ASE formation. The switch pulse was delayed with the probe pulse, when time zero was obtained there was a drop in the signal because the switch pulse would push the excitons to the upper excited state, S_n thus reducing the amplification of the probe signal. Once time zero

[1] The thickness was measured with the dektak

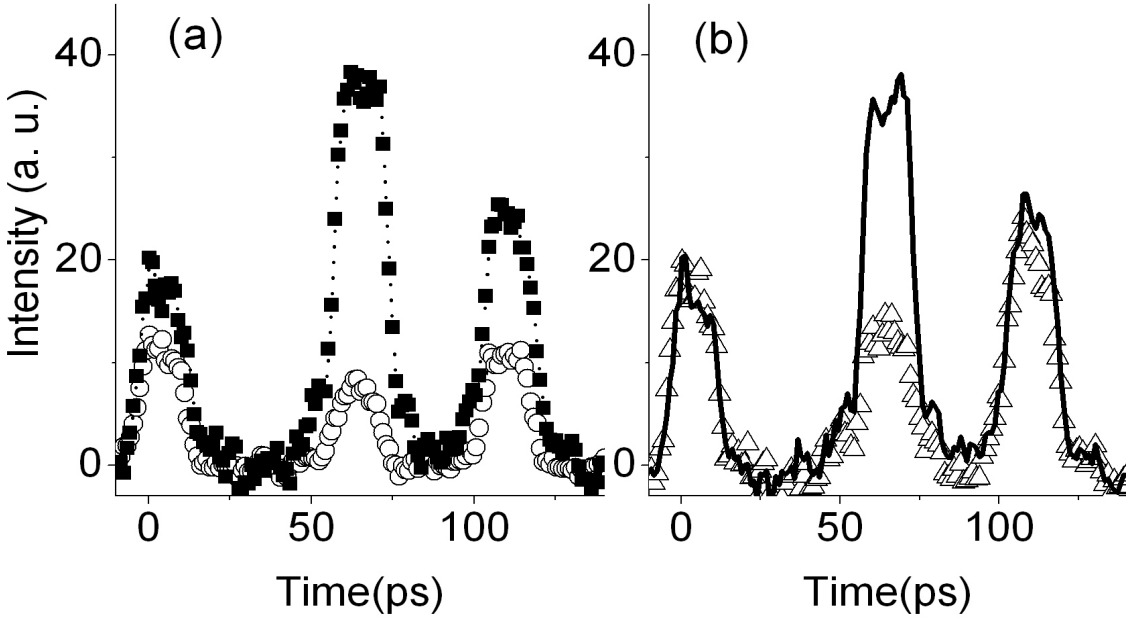

Figure 6.13: Spin coated film of GP1302.(a) Unamplified pulse sequence (*open symbols*) and amplified pulse sequence (*closed symbols*). (b) Amplified pulse sequence when switch pulse was applied (*open symbols*) and amplified pulse sequence after the switch pulse was applied (*solid line*) [128].

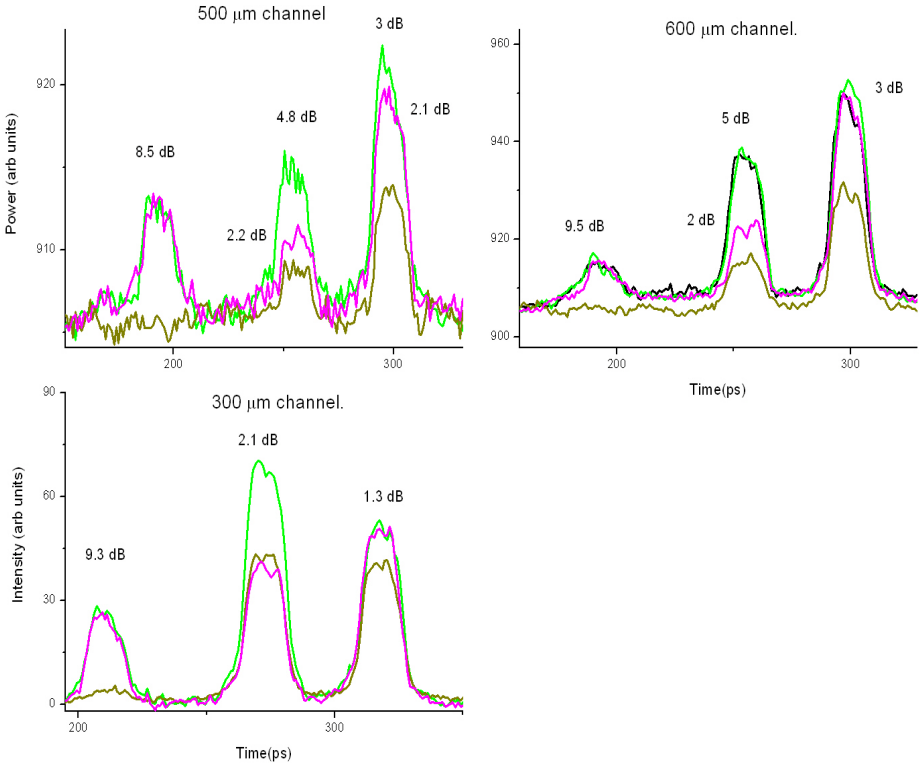

Figure 6.14: Switching in 300, 500 and 600 μm waveguide lengths. The *yellow line* is the unamplified probe, the *green line* is the amplified probe with the switch blocked, the *pink line* is the amplified probe with the switch unblocked and the *black line* is the amplified probe after the switch had been applied.

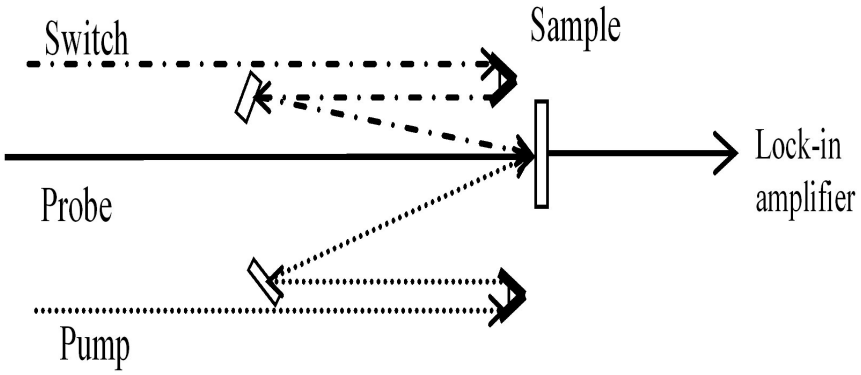

Figure 6.15: Schematic of the transient absorption setup for recovery time measurement.

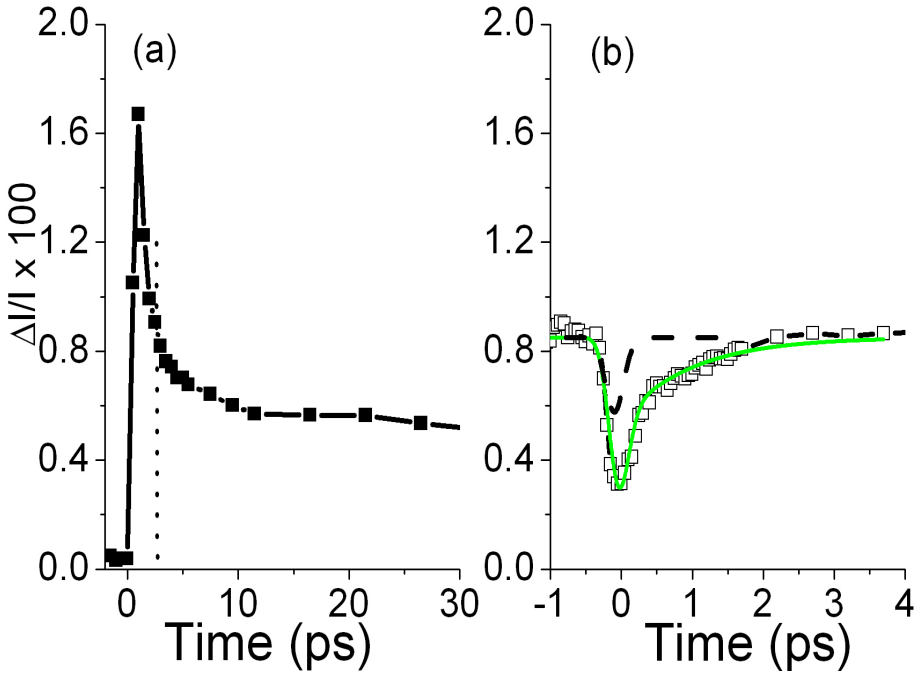

Figure 6.16: Polymer GP1302. (a) Gain dynamics against time of pump (at 400 nm) and probe (at 550 nm). (b) *Open symbols* is the recovery of switched pulse, *dotted line* is the instrument response and the *green line* is the biexponential fit.

was passed, the gain recovers because the excitons relax from the S_n state to the S_1 state. This occurs in 2 ps, as shown in Figure 6.16(b). The data was fitted to a biexponential decay function which showed that there was a fast and slow time component of 0.5 and 1 ps respectively. The fast component can be due to internal conversion from the S_n to the S_1 state where the energy is converted to vibrational energy which was dissipated amongst the vibrational modes. Excess energy stored in active vibrational modes can transfer energy to unexcited molecules, explaining the long 1 ps component. The recovery dynamics for different switching energies were measured. Figure 6.17 shows these traces, and they show that even though the recovery time changes by ± 1 ps, there is no dependence on the switching energy. The percentage switched fluctuates from 70 % to 50 %. This indicates that there is still quenching of the switch signal occurring making it not possible to get 100 % switching.

The switching and recovery of ADS233YE was also measured. This material was purchased through American Dye Source (ADS) as it showed an absorption and emission spectra similar to GP1302, and was commercially available. ADS233YE

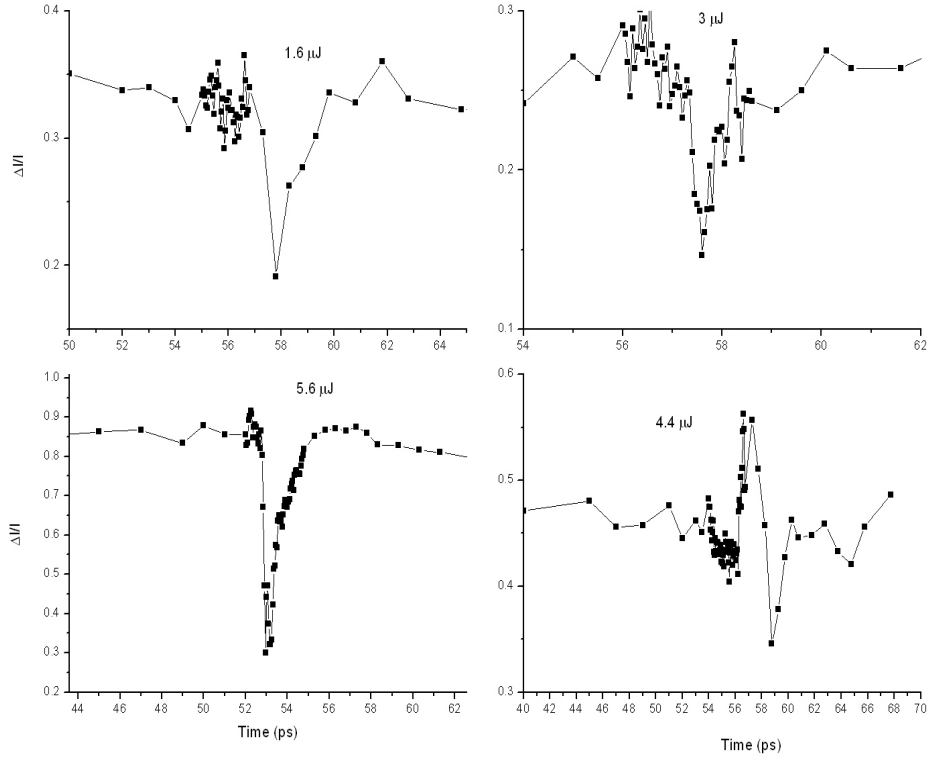

Figure 6.17: Recovery dynamics for different switch energies of 5.6, 4.4, 3 and 1.6 μJ, in GP1302.

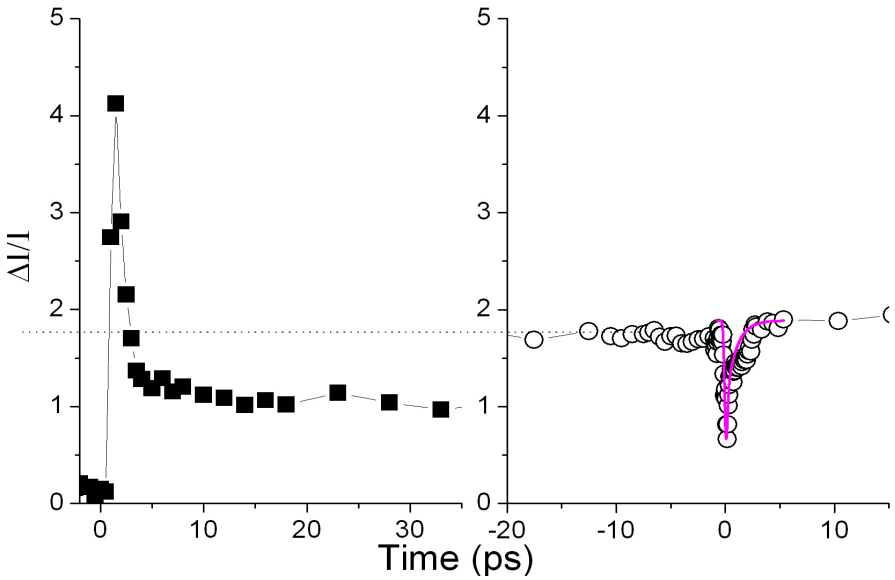

Figure 6.18: Polymer ADS233YE. Left: Gain dynamics against time of pump (at 400 nm) and probe (at 550 nm). Right: *Open symbols* is the recovery of switched pulse and the (*pink line*) is the biexponential fit.

was spin coated at 800 rpm from a solution of 50 mg/ml on a quartz disk. The probe, pump and switch wavelengths and energies remained the same as that in GP1302. Figure 6.16 shows the gain recovery dynamics. The material recovered fully in 2 ps. Switching of ADS233YE as an amplifier device was only attempted at 50 kHz which did not work as described in chapter 8.

However the recovery experiment showed switching of ADS233YE by 70 % with a 2 ps pulse recovery time, as shown in Figure 6.18. The data was fitted to a biexponential decay function with the same time constants of 0.5 and 1 ps. With the recovery time of GP1302 and ADS233YE established, F8BT was tested. F8BT was spin coated at 1000 rpm from a solution of 30 mg/mL on a quartz disk. The probe, pump and switch wavelengths were 550, 400 and 800 nm and the energies were 40 nJ, 0.24 μJ and 6.4 μJ respectively. The reduction in the gain of 47 % is shown in Figure 6.19 and the signal does not fully recover. The gain recovers for 20% and remains at this point for $>$ 20 ps. This long recovery and 50 % switch off is consistent with the switching behaviour seen in the F8BT amplifier device. Transient absorption of F8BT had been studied by *Stevens et al.* [129] who indicated that in F8BT, the signal does not fully recover due to charge transfer from the upper excited state forming long lived polarons, reducing the number of excitons that relax to the lowest excited

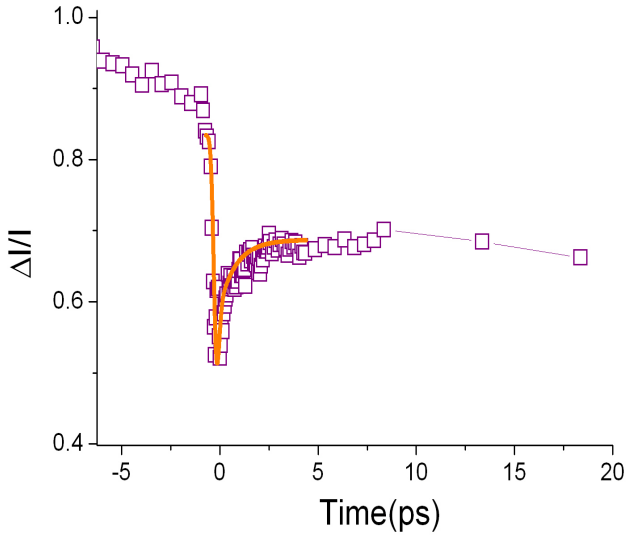

Figure 6.19: Recovery dynamics of F8BT (*symbols*) and biexponential fit (*orange line*).

state. The data was fitted to a biexponential decay function with the time constants of 0.7 and 1 ps for the 20 % recovery.

6.4 Switching of a polymer laser

Switching was also attempted on a conjugated polymer laser. The work was a collaborative project between Imperial College London and St Andrews University. The conjugated polymer used was Red-F and the distributed feedback laser (DFB) structures were brought by Dr. Ruidong Xia and Cora Cheung. The pump and switch pulses were obtained from the 5 kHz OPA, this was stretched by a TF-10 glass block so that the pulses were within the resolution of the streak camera. The second harmonic of the control pulse was recorded on the streak camera [131]. Because the two beams were interconnected in the OPA, changing the switching wavelength would change the pump wavelength as well. Two sets of pump and switch wavelengths were used 498 nm and 1.3 μm, 492 nm and 1.28 μm. The Red-F was spin coated to form a film thickness of 250 nm. Switching was obtained with a switching energy of 2 μJ at 1.28 μm. The pump energy was 40 nJ and the lasing threshold and wavelength were 25 nJ/pulse and 692 nm respectively. Figure 6.20 shows the effect on the laser pulse

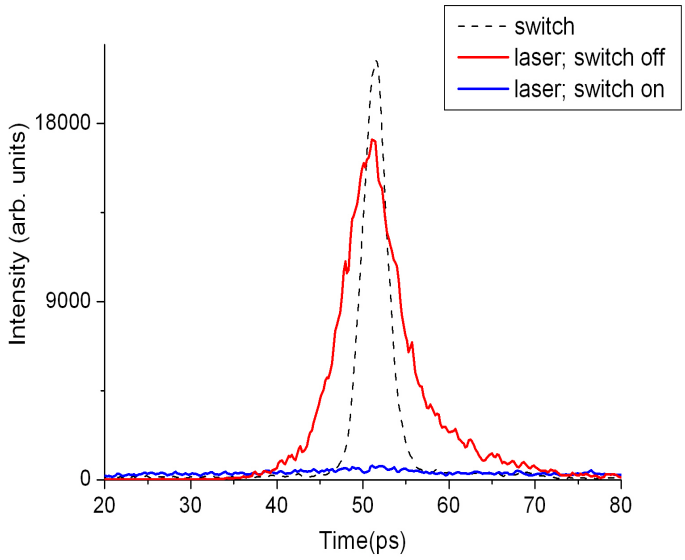

Figure 6.20: Switching of laser pulse at 692 nm. The pumping and switching wavelengths were 492 nm and 1.28 μm. The pumping and switching energies were 40 nJ and 2 μJ.

with the switch pulse on and off.

Measurements were also taken with a weak switching energy (50 nJ). This is shown in Figure 6.21 with a lasing wavelength of 692 nm and pump and switching wavelengths of 1.28 μm and 492 nm. The pump energy was 200 nJ. The resulting spectra shows strong PL background once the lasing has been terminated. Partial switching was also obtained by temporally delaying the switch pulse relative to the pump pulse. The switching and pump energies used were 200 and 80 nJ and the switching and pump wavelengths were 1.3 μm and 498 nm which had a lasing wavelength and threshold of 675 nm and 18 nJ/pulse respectively. This is shown in Figure 6.22. In this measurement the switch pulse was timed to arrive a few picoseconds after the pump pulse resulting in 35 % drop in the intensity of the lasing pulse, shown in Figure 6.22(b). The resulting output lasing pulse arrived 3 ps after the switch pulse as shown in Figure 6.22(a). The delay is because when the excitons pushed to the upper excited state S_n, relax back to the S_1 state, they repopulate it and the resulting lasing signal is delayed [131].

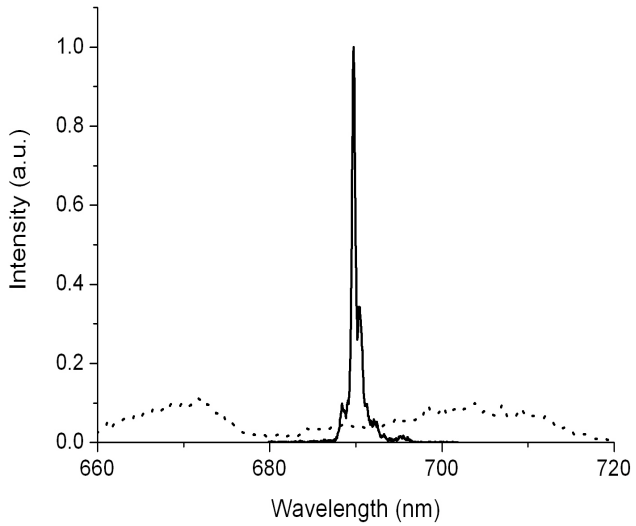

Figure 6.21: Switching of laser pulse at 692 nm. Spectral profile of emission from laser with (*dotted line*) and without (solid line) switching pulse. The pumping and switching wavelengths were 492 nm and 1.28 μm. The pumping and switching energies were 200 and 50 nJ.

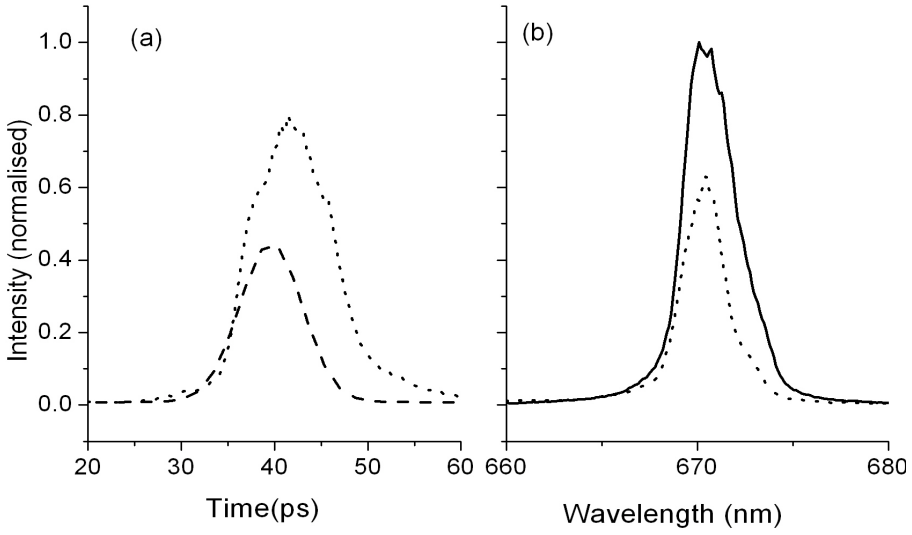

Figure 6.22: Switching of laser pulse at 675 nm. The pumping and switching wavelengths were 498 nm and 1.3 μm. The pumping and switching energies were 80 and 200 nJ. Temporal (a) and spectral (b) profiles are shown for the lasing pulse with (*dotted line*) the switching pulse applied (*dashed line*). The switching pulse arrives a few pico seconds after the peak of the unaffected laser pulse (*solid line*). The subsequent laser emission is delayed by $\sim$ 3 ps from the switch pulse.

6.5 Conclusion

The amplified signal in F8BT did not fully switch off and had a long recovery. This is because not all the excitons are excited to the upper state S_n and those which are, form inter-chain charge pairs. It is possible that when some switching occurred, it was not more than 50 % because there was insufficient energy of the switching pulse to push all the excitons into the higher excited state. The recovery experiment used a higher switching energy of 5.6 μJ than used in the amplifier device experiment and obtained a similar reduction of the amplified signal (in F8BT) by 47 %. This indicates that the energy in the amplifier device experiment was sufficient, but possibly there was quenching of the switching signal, i.e. the switch pulse was not being absorbed by the F8BT chromphores and was possibly being directly absorbed by defects or traps in the material. This quenching would reduce the effect of the switch on the amplified signal and hence only part of the amplified signal would be suppressed. To reduce quenching of the switching signal, the co-polymer, GP1302 was used. The co-polymer was a combination of PFO and F8BT. By exciting the F8BT, the PFO chromophore can act as a spacer to reduce any quenching of the switch signal occurring.

However, laser switching of F8BT was possible by *Perissinotto et al.* [130]. They obtained 90 % switching. This was because switching of a laser pulse requires a reduction of the gain to just below the lasing threshold to switch the laser off. In contrast, amplifiers do not have a threshold, and hence would require a larger reduction of the population to switch off the gain. Moreover, *Perissinotto et al.* also observed switching for 8 ps when the switch pulse was no longer temporally overlapped with the pump pulse. They attributed this to the formation of charge pairs.

Previous work conducted has demonstrated optical control of the probe signal [97, 98]. *Frolov et al.* demonstrated this by 'dumping' the gain [98]. A pump beam was used to generate excitons, to which a 'dump' beam, tuned within the stimulated emission spectral range, was applied. A probe pulse tuned into the photo absorption bands was used to measure the effect. *Lanzani et al.* demonstrated switching and analysis of the recovery time using transient absorption measurements conducted on isolated PFO chains suspended in a PMMA matrix. They obtained a partial recovery of 3 ps [97]. They also analysed the switching effects of clustered and isolated PFO chains [44]. In the film with densely packed PFO chains the switch did not recovery due to the formation of long lived inter-chain charge pairs. Whereas in the film with

isolated PFO chains, they obtained full recovery of the switched signal. They were able to fit the recovery dynamics to a $t^{-1/2}$ power law, which is a predicted dynamic for geminate recombination. They assigned the switching effect to the recombination of geminate charge pairs. The recovery dynamics in GP1302 and ADS233YE show no formation of inter-chain charge pairs indicated by the full recovery. Moreover, the data fits to a biexponential decay function and not to a $t^{-1/2}$ power law, indicating that the switching effect was not from intra-chain charge pairs either. This indicates that the switching effect was to the upper excited state with no polaron generation.

Laser switching has also been demonstrated, with a 100 % switching effect in a Red-F laser for a switch and pump energy combination of 2 μJ and 40 nJ at a switching wavelength of 1.3 μm and 50 and 200 nJ at a switching wavelength of 1.28 μm. Temporally delaying the switch pulse by a few picoseconds from the pump pulse still provided sufficient overlap to have a 35 % reduction in the intensity of the output lasing pulse and a 3 ps shift relative to the control pulse, suggesting that re-timing of the output lasing pulse is possible with the temporal position of the switch pulse.

For a switching energy of 1 μJ the amplifier showed a 70 % switch with $\sim$ 5.5 dB extinction ratio and a full recovery of 2 ps which indicates that the switching rate can be as high as 500 GHz. SOAs have demonstrated switching with lower energies of up to 1 pJ and extinction ratios of $>$ 17 dB. However the fast and full recovery is comparable to the recovery times stated in SOAs [110, 114–119, 132]. Moreover the device does not suffer from cross talk effects or have complex growth and processing techniques [113].

This work has demonstrated an all optical switching device operating at 5 kHz repetition rate using resonant switching technique. Organic polymers have the advantage of being simple to process and can be coated on any surface. Further work needs to be conducted on an encapsulated structure to produce a device with performance that is comparable to that in all-optical SOA switches.

Chapter 7

Non-collinear Optical Parametric Amplifier

This chapter discusses the theory and the work involved in the development of a noncollinear optical parametric amplifier (NOPA) for spectroscopic applications. Initial work had been performed by a project student, Emmanuel Gaubet, under the direction of Dr. Arvydas Ruseckas, and the source was further developed by myself as described below.

Parametric amplifiers are of great use because they can provide an amplified signal over a large bandwidth. This is a huge advantage over lasers because a laser provides a more limited wavelength range which is dependent on the gain medium. Figure 7.1 shows the tuning range of different lasers compared to that of a NOPA. The concept of tuning over a large bandwidth by simply changing the distance, and hence the time, traveled by the input (pump) beam is very convenient and research is being carried out to enable stable and broadband amplification at high repetition rates.

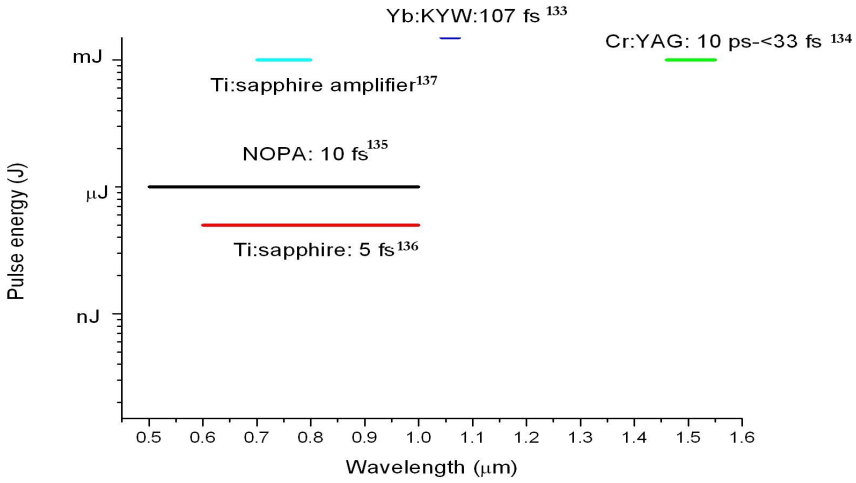

Figure 7.1: Graphical representation of the tunability from some different spectroscopic sources with the corresponding pulse widths [133–137].

7.1 Parametric Amplification

A light wave of an electric field E incident on a dielectric material, induces an electric polarisation P and can be related by a tensor equation of [49, 112, 138]:

$$P = \epsilon_o \chi E \tag{7.1}$$

where χ the dielectric susceptibility and ϵ_o is the permittivity of free space. For higher powers the polarisation response is [138]:

$$P = \epsilon_o(\chi^{(1)}E + \chi^{(2)}E^2 + \chi^{(3)}E^3) \tag{7.2}$$

The $\chi^{(2)}$ susceptibility is responsible for the frequency conversion obtained in parametric amplifiers. The $\chi^{(2)}$ effects are only found in non-centrosymmetric crystals [112, 138]. The $\chi^{(3)}$ susceptibility is found in both centrosymmetric and noncentrosymmetric media [138] and is responsible for self-phase-modulation which is discussed later in the chapter [112, 138].

The parametric amplification was produced in a non-centrosymmetric birefringent

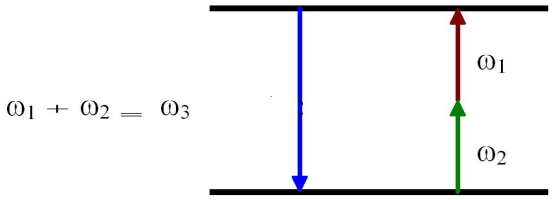

Figure 7.2: Illustration of sum frequency mixing [138].

crystal. A birefringent crystal is optically anisotropic, i.e. the optical properties are not the same in all directions and has different refractive indices for different polarisations of light [139]. Light passing through a birefringent material splits into two waves: the *extraordinary* and *ordinary* waves. The velocity of each wave is associated with the two refractive indices as the speed of light traveling in a medium is dependent on the refractive index of the medium:

$$v = \frac{c}{n} \tag{7.3}$$

where v is the speed of light in the medium, c is the speed of light in a vacuum and n is the refractive index of the medium. The wave which experiences a higher refractive index will travel slower than the wave that experiences a lower one. The magnitude of the birefringence can be measured by the relationship [138, 140]:

$$\Delta n = n_e - n_o \tag{7.4}$$

where n_o and n_e are refractive indices perpendicular and parallel to the optical axis [112].

Parametric amplification is a three wave process, which are the pumping wave, ω_3, the signal wave, ω_1 and the idler wave, ω_2.

Two waves of different frequency (ω_1 and ω_2) are mixed in the birefringent crystal. This could be sum or difference frequency mixing, where in the former case the

pump frequency (ω_3) is the sum of the two frequencies (as shown in figure 7.2) [138]:

$$\omega_{3,\text{pump}} = \omega_{1,\text{signal}} + \omega_{2,\text{idler}}. \tag{7.5}$$

and in the latter, the pump frequency is the difference of the two frequencies:

$$\omega_{3,\text{pump}} = \omega_{1,\text{signal}} - \omega_{2,\text{idler}}. \tag{7.6}$$

7.2 Phase-matching

In order to have parametric amplification the three waves need to be *phase matched*. This is the criteria needed to have a high conversion efficiency of the output from the input. The phase matching conditions are [138]:

$$\omega_1 + \omega_2 = \omega_3 \tag{7.7}$$

$$\underline{k}_1 + \underline{k}_2 = \underline{k}_3 \tag{7.8}$$

which can be seen as the conservation of energy [138]; $\hbar\omega_1 + \hbar\omega_2 = \hbar\omega_3$ and conservation of momentum $\hbar\underline{k}_1 + \hbar\underline{k}_2 = \hbar\underline{k}_3$,
where $\hbar$ is Planck's constant, ω is the angular velocity and $\underline{k}$ is the vector of momentum. Equation 7.7 is the conservation of photon energy and Equation 7.8 is the conservation of photon momentum.

Phase matching will produce a system of low phase mismatch (caused by chromatic dispersion). A non-zero phase mismatch will reduce the conversion efficiency and result in a lower output power. If the waves were phase matched, the direction of energy transfer of the signal beam would be in a constant direction and the output energy would grow in proportion to the square of distance traveled in the crystal. If phase matching was not sustained, the energy transfer would oscillate and the output energy would remain low [83, 138], a graphical illustration of this is shown in Figure 7.3.

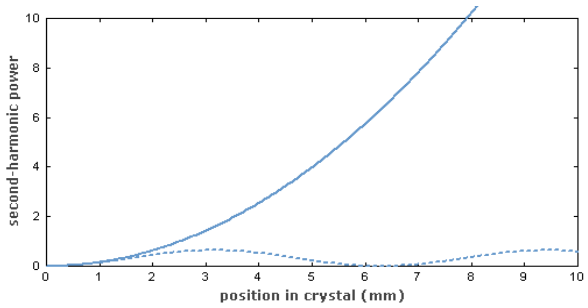

Figure 7.3: The plot shows how the growth of power of second harmonic light varies when phase matched *solid curve* and phase mismatched *dotted curve*. The phase matched case shows that the power grows in proportion to the square of the propagation distance. The non phase matched case shows that the power of the second harmonic light will oscillate [83, 138].

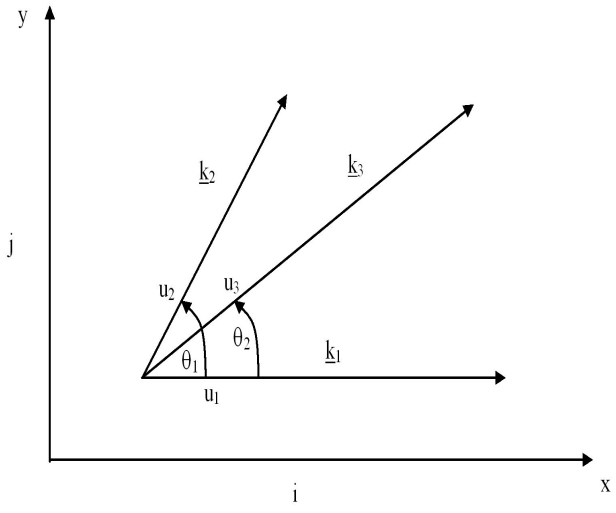

Figure 7.4: Illustration of phase matching, adapted from [141].

In non-collinear phase matching, the vectors are in different directions, as shown in Figure 7.4, the non-collinear phase matching condition is given by [141, 142]:

$$\underline{k}_i = n_i(\omega_i)(\omega_i/c)u_i \tag{7.9}$$

where $\underline{k}_i$, $n_i(\omega_i)$and ω_i are the wavevector, refractive index, frequency and of the ith wave, u_i is the unit normal to the wave front. Equation 7.8 can be re-written as [141, 142]:

$$n_1\omega_1 u_1 + n_2\omega_2 u_2 = n_3\omega_3 u_3 \tag{7.10}$$

The angular relationship between the wave vectors were derived as [141, 142]:

$$sin\theta_1 = \left(1 - \left[\frac{2n_3(2\omega)^2}{n_1(\omega)n_2(\omega)} - \frac{n_1(\omega)}{2n_2(\omega)} - \frac{n_2(\omega)}{2n_1(\omega)}\right]^2\right)^{\frac{1}{2}} \tag{7.11}$$

$$sin\theta_2 = \left(\frac{n_2(\omega)^2}{4n_3(2\omega)^2} - \left[\frac{n_3(2\omega)}{n_1(\omega)} - \frac{n_1(\omega)}{4n_3(\omega)} - \frac{n_2(\omega)^2}{4n_1(\omega)n_3(2\omega)}\right]^2\right)^{\frac{1}{2}} \tag{7.12}$$

where θ_1 and θ_2 are the noncollinear angles between the wave vector of the pump and that of the idler and signal waves.

The crystals used are either type I or type II phase matching. Type I phasematching refers to mixing of waves of the same polarisation and Type II phase matching refers to mixing of waves of different polarisations. Type I phase matching was used in this NOPA. Phase matching was achieved by aligning the crystal to the phase matching angle. The crystal was roughly set to the phase matching angle. Then the crystal angle was altered by fine tuning using the controls on the stand on which the crystal was mounted.

7.3 White light generation

The seed signal is a continuum which is spectrally and temporally broad, ranging from $\sim$ 420 - 750 nm and a temporal pulse width of $\sim$ 1 ps. Visually, it contains

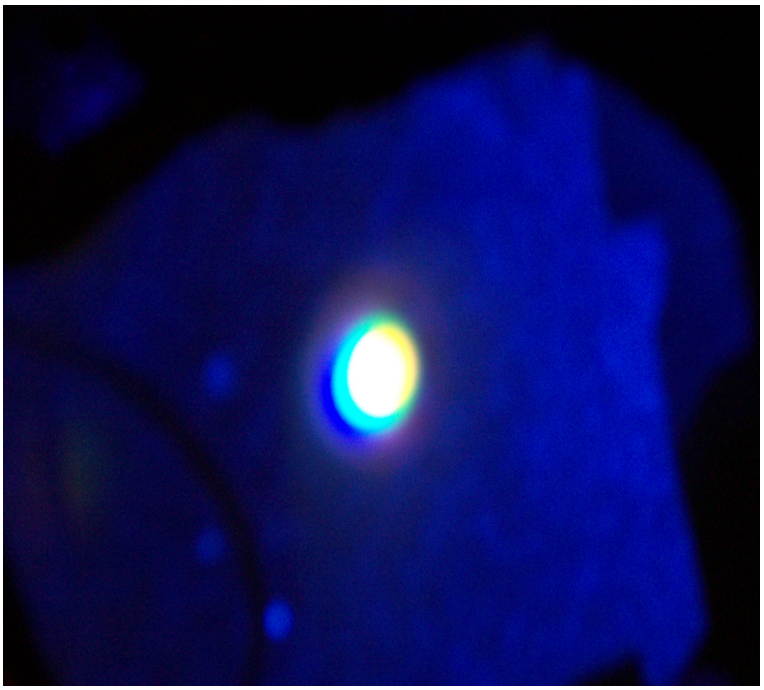

Figure 7.5: Picture of continuum.

an outer ring of red and blue and an inner ring of green and yellow and a white center. The single filament form of the continuum is when the concentric rings are symmetric and clearly visible. Figure 7.5 is an image of this. In this form the intensity of the signal pulse is maximized, possibly because the overlap of the pump and the selected wavelength through the continuum is distinct and allows for conversion to be concentrated at a clearly defined wavelength. The continuum is produced by a 800 nm beam in a sapphire, Al_2O_3, plate by self phase modulation described below.

7.3.0.1 Self-phase modulation

Self-phase modulation occurs in materials with a third order nonlinearity; $\chi^{(3)}$ susceptibility. The refractive index of a material has two parts: one linear and the other nonlinear [112, 138].

$$n = n_0 + n_2 I(t) \tag{7.13}$$

where n is the refractive index, n_0 is the linear refractive index and n_2 is the nonlinear refractive index.

This results in self phase modulation and other self focusing effects as the phase of the pulse is dependent on the refractive index by the relationship [138].

$$\phi(t) = -\frac{n_2 I(t)\omega_o l}{c} \tag{7.14}$$

$$\omega(t) = \omega_o + \delta\omega(t) \tag{7.15}$$

$$\delta\omega(t) = \frac{d}{dt}\phi(t) \tag{7.16}$$

where $\Delta\phi$ is the phase shift, ω_o is the angular frequency, $\omega(t)$ is the instantaneous frequency of the pulse, $\delta\omega(t)$ is the variation of the instantaneous frequency and l is the length of the material. If the pulse has a rapidly varying intensity of the wave, it will induce a phase shift and hence a frequency shift on the pulse. The leading edge shifts to longer wavelengths and the trailing edge will shift to shorter wavelengths. This results in a spectral broadening of the pulse. As the pulse ends up modulating its own phase, it is called 'self phase modulation'.

7.4 Noncollinear OPA

Two beams called the pump (at 400 nm) and the seed (at 800 nm) were used to generate parametric amplification, as shown in Figure 7.6. The home built system uses a non-collinear approach where the pump and seed do not enter the crystal parallel or collinear. The noncollinear geometry eliminates the problem of group velocity mismatch (GVM) that is present in a collinear geometry [143]. Group velocity is defined as [140]:

$$v_g = (\frac{d\omega}{dk}) \tag{7.17}$$

Group velocity mismatch is when two or more waves, initially with the same group velocity, are separated after propagating a distance and no longer share the same group velocity. GVM will affect the spectral range over which phase matching can be obtained.

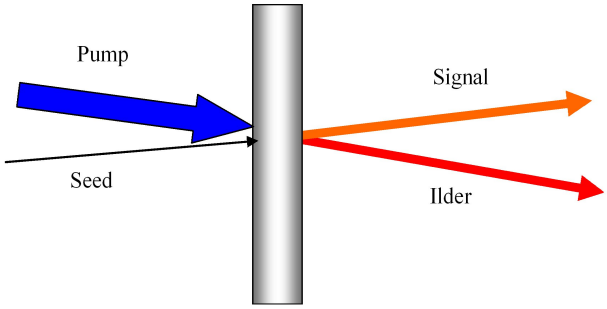

Figure 7.6: Illustration of pump, seed, idler and signal waves with crystal.

Phase matching does not ensure the matching of the group velocities. In a collinear set up, the output is dependent on the group velocity mismatch (GVM) of the pump pulse and the generated signal and idler. A non zero GVM will result in the idler wave traveling faster than the signal wave and would be temporally offset from the signal pulse, hence lengthening the resulting signal [135, 143].

In a non-collinear geometry, the GVM between the pump, signal and idler waves can be compensated as only the projection of the idler group velocity on the signal vector is required and the GVM is only important between the pump and the seed [135, 143–145]. This is equivalent to [135, 143]:

$$v_{g,1} = cos(\Omega) v_{g,2} \tag{7.18}$$

where $v_{g,1}$ and $v_{g,2}$ are the signal and idler group velocities and Ω is the angle between them. A suitable angle, Ω, will result in both having the same group velocity, hence no lengthening of the resulting signal [143]. The GVM of the seed and the pump can easily be set to zero by ensuring the distance (and hence time) traveled by pulses in both beams is the same. The interaction of the pump and the seed produce the signal and idler waves. The noncollinear geometry allows larger spectral pulse widths to be obtained than in collinear OPAs [135, 144].

7.5 Existing construction

The construction of the setup involved two sections, construction prior to my PhD studies commencing, and construction after. The set up was partially built by a short term student and parametric amplification was achieved. The set up layout is shown in Figure 7.7 and it gave parametric amplification from 500 to 750 nm. It had a conversion efficiency of $\sim$ 10 % using a double pass configuration with the first pass giving $<$ 5 % conversion efficiency. The conversion efficiency is calculated as a ratio of the signal output power minus the background power to the pump power input. The development to the system is detailed below.

In order to use the amplified signal for material analysis improvements were made to the set up which were;

1. Improving the conversion efficiency.

2. Produce a compact layout for the system.

3. Adjust for beam divergence.

4. Set up pulse width measurement system.

5. Implement dispersion compensation.

7.6 System development

Input to the NOPA was from a regenerative amplifier at 50 kHz, which was seeded by the Ti:sapphire oscillator. The seed beam was $\sim$ 10 % ($\sim$ 15 mW) of the input signal and was used to produce a white light continuum through self phase modulation. The continuum can be maintained for several days using a UV resistant material, in this case a sapphire plate (Al_2O_3). Phase matching was obtained with a Type I BBO crystal cut at 29^0, which was the phase matching angle to the pump. At this angle, the pump wave generates a superfluorescence cone. If the seed beam is pointed

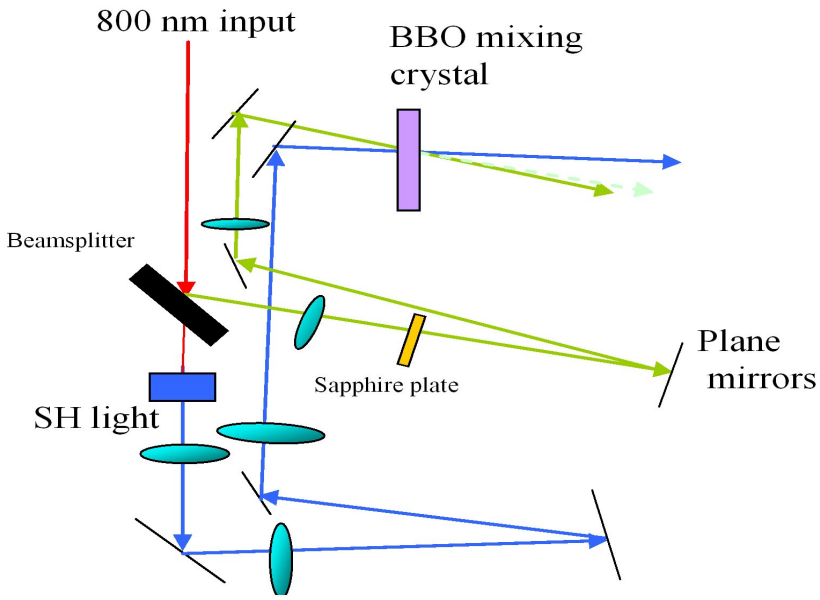

Figure 7.7: Illustration of previous NOPA setup.

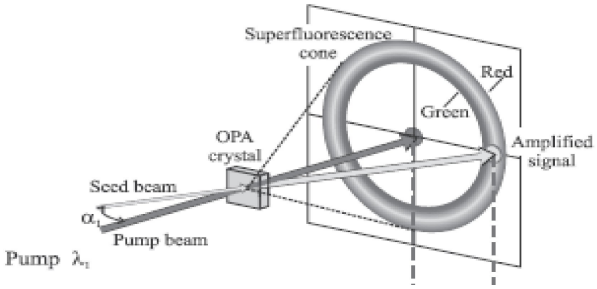

Figure 7.8: Schematic of a non-collinear geometry showing a superfluorescence cone generated by a pump pulse and the seed pulse amplified [145].

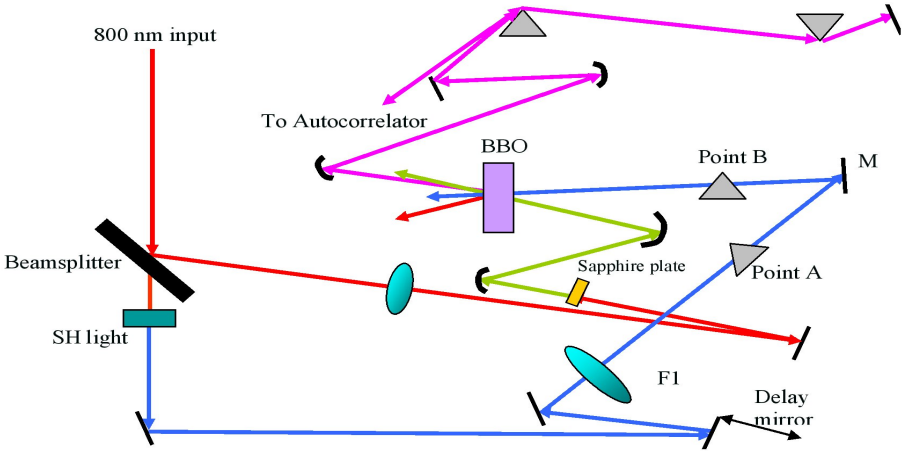

Figure 7.9: Illustration of current NOPA setup.

in the same direction it can be amplified producing the amplified signal wave [145]. This is shown in Figure 7.8. The pump wave was an extraordinary wave and the signal and idler waves were ordinary waves. Spatial walk off was not an issue as it only affects the extraordinary wave. The angle between the pump and the seed, just before the birefringent crystal, is called the external angle, α_E. Within the crystal, due to refraction, this angle changes. It is either called the seeding, noncollinear [141, 146] or internal angle [135] α or ψ, and is the angle between the wave vectors of the pump and the signal wave. This will be referred to as the noncollinear angle and can determine the spectral bandwidth of the signal wave [143, 146] as the noncollinear angle is related to Ω and the signal and idler wavelengths (for a Type I phase matching in BBO crystal) as [135]:

$$\psi = \frac{\Omega(\lambda_{\text{signal}})}{1 + \frac{\lambda_{\text{signal}}}{\lambda_{\text{idler}}}} \tag{7.19}$$

Tuning of the signal wavelength was obtained by varying the time delay between the pump and the seed. When the phasematching and noncollinear angles are set, the signal wavelength can be changed by altering the timing of the spectral component of the continuum with the pump. This is achieved by changing the temporal delay between the two waves. The amplifier was tunable in the visible range, 420 - 650 nm enabling it to be used on a wider range of materials than possible with the Ti:sapphire laser. The construction was changed to optimise and increase the conversion efficiency, make the set up more compact and stable, and introduce dispersion compensation. The new configuration is shown in Figures 7.9 and 7.10.

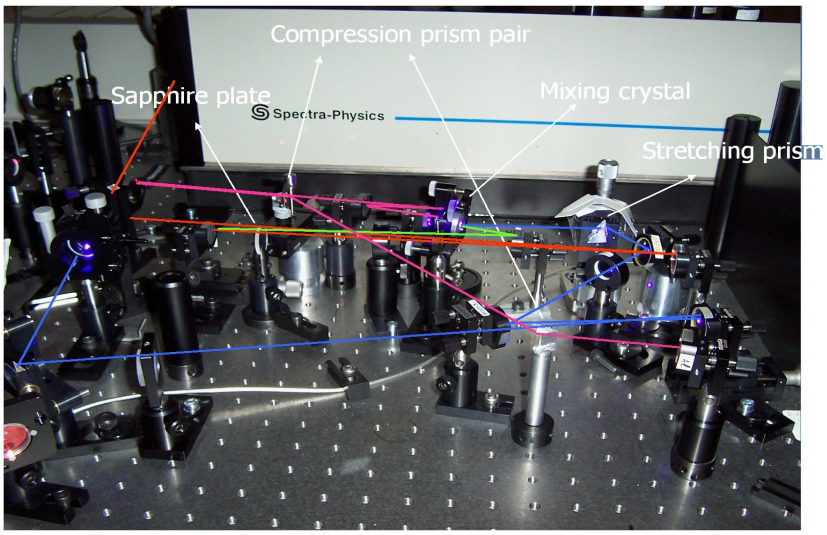

Figure 7.10: Current NOPA setup. The *red line* is the 800 nm input from the Ti:sapphire laser. The *blue line* is the pump signal. The *green line* is the continuum. The *pink line* is the amplified output.

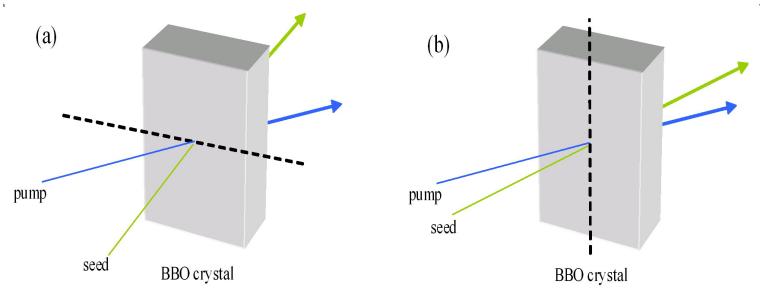

Figure 7.11: Phase matching shown in the horizontal (a) and vertical (b) plane.

Signal efficiency is determined by many factors, these included the amount of aberrations applied to the signal, the intensity of the pump pulse, the noncollinear angle, α, the group velocity match between seed and pump, and signal and idler and the phase matching angle. Phase matching was changed from the horizontal plane to the vertical plane to reduce losses, a visual schematic is shown in Figures 7.11(a) and 7.11(b). Phase matching in the vertical plane required the pump to be horizontally polarized. As the amplified signal would share the same polarisation, the vertical plane phase matching would allow a better configuration of the prism compressor and allow them to be set at the Brewster angle to reduce losses.

A seeding angle of $\sim$ 3 - 4^o allows for a suitable tuning range in a Type I BBO crystal [135, 145]. An external angle of about 4.6^o was used to obtain tunability over $\sim$ 420 to 650 nm. Aberrations were reduced by replacing lenses with focusing mirrors which had the problem of spatially elongating the beam. This was reduced by keeping the reflection angles small which had the additional advantage of compressing the layout of the set up.

The pump power was 88.9 mW and the maximum output power was $\sim$ 12.10 - 16 mW, providing a conversion efficiency of 13 to 18 % from a single pass making a second pass unrequired. This value is comparable to conversion efficiencies obtained by single pass configurations in a other non-collinear set ups which were in the range of $\sim$ 15 - 25 % [135, 147–149].

7.6.1 Output characterisation

The characterization of the output is explained in two sections: the optimization, which involves improving the configuration of the setup to reduce losses and increase the conversion efficiency, and the pulse compression which leads onto autocorrelation traces.

7.6.2 Optimization

The optimization of the output was focused on maximising the conversion efficiency.

The conversion efficiency is dependent on the power per unit area of the pump signal. In order to obtain high conversion efficiencies, phase matching needed to occur at the beam waist of the pump beam. The highest intensity was at the focal plane of the focused pump signal, but this would burn and critically damage the birefringent crystal, which was only 1 mm thick. To avoid this, *Riedle et al.* [150] had stretched the pump signal temporally, using a sapphire plate. This allowed the crystal to be placed at the focal plane of the pump beam and the high intensity at the focus allowed for a more intensely amplified output. *Riedle et al.* state that the stretched pump beam would extend the phase matching bandwidth allowing for amplification over a broader range [145, 150]. A longer crystal and so a larger pump beam could have been used, however this will not result in femtosecond pulse generation. The longer crystal will introduce chirp on the pulse which could stretch it by a large amount.

With the un-stretched pump beam, the conversion efficiency of the parametric process was ~ 6 %. To stretch the pump beam, a quartz prism was used. The output was analyzed with the prism placed at two points in the setup; point A and B, as shown in Figure 7.9. With the prism in place, the conversion efficiency showed 16 % for point A and 13 % for point B. The prism was used at point B because by placing it closer to the crystal, any changes made to the prism position will not shift the position of the pump beam. Further adjustments were made to the mirrors and the prism to improve the overlap and the external angle and hence the noncollinear angle. It should be noted that the conversion efficiency at the two points were only different because adjustments made to the optics resulted in those values. With further adjustments, the same amount of conversion efficiency would be obtainable in both points A and B.

The angle of the incident light on the prism produced an astigmatism on the pump beam, which was an elongation of the pump beam in either the vertical or horizontal plane depending on the incident angle. To maintain a fixed angle, the prism is glued in place. Shrinkage of the adhesive was unavoidable and induced stress on the glued materials. The position of the lens focussing the pump on to the prism, F1, was varied to find the optimal position. Figure 7.12 shows the output power of the amplified signal for the different positions of the focussing lens. This indicated that

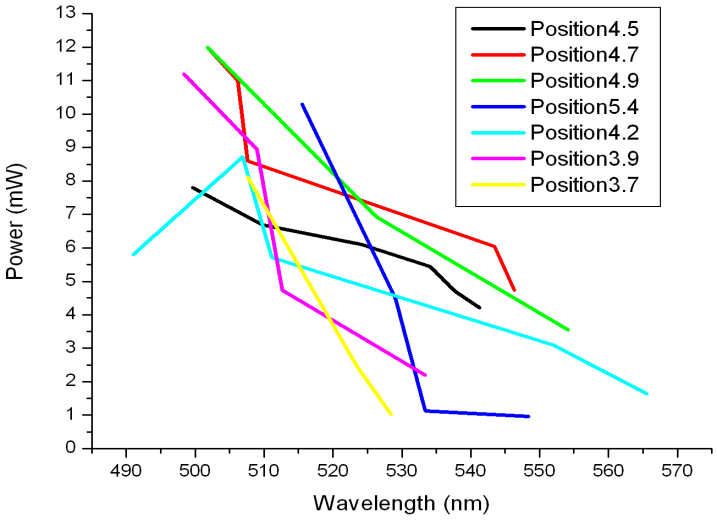

Figure 7.12: The output power for different wavelengths for a range of positions of lens F1 from mirror M.

the lens should be placed 4.9 cm from the mirror as it had a high output power for that wavelength range. It remained at this point.

The output from the NOPA had a large horizontal divergence. Prior to entering the compressor stage, this beam had to be collimated to limit the divergence. Collimation and correction of the horizontal divergence was made with a cylindrical mirror and two spherical mirrors in a double pass configuration which is shown in Figure 7.13. With a plane mirror and spherical mirror gave a beam width which was about 20 mm wide. When the plane mirror was replaced with a spherical mirror, the beam width was reduced to 6 mm.

7.6.3 Pulse compression

For the 6 mm beam configuration, the pulse width was compressed with a pair of quartz prisms. This beam was chirped due to positive dispersion introduced by the 3 mm thick sapphire plate and other optical elements, such as lenses. The stretching prism on the pump beam introduced a small amount of positive group velocity dispersion (GVD) on the signal output. In order to get near transform limited pulses,

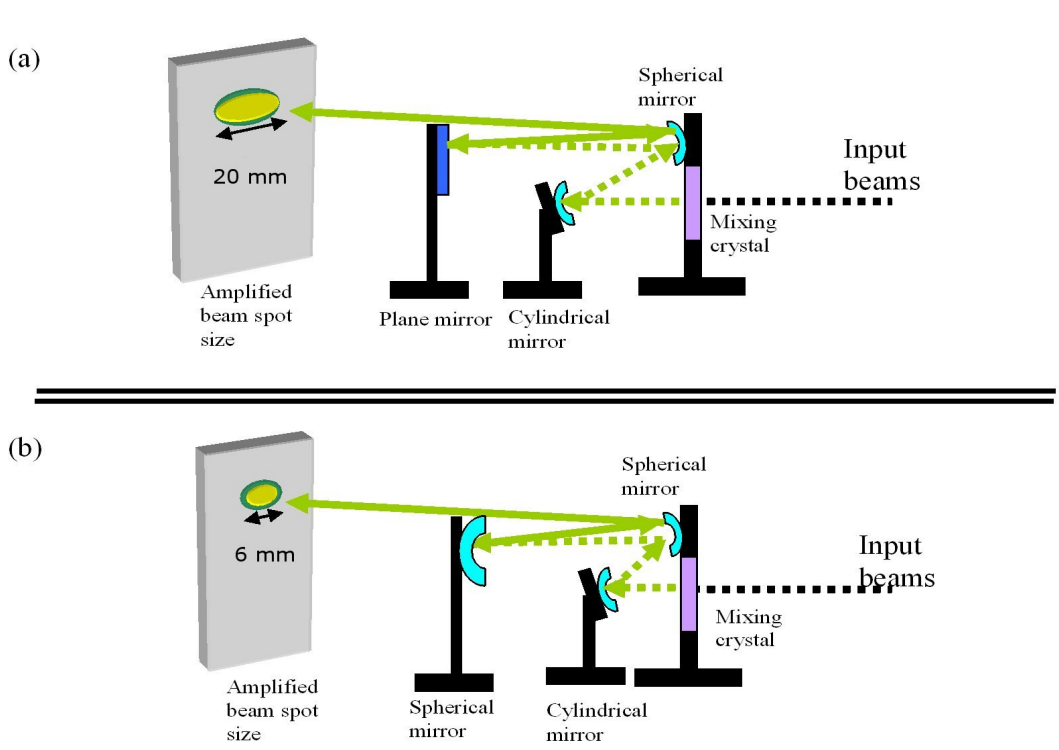

Figure 7.13: Beam reshaping and collimation. Figure (a) shows a 20 mm wide output using a plane mirror and figure (b) shows a 6 mm beam with a spherical mirror.

the positive GVD was compensated with a prism pair which would introduce negative GVD to the input pulses [48, 151]. For a Gaussian pulse, the transform limit is:

$$\Delta v \Delta t > 0.441 \tag{7.20}$$

where Δv is the bandwidth and Δt is the pulse width. Some positive GVD can also be introduced by the prism pair by inserting more glass of the prism.

The amplified output is double passed through the prisms as shown in Figure 7.14. The compensation for GVD by the prism pairs is based on the angular dispersion induced by the prisms on the beam. The beam is incident on the apex of the first prism and the dispersed beam hits the apex of the second prism, illustrated in Figure 7.14. The prisms were placed at the Brewster angle to reduce the reflection losses. Negative GVD is controlled by the distance between the prisms. The output was frequency doubled in a second harmonic generation (SHG) BBO crystal. The beam then passed to a power meter via a filter as shown in Figure 7.15. The intensity of

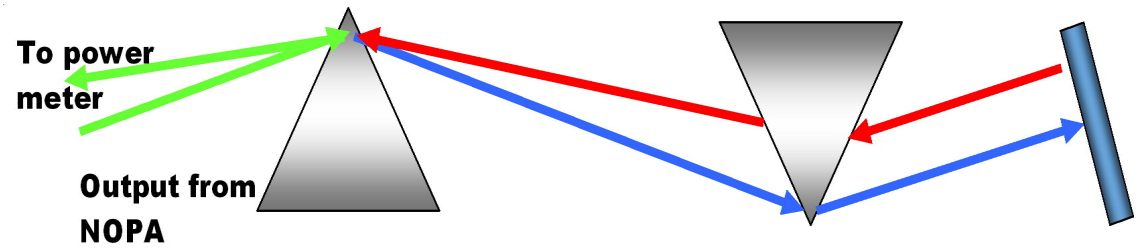

Figure 7.14: Schematic of compressor with output recorded by a power meter.

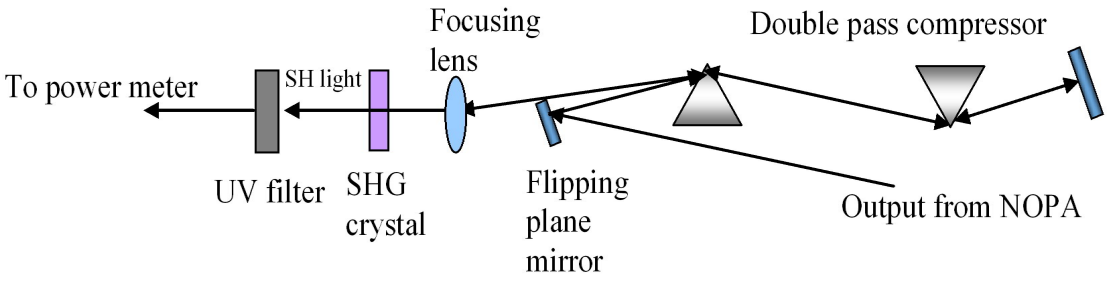

Figure 7.15: Compressor setup for pulse optimum pulse compression.

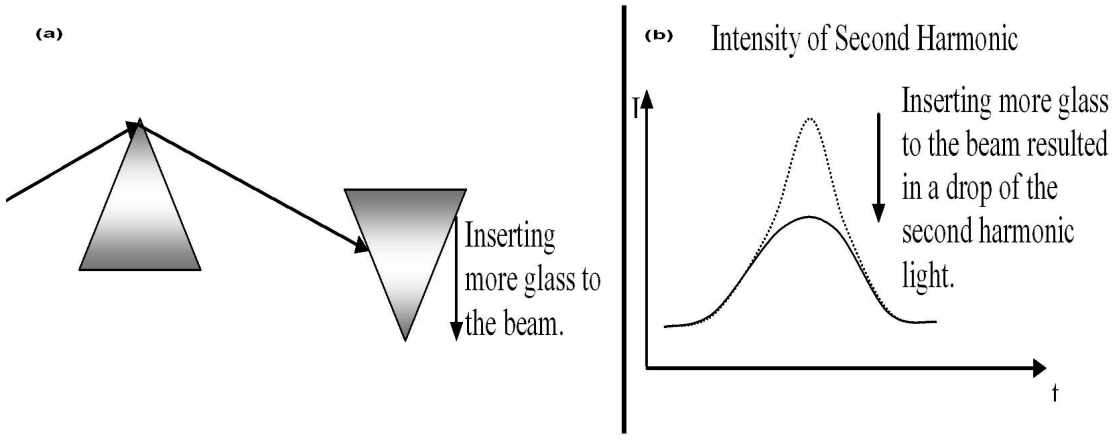

Figure 7.16: Figure (a) illustrates how more glass is introduced. Figure (b) shows that if inserting more glass caused a drop in the second harmonic intensity. There is not enough negative GVD from the prism compressor to compensate for the positive GVD produced before the crystal.

the second harmonic of the signal output from the compressor was used as a method of measure, in order to establish initial prism distances and positions. An increase of the second harmonic light would indicate that the pulse duration was close to the transform limit. This implied that the pulses were as short as possible for their bandwidth. Positive GVD was induced on the beam by increasing the amount of glass traveled by the signal. This could be controlled by translating the prisms inward or outward with respect to the beam.

On inserting more glass, the amount of positive GVD increased. If this caused the intensity of the second harmonic light to drop, it was because the negative GVD of the prism compressor could not compensate for the positive GVD produced by the pump and seed beams and the glass in the prism. This is illustrated in Figure 7.16. In this case, it was an indication that the prism separation needed to be increased to increase the amount of negative GVD produced by the prism pair.

If the intensity of the second harmonic light remained fairly steady when a small amount of glass is inserted into the beam path, this indicated that there was ample negative GVD compensation produced by the prism compressor.

7.6.4 Autocorrelation

Autocorrelators are used to measure the width of ultra short pulses, particularly in the femtosecond or picosecond regime, as even fast photodiodes are too slow. An autocorrelator set up was built to measure the width of the compressed pulse, as shown in Figure 7.17. The input to the setup was the signal wave from the NOPA. This was split into two beams by a beamsplitter and recombined in a nonlinear crystal. The crystal used was a BBO crystal. Sum frequency mixing occurs within the crystal and a signal of shorter wavelength will output through the crystal when the two input beams are temporally and spatially overlapped. The type of autocorrelator used was an *intensity autocorrelator*, where the intensity of the autocorrelated signal can be varied when changing the temporal overlap of the two input beams. This is shown in Figure 7.18. When the two beams arrive at the same time it is the maximum point of the autocorrelated signal. At full width half maximum of the autocorrelated signal occurs when the input beams are half overlapped temporally and at the point of no autocorrelated signal there is no temporal overlap. This dependence on the

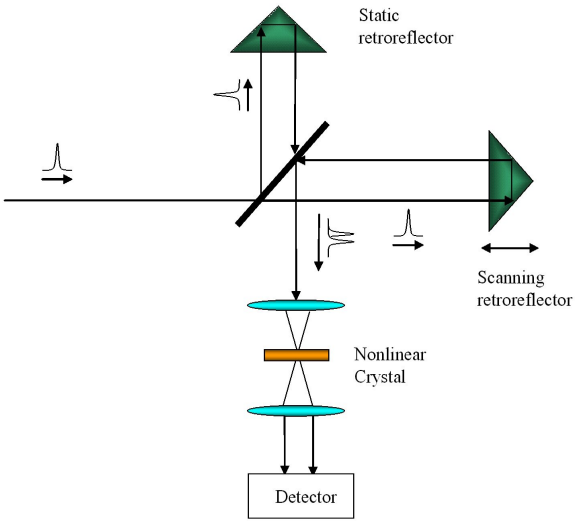

Figure 7.17: Setup of autocorrelator [152].

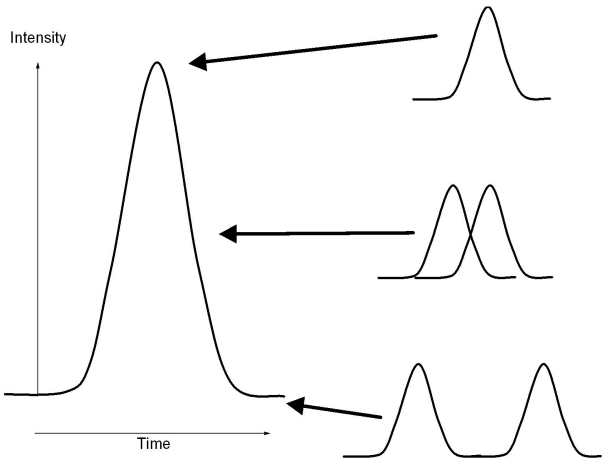

Figure 7.18: Formation of autocorrelated signal through the temporal overlap of the two input beams. On the left hand side is the autocorrelated pulse. On the right hand side is the degree of temporal overlap between the two input beams. The degree of temporal overlap will affect the intensity of the autocorrelated signal [152].

autocorrelated signal can be expressed as [152, 153]:

$$G_{ac}(\tau) = \frac{\int I(t)I(t+\tau)dt}{\int I(t)^2 dt} \tag{7.21}$$

where I(t) is one input beam, I(t + τ) is the second input beam delayed by τ and I(t)^2 dt is the normalizing factor. The width of the autocorrelated signal is directly related to the width of the measured pulse. To determine the pulse duration, one needs to assume a pulse shape, in this case a Gaussian pulse. Therefore, the pulse width was calculated using [152]:

$$\frac{\Delta\tau_G}{\Delta\tau} = 1.414 \tag{7.22}$$

where $\Delta\tau_G$ is the width measured from the autocorrelated signal and $\Delta\tau$ is the width of the measured pulse, to be calculated.

With the compressor setup using the SHG method mentioned previously, initial scans with the autocorrelator showed a pulse width of about 300 fs. This was because the signal pulse was temporally stretched to $>$ 100 fs by the stretching prism on the pump and the SFM on the seed. The SHG method should have given a pulse width of $<$ 100 fs. As this was not the case, it indicated that the SHG method to find the optimum spacing and glass depth was not efficient. Hence the autocorrelator was used to get a measurement of the pulse width alongside changes made to the compressor set up. These changes involved altering the amount of glass traversed by the beam and the spacing between the prisms.

Autocorrelations were taken at different prism distances at a step interval of 1 ps. From these results (shown in Figure 7.19) I was able to determine what prism distance to choose and scanned within this range with smaller steps. Further autocorrelations with a step interval of 0.5 ps, led to a prism separation range of 41 to 50 cm, autocorrelations for these distances are shown in Figure 7.20. Prism separations of 44 cm and 50 cm gave pulse widths of 172.33 and 164.35 fs respectively. A prism separation of 50 cm had previously given a larger pulse width. This encouraged me to focus on the separation distance of 44 cm and carry out autocorrelations at a shorter step interval of 0.25 ps, shown in Figure 7.21. Figure 7.21 show a main peak with two

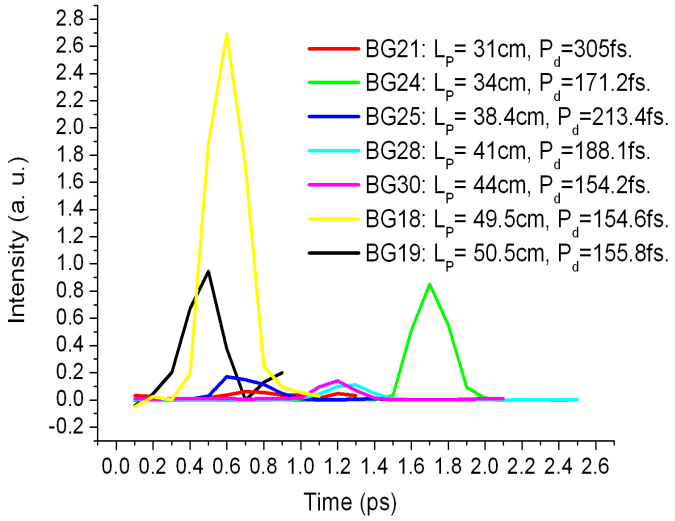

Figure 7.19: Autocorrelations for different prism separations, L_p. The legend displays the corresponding pulse widths.

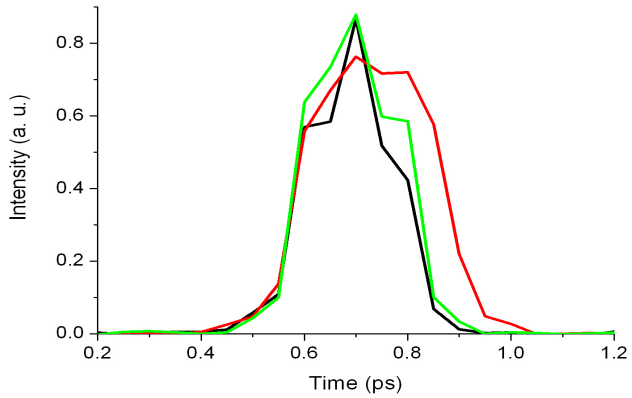

Figure 7.20: Autocorrelations for prism separations of 41, 44 and 50 cm. Scans were taken with a step interval of 0.5 ps.

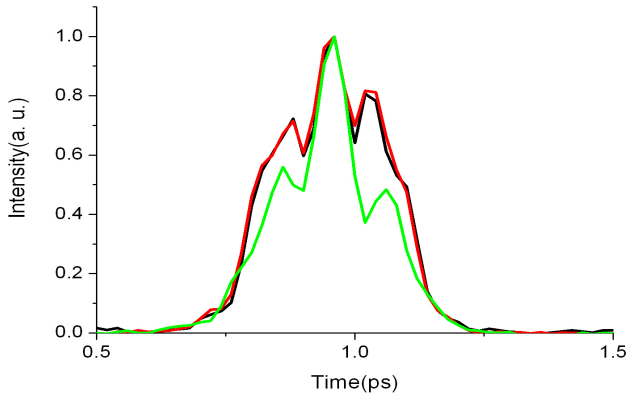

Figure 7.21: Autocorrelations for a prism separation of 44 cm. Scans were taken with a step interval of 0.25 ps.

side lobes present on either end. It is probable that the trace is showing four pulses overlapping instead of two. The pulse width was measured to be $\sim$ 120.2 fs. This was kept as a suitable pulse width for the tunable output of the NOPA.

7.6.5 Tunability

The amplified output was tunable over the visible range as shown in Figure 7.22. An optical fiber was used to collect scatter from the output. Scatter was collected instead of direct light to avoid damaging the fiber tip. With a repetition rate of 50 kHz on the Ti:sapphire regenerative amplifier, the energy per pulse was 0.242 μJ. Figure 7.22 shows the output from 455 to 650 nm. The spectra of the idler and continuum are also shown in Figure 7.22.

7.7 Conclusion

The OPA and TOPAS-white allow tunability along the entire visible region at 5 kHz. The NOPA bridges the gap between the tunable 5 kHz (OPA and TOPAS) and the 80 MHz (Mai:Tai) femto-second spectroscopic sources. It delivers femtosecond pulses in a 252 THz range with a conversion efficiency of 13 - 18 %. The pulse width is between

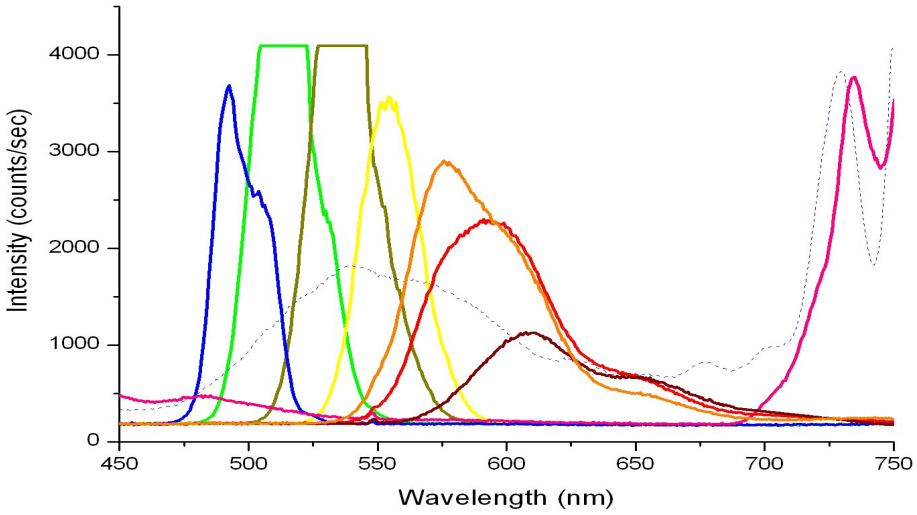

Figure 7.22: Tunability of the signal is shown from 450 to 650 nm. The lines represent the spectra observed at different delays. The idler and continuum are the pink and dotted lines respectively.

100 - 200 fs. Further work needs to be carried out to obtain a sub femtosecond pulse width which has been produced in other home build NOPA systems [135, 154, 155].

Conjugated polymer amplifier devices have been demonstrated to be capable of operating at high repetition rates up to 5 kHz [43, 69]. Working at high repetition rates is a challenge due to fast triplet build up and degradation. However the operation of the amplifier at a higher repetition rate of 50 kHz was explored and the output was detected with the streak camera. This was possible due to the construction of the NOPA. The 50 kHz repetition rate allowed to probe the material for a different energy range and the tunability of the NOPA made it possible to investigate multiple conjugated polymers of different emission spectra. This work is discussed in more detail in the following chapter.

Chapter 8

Optical amplifier operating at fifty kilohertz

Digital bandwidths to the home and office areas are at a rate of 4 Mbits/sec [24] and this will soon increase to 100 Mbits/sec [156]. Hence in order for polymer amplifier or laser devices to function in real world applications they need to be operable at high repetition rates. However operating polymer lasers or amplifiers at high repetition rates or even in the continuous wave mode is an issue, due to loss mechanisms such as fast triplet build up and degradation [17]. Most work has demonstrated thin film polymer lasers [15, 17–21, 157] or amplifiers [72–74] at repetition rates below 1 kHz . Few have demonstrated solid state polymer lasers and amplifiers operating at higher repetition rates; *Heliotis et al.* were the first to demonstrate a conjugated polymer laser operating at 5 kHz [158] and two years later, the same repetition rate was used by *Vasdekis et al.* in their demonstration of a low threshold solid state laser [14]. The highest operating repetition rate for a laser so far was demonstrated by *Rabe et al.* with packets of pulses at 5 MHz [159]. The highest repetition rate demonstrated for an optical amplifier to date has been at 5 kHz [43, 69].

The amplifier device was tested at a higher repetition rate of 50 kHz which was available from the noncollinear optical parametric amplifier (NOPA) described in the

previous chapter. The signal output of the NOPA provided the probe beam. The residual pump from the parametric process, which was at 400 nm, was used to excite the polymer. The output was recorded with the streak camera.

This chapter explains the process by which amplification and switching of light was attempted with different polymers at a repetition rate of 50 kHz. Amplification of light was attempted with the following conjugated polymers; F8BT, GP1302, ADS233YE and MEH-PPV. Attempts were also made to switch off the amplification of light in some of the polymers. The switching wavelength was 800 nm, and was obtained from the 50 kHz regenerative amplifier.

For longer waveguide lengths (> 600 μm) more probe energy (0.120 nJ) was required than used in the 5 kHz set up for the data amplifier (0.04 nJ) which is explained in the discussion section of this chapter. Hence either the probe power had to be increased when testing long waveguides > 600 μm, or shorter waveguides were used. With longer waveguides amplification was low, in the order of 3 dB. This was because more probe energy was required, which would have depleted the population inversion and reduced the maximum gain obtained. Experiments were conducted on shorter waveguides which were < 822 μm.

8.1 F8BT amplifier at 50 kHz

Amplification of light was attempted with a polymer that had been previously tested at 5 kHz. Amplification with F8BT showed high gains of 16 and 12 dB for waveguides of length 422 and 322 μm, shown in Figure 8.1. The gain cross section, σ, was calculated from these measurements using Equation 4.4. The gain cross-section was calculated to be $\sigma = (2.75 \pm 1.18)\text{x } 10^{-16}$ cm^2. This is comparable to the values for the same material in previous work, which were in the range of 10^{-16} to 10^{-17} cm^2 [19, 61, 69, 72].

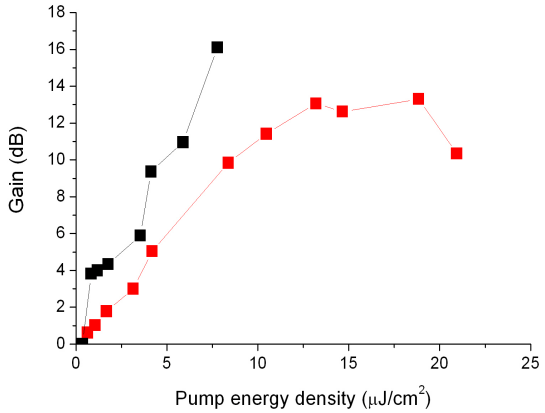

Figure 8.1: Amplification in F8BT in waveguide lengths of 322 (*red symbols*) and 422 μm (*black symbols*) at a repetition rate of 50 kHz with probe energy of 0.04 nJ.

8.2 The copolymer GP1302

Some amplification was obtained for a probing wavelength of 530 nm with a material concentration of 6 mg/ml and is shown in Figure 8.2. The probe energy was 0.012 nJ just after the input coupler. The probe wavelength was 580 nm and the concentration was kept the same as in the previous experiment as there was good waveguiding and the optical density was sufficient at an excitation wavelength of 400 nm to give 82 % absorption. Amplification was was poor and is discussed further in the discussion section of this chapter.

8.3 The copolymer ADS233YE: absorption and photoluminescence

ADS233YE is a light emitting copolymer of benzothiadiazole and fluorene units to the ratio [1]of 1:4 and was obtained from American Dye Source (ADS). It was chosen because it has similar absorption and emission spectra to GP1302 and was commercially available. Figure 8.3 shows the absorption and emission spectra of ADS233YE.

[1]The ratio is the absorbance at 370 nm to 440 nm taken from the absorption spectrum.

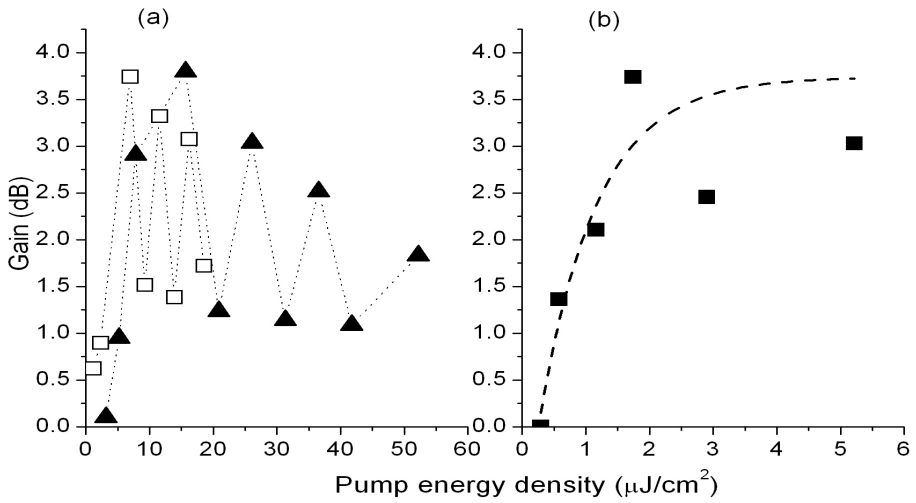

Figure 8.2: Amplification of GP1302 in waveguide lengths of (a) 222 μm (*closed symbols*), 322 μm (*open symbols*) and (b) 622 μm for pump and probe wavelengths of 400 and 530 nm.

It is a yellow powder which was made into solution with toluene. Amplification of ADS233YE was only attempted at 50 kHz.

8.3.1 ASE spectra of ADS233YE

ASE measurements were conducted on a 460 nm thick film of ADS233YE, excited at 400 nm, which had 96 % absorption. Figure 8.4 shows the ASE spectra variation with pump energy and Figure 8.5 shows the peak intensity variation with pump energy. The ASE threshold and wavelength were 3.25 μJ/cm^2 and 560 nm respectively.

8.3.2 Amplification of light in ADS233YE

Amplification of light in ADS233YE was attempted for two probe wavelengths; 530 and 580 nm as the former was the PL peak and the latter would have demonstrated tunability of the material. At the PL peak it should be possible to obtain amplification. The film was spin coated at 800 rpm from a toluene solution concentration of 46 mg/ml to form a 409 nm thick layer. Figures 8.6 and 8.7 show the gain obtained at probe wavelengths of 530 and 580 nm respectively. The probe energy was 0.024

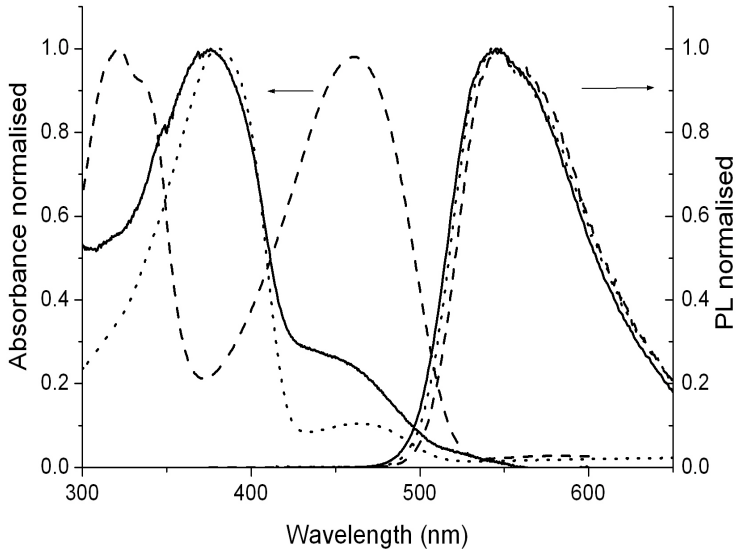

Figure 8.3: Absorption and emission spectra of ADS233YE (*solid line*). For comparison the absorption and emission spectra of GP1302 (*dotted line*) and F8BT (*dashed line*).

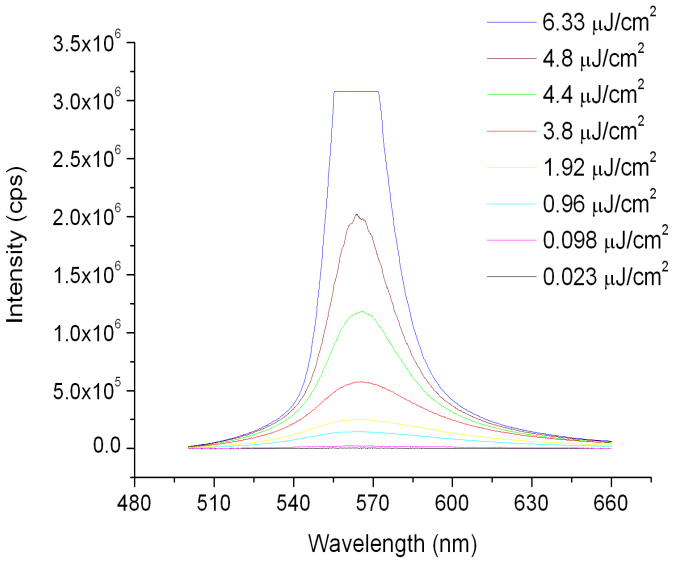

Figure 8.4: ASE emitted from ADS233YE copolymer film for different pump energies.

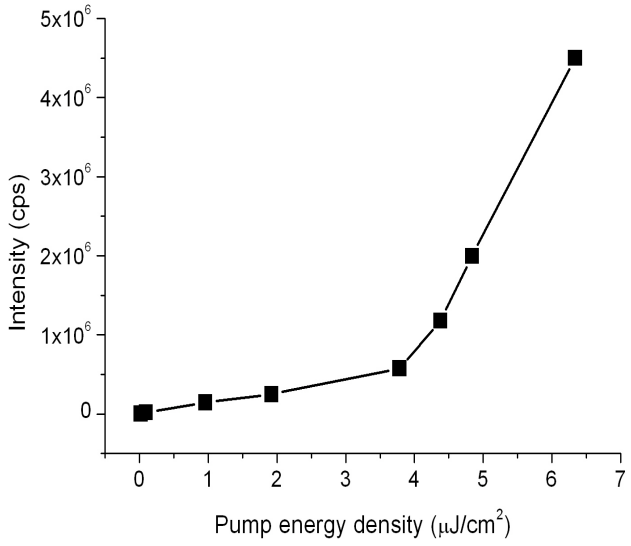

Figure 8.5: ASE intensity peak variation against pump energy for ADS233YE.

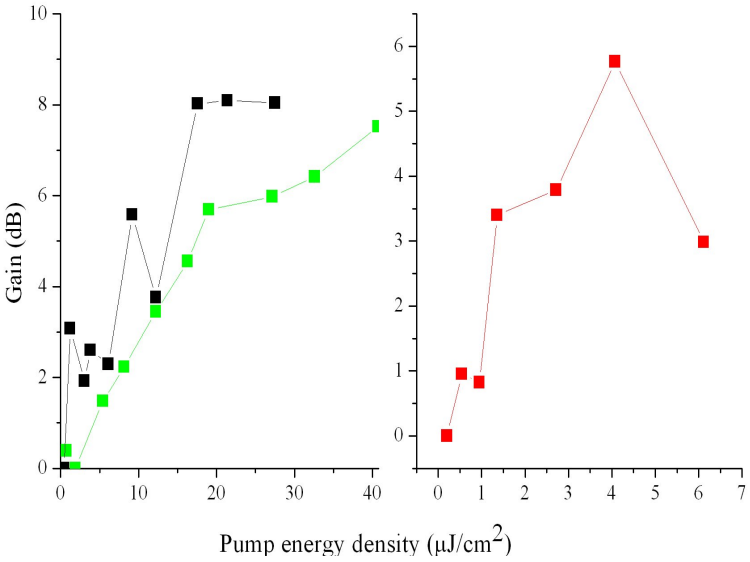

Figure 8.6: Amplification of ADS233YE in waveguide lengths of 322 (*green symbols*), 422 (*black symbols*) and 622 μm (*red symbols*) for pump and probe wavelengths of 400 and 530 nm respectively.

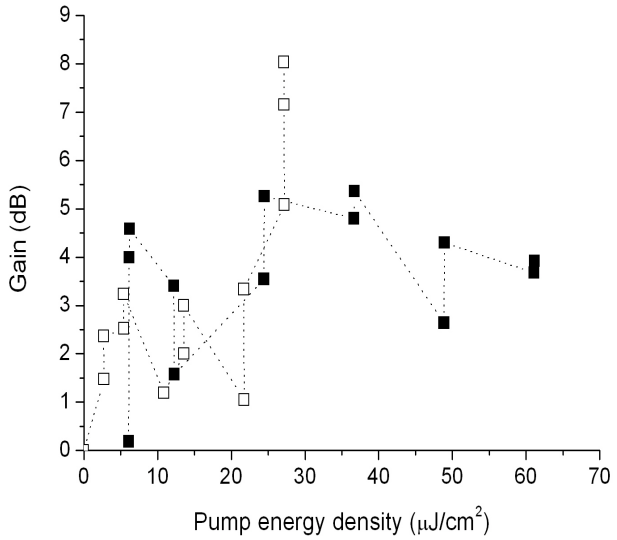

Figure 8.7: Amplification of ADS233YE in waveguide length of 222 μm (*closed symbols*) and 322 μm (*open symbols*) for pump and probe wavelengths of 400 and 580 nm respectively.

nJ (just after the input coupler) for both wavelengths. The highest achievable gain at 530 nm was 8 dB in a waveguide of length 422 μm. A gain of 5 dB was obtained with a probe wavelength of 580 nm in a 222 μm long waveguide and $\sim$ 8 dB in a 322 μm long waveguide. The gain cross section was calculated for a probe wavelength of 530 nm to be $\sigma = (4 \pm 3.3)$ x 10^{-18} cm^2. This value is an order of magnitude lower than expected. Expected values would be in the range of 10^{-16} to 10^{-17} cm^2.

Switching was possible. Switching with an extinction ratio of 3.67 dB in a 222 μm long waveguide was obtained. This is shown in Figure 8.8 (a), (b) and (c). Figure 8.8(d) shows partial switching with an extinction ratio of 2.9 dB, in a waveguide length of 300 μm. The resulting trace, after subtraction of the PL spectrum, was very noisy. This was because the PL spectrum was very noisy.

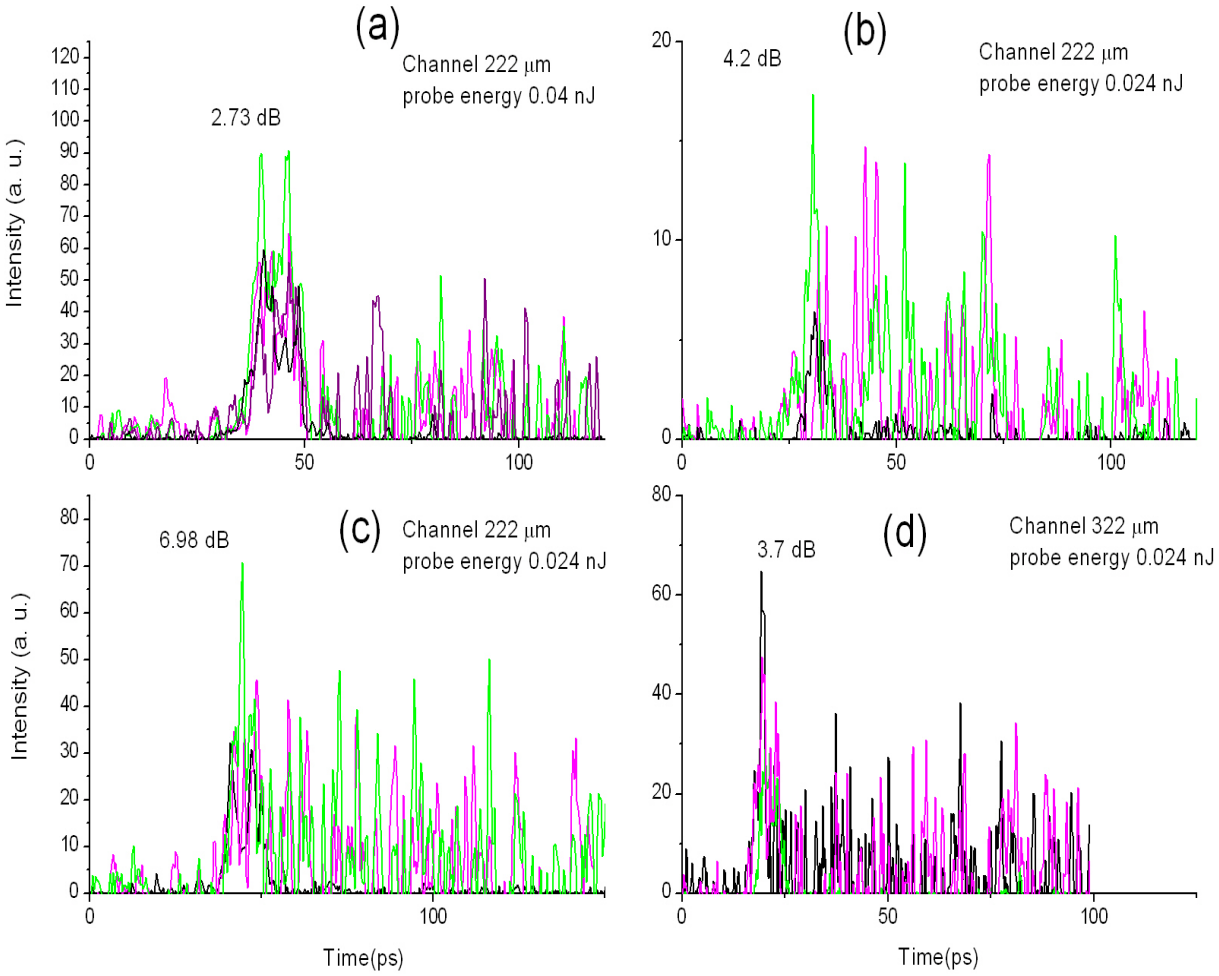

Figure 8.8: Figures (a), (b) and (c) show switching of probe signal in a waveguide length of 222 μm. Figure (d) shows 50 % switching in waveguide length of 322 μm. The *black line* is the unamplified probe, the *green line* is the amplified probe and the *pink line* is the amplified probe with the switch pulse unblocked. The pump, probe and switch energies were 7 nJ, 24 pJ (40 pJ for figure (a)) and 80 nJ.

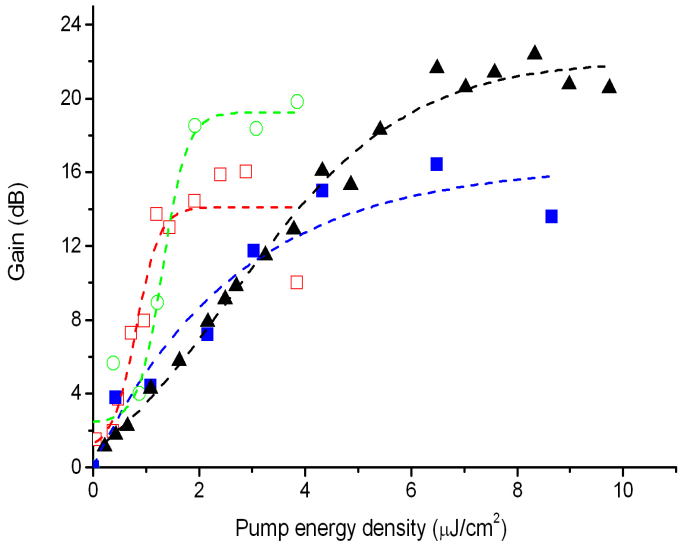

Figure 8.9: Gain obtained for different pump energy densities for different waveguide lengths of 622 μm (*red open square symbols*), 422 μm (*black triangular symbols*), 322 μm (*green open circular symbols*) and 222 μm (*blue closed square symbols*) in MEH-PPV. The film thickness was 100 nm, the probe wavelength was 630 nm at 50 kHz. The *dashed lines* are a guide to the eye.

8.4 Amplification and switching of light in MEH-PPV

Amplification was obtained for waveguides of length 622, 422, 322 and 222 μm, shown in Figure 8.9. The probe wavelength was 630 nm. The probe energy was 0.04 - 0.06 nJ (just after the input coupler) for waveguides of length $<$ 622 μm and 0.12 nJ (just after the input coupler) for the waveguide of length 622 μm. The gain cross-section was calculated from the linear region of the slope, using Equation 4.4, as shown in Figure 8.9, to be (2.17 ± 0.9) x 10^{-16} cm^2. This value is comparable to that calculated in Chapter 4 and with other polyparaphenylenevinylene, which were in the order of 10^{-17} cm^2 [67].

The gain variation was also measured for a small range of the probe energy, and is shown in Figure 8.10. In this measurement, the gain of $\sim$ 8 dB was obtained for the same probe energy and pump energy density (0.04 nJ and 2 μJ/cm^2 respectively), in a waveguide length of 422 μm, as that in the pump dependency measurement shown

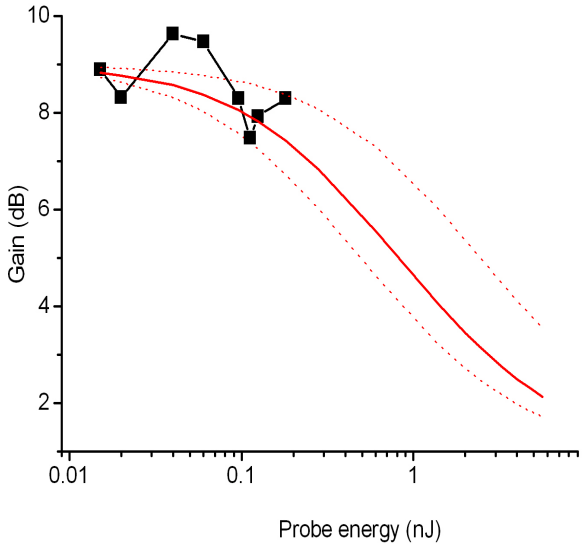

Figure 8.10: Gain dependence on probe energy for MEH-PPV at 50 kHz in a waveguide length of 422 μm. Pump energy density remained constant at 2 μJ/cm^2. The *symbols* are the experimental data and the *solid red line* is the theoretical fit, the *dotted lines* are the fits for the stated error in the text.

in Figure 8.9. The data were fitted to the theoretical equation of the homogeneous saturated amplifier [82], Equation 4.8. From this fit a small signal gain, G_0, of 9 dB and a gain cross-section of (3 $\pm$ 2) x 10^{-16} cm^2 were obtained. This value is within the value calculated using Equation 4.4 and is comparable to the value calculated in Chapter 4 and another report polyparaphenylenevinylene, which were in the order of 10^{-17} cm^2 [67].

Different probe wavelengths were coupled in at different angles. The gratings in each column were etched at different grating periods so that a range of coupling angles and thus coupling wavelengths could be used. Hence, for a given probe wavelength, gratings in one column could only be used. Due to fast degradation of the polymer at 50 kHz, this was a limited choice and so amplification was attempted at a lower repetition rate. A chopper at 3 kHz was used to chop the 50 kHz beam. The chopper allowed about 15 pulses between chops. This gave a gain of 9 dB in a 300 μm waveguide, shown in Figure 8.11. This was abandoned because work progressed towards gain recovery explained in chapter 6.

Switching of the amplification in MEH-PPV was attempted. The switching wave-

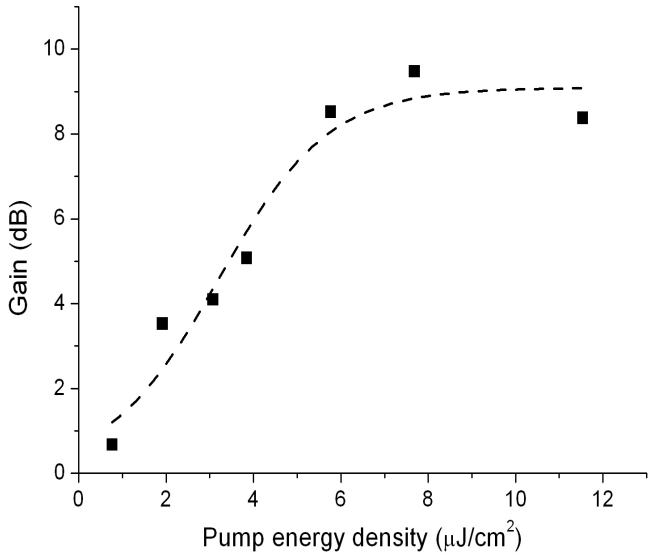

Figure 8.11: Amplification of light with MEH-PPV in a waveguide length of 322 μm with a 3 kHz chopping frequency applied on the 50 kHz signal. The probe power was 0.2 nJ. The *dashed line* is a guide to the eye.

length was 800 nm as transient absorption measurements had shown that there was excited state absorption at 800 nm for MEH-PPV [160]. Switching of MEH-PPV showed either

(i) Switching of the amplified signal

(ii) Long signal recovery.

(iii) Fluctuation in the switching effect.

Figures 8.12 and 8.13 show measurements taken in consecutive order. Extinction ratios of 3 - 5 dB were obtained. Figure 8.12 shows that the amplification was switched off by 50 % in a waveguide length of 200 μm. This remained switched for two further consecutive recordings. A recording takes 2 - 5 seconds. Hence the switch was applied for 6 seconds and the signal remained switched for this duration. On removing the switch pulse, the signal does not recover immediately. The signal recovers after three consecutive measurements, a total of 6 seconds. The behaviour of MEH-PPV indicated that there were long lived species which affected the recovery of the signal. Figure 8.13 shows switching occur with the initial measurement. However, the two

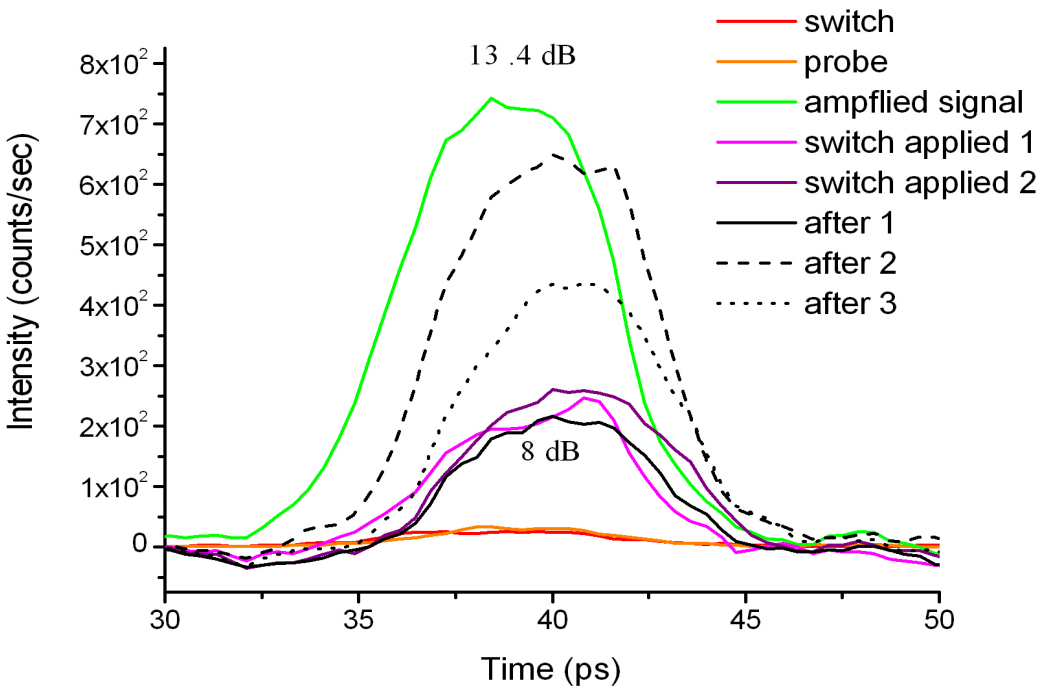

Figure 8.12: Switching of amplified light in MEH-PPV with a waveguide length of 222 μm. The amplification of the signal was switched off by 68 %. The *yellow line* is the unamplified probe, the *red line* is the switch pulse and the *green line* is the amplified probe. The *pink lines* are the multiple measurements of the amplified probe taken with the switch beam unblocked in consecutive order. The *solid black line* is the amplified probe after the switch is blocked. The *dotted black line* is the second consecutive measurement of the amplified probe with the switch blocked and the *dash line* is the third consecutive measurement of the amplified probe with the switched blocked. The probe, pump and switch energies were 0.04, 2 and 120 nJ respectively and the wavelengths were 630, 400 and 800 nm respectively.

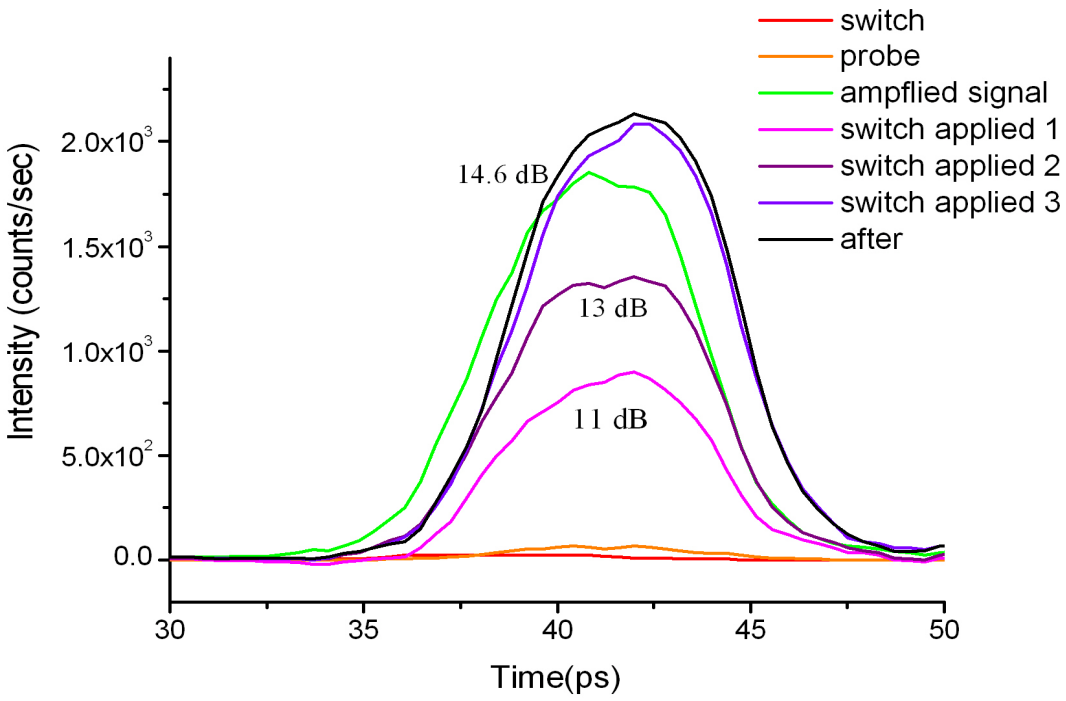

Figure 8.13: Switching of amplified light in MEH-PPV with a waveguide length of 222 μm. The amplification of the signal was switched off by 51 %. The *yellow line* is the unamplified probe, the *red line* is the switch pulse and the *green line* is the amplified probe. The *pink lines* are the multiple measurements of the amplified probe taken with the switch beam unblocked in consecutive order. The *solid black line* is the amplified probe after the switch is blocked. The probe, pump and switch energies were 0.04, 2 and 120 nJ respectively and the wavelengths were 630, 400 and 800 nm respectively.

consecutive measurements after that show the amplification recover even with the switch pulse still unblocked, indicating that switching was ineffective.

8.5 Discussion and conclusions

8.5.1 F8BT

Figure 8.14 compares the F8BT results at 50 kHz with those of similar waveguides of length 322 and 622 μm at 5 kHz. *The probe energy in both cases were the same at 0.04 nJ.* A waveguide length of 322 μm shows the same gain obtained at both repetition rates, this is shown in Figure 8.14(a). A waveguide of length 422 μm at 50 kHz is compared with a waveguide of length 622 μm at 5 kHz, shown in Figure 8.14(b). In this comparison (Figure 8.14(b)), results at 50 kHz have not reached saturation point and is still rising. However in both length of waveguides, the rise rate appears to be faster than with the 5 kHz repetition rate, which is clearer in Figure 8.14(a) than in Figure 8.14(b), is possibly because of the pulse widths. The pulse widths were ~ 0.3 and 10 ps for the 50 and 5 kHz repetition rates. It is probable that the faster rise is due to the shorter pulses experiencing the maximum population inversion at the peak intensity of the pump and probe pulses.

8.5.2 GP1302 and ADS233YE

High gain was not obtained with **GP1302** at 50 kHz. At a probe wavelength of 530 nm, high gain was not obtained due to ground state losses. Probing closer to the ASE peak, 570 nm, would have been better because at this wavelength there are lower ground state losses and higher net gain. However no gain was observed at a probing wavelength of 580 nm. **ADS233YE** showed gain when probed at 530 nm, however the gain obtained at 580 nm was not very high.

Gain characteristics measured subsequently, shown in Figure 8.15, at 5 kHz on ADS233YE showed that the pump energy densities used at 50 kHz were at the rising edge of the

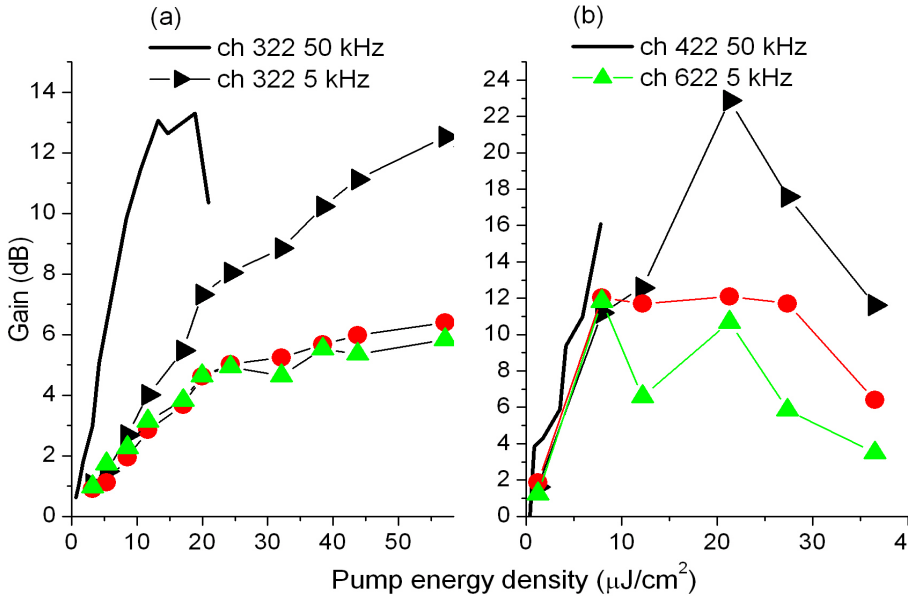

Figure 8.14: Amplification of light in F8BT with waveguide lengths of 322 (a) and 422 μm (b) (*solid lines*) at a repetition rate of 50 kHz with probe energy of 0.04 nJ. To compare with the amplification of F8BT at 5 kHz for waveguide lengths of 322 and 622 μm (*symbols*) are shown, which are the amplification of three pulses.

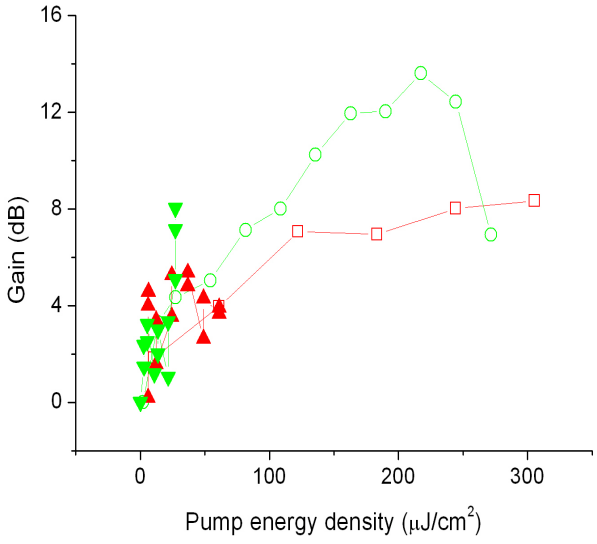

Figure 8.15: Gain curves for ADS233YE at a repetition rate of 5 kHz (*open symbols*) and 50 kHz (*closed symbols*) in waveguide lengths of 222 μm (*red symbols*) and 322 μm (*green symbols*).

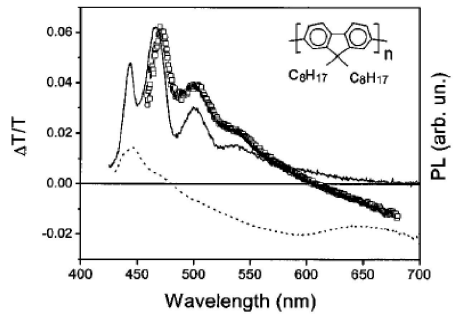

Figure 8.16: Transient transmission of PFO in film (*dotted line*). The remaining traces can be ignored [97].

gain curve. In order to get the necessary maximum gain with ADS233YE and GP1302, higher pump energy densities should have been used, as in Chapter 6 (176 μJ/cm^2). This was not the case because the gain for GP1302 had not been characterised for different pump energy densities at 5 kHz. The pump energy density used was considered appropriate at the time through comparison of the results using F8BT at 5 kHz where saturation occurred at pump energy densities in the range of 20 - 40 μJ/cm^2, the range explored with ADS233YE and GP1302 at 50 kHz.

The reason the gain obtained in ADS233YE was higher than in GP1302 was due to the excitation wavelength and the ratio of the PFO and F8BT units. In ADS233YE, the ratio of F8BT to PFO is 1:4. In GP1302, the ratio is 1:10. The pump wavelength of 400 nm would excite the PFO chromophores and it is possible that the probe wavelength, which overlaps with the absorption of the excited state of the PFO, is absorbed by the material. Figure 8.16 is the transient transmission of PFO film (*dotted line*) which shows the maximum of the photoinduced absorption is at 580 nm.

Amplification of light in **ADS233YE** at the probe wavelength of 530 nm, shown in Figure 8.6, had gain saturation at a lower pump energy density in the longer waveguide of length 622 μm. This was because the probe energy was increased to 0.12 nJ from 0.024 nJ. The latter energy was possibly being absorbed by the material and so, was insufficient to propagate to the output coupler. As a consequence, the higher probe energy would deplete the population inversion and lead to gain saturation at a low value.

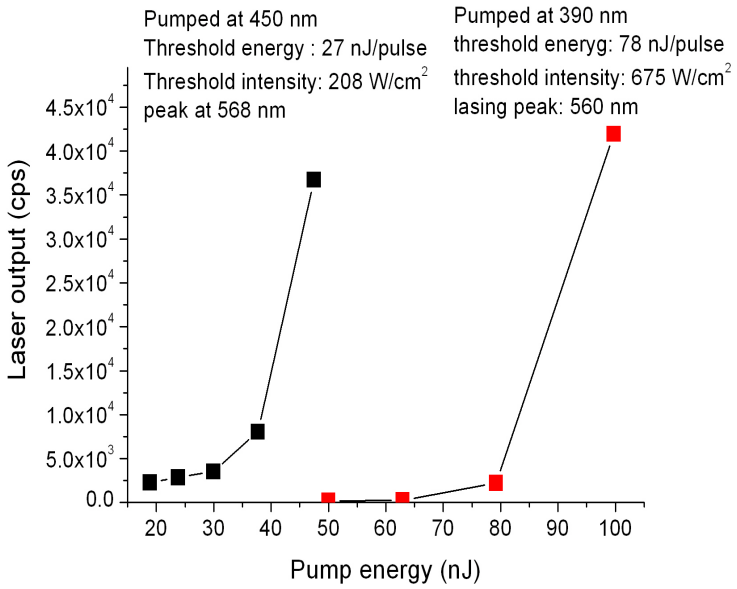

Figure 8.17: Laser output variation with pump energy. Pumping wavelengths of 450 nm (*black symbols*) and 390 nm (*red symbols*).

A higher probe energy was required for longer waveguide lengths than in the 5 kHz regime (0.04 nJ in 1 mm waveguide), possibly because there was reabsorption of the signal out due to the wavelength being within the PFO excited state absorption spectrum, as described earlier. Given that 0.024 nJ was sufficient for short waveguide lengths (< 600 μm), an increase in the waveguide length would then require an increase in energy of the probe.

Laser experiments had been conducted by a group member, Ying Yang, with ADS233YE using a ns OPO as a tunable excitation source. When the laser was pumped at 450 nm (within the F8BT region), the lasing threshold was 27 nJ/pulse. When pumped at 390 nm (within the PFO region), the lasing threshold was 78 nJ/pulse, both are shown in Figure 8.17. This threefold increase in threshold energy is consistent with the proposed role of excited state absorption in the fluorene-based amplifier. Moreover, the ASE measurement conducted on a 600 nm thick film of GP1302 at an *excitation wavelength of 400 nm*, shown in Figure 8.18, has, at the maximum available excitation energy of 27.7 μJ/cm^2, ASE just beginning to form and no line narrowing present at this point. Whereas F8BT and ADS233YE showed ASE thresholds at pump energy densities of 0.8 (Figure 5.4) and 3.25 μJ/cm^2 (Figure 8.5), pumped at 497 and 400

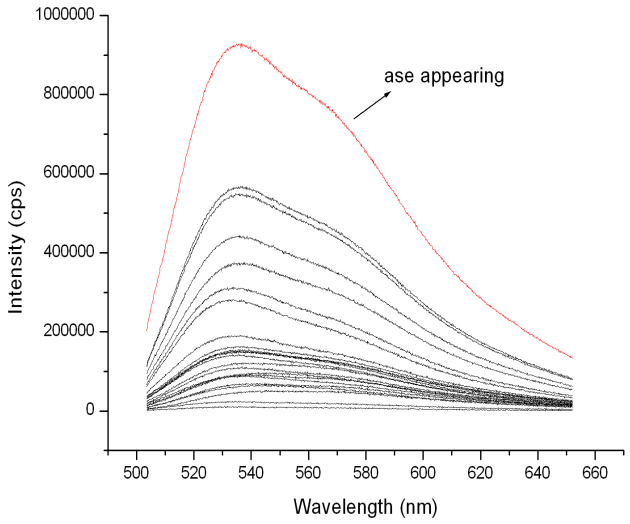

Figure 8.18: ASE of GP1302 excited at 400 nm.

nm respectively. A further indication that the excitation wavelength of 400 nm was inhibiting amplification of light in GP1302 more than ADS233YE. ASE measurements had not been conducted on GP1302 at 497 nm because the PL was similar to that of F8BT. Hence the ASE wavelength was assumed to be the same wavelength as F8BT. The strong amplification of light, with an excitation wavelength of 497 nm, as described in chapter 6 (for GP1302), showed that an excitation wavelength of 497 nm did not inhibit the gain in GP1302.

8.5.3 MEH-PPV

The gain cross-section calculated for MEH-PPV in this chapter is higher than that calculated in the 'Gratings based amplifier' chapter. This is because the lower probe energy allows for a more accurate measurement as it amplifies without depleting the population inversion and so would not affect the gain curve.

Furthermore, the gain values are much higher than those obtained in MEH-PPV in the longer waveguide lengths of 1 mm at 5 kHz. This is because a lower probe energy was used in the 50 kHz experiment. A lower probe energy would not deplete

the population inversion and thus does not limit the maximum obtainable gain. A higher probe energy depletes the excited state and hence result in a low gain maximum. At 5 kHz, in a 0.4 mm waveguide, the probe energy was 2 nJ and gave a gain of 2 dB at 2 μJ/cm^2. At 50 kHz, extrapolating the theoretical fit of the probe variation at 50 kHz in the 0.4 mm long waveguide (Figure 8.10), showed that at a probe energy of 2 nJ, the gain is (3 $\pm$ 2) dB, which is within the range of the value of 2 dB recorded at 5 kHz, indicating that the higher gain is because of the lower probe energy.

It was possible to switch the amplified signal in MEH-PPV up to 68 % which gave an extinction ratio of 3 - 5 dB. However this was followed by either long recovery possibly due to long live species at higher excited states or no switching with the switch beam still applied. In the latter, the amplification recovered, which is an indication that the material had not degraded. Given that the switching worked, as shown in Figure 8.12, it is an indication that the switching energy is effective, but not reliable, perhaps a higher switching energy would have been better. The results showed that MEH-PPV was not a suitable material for switching in this structure at the switching wavelength used of 800 nm.

8.5.4 Amplification and switching of all polymers

F8BT and MEH-PPV showed amplification of light without hinderance as was observed with GP1302 and ADS233YE. The gain curves were not oscillating as was with GP1302 and showed a smooth rise to saturation point with MEH-PPV giving a higher gain maximum than F8BT which has also been observed in the previous chapters. For the same probe energy of 0.04 nJ in a 422 μm long waveguide, F8BT and MEH-PPV gave gains of 16 and 22 dB respectively. In a 322 μm long waveguide, gains of 13 and 18 dB were obtained for F8BT and MEH-PPV respectively. The gain cross-section for both materials was calculated to be within the same order of 10^{-16} cm^2. However the gains obtained were very different, with one material showing much higher gain. This is because other factors, such as effect of excitation wavelength on material, behaviour of excitons in the material and material quality.

ADS233YE and GP1302 could have shown higher amplification if pumped much beyond the pump energy density regime of F8BT.

Switching of F8BT and MEH-PPV showed similar affect of ineffectiveness of the switch pulse on the gain. The results indicated the presence of long lived species and showed that consideration of the material structure is a requirement for optical switching of a conjugated polymer. Switching of ADS233YE was possible, but was low with an extinction ratio of 2.9 dB.

8.5.5 Amplifier operation at 50 kHz

At a 50 kHz repetition rate, the material would degrade very quickly, occurring in 5 - 10 minutes, whereas in the 5 kHz set up, degradation would occur after 40 minutes. However, the operational time at 50 kHz is equivalent to the same number of pulses as at 5 kHz.

The streak camera was used as it can take measurements very quickly. A scan took 2 seconds. Figure 8.19 shows PL measurements taken on continuous exposure up to 50 seconds for pump energy densities of 27, 19 and 13.6 μJ/cm^2 in ADS233YE. It shows that on continuous exposure below 27 μJ/cm^2, no degradation is observed up to 50 seconds, a time duration in which 25 scans could be taken at high pump energy (27 μJ/cm^2).

To conclude with the increase in the repetition rate, the operational time is reduced. This makes operation of conjugated polymers in the practical world a problem. To improve the performance of these devices, materials with longer operational times are needed.

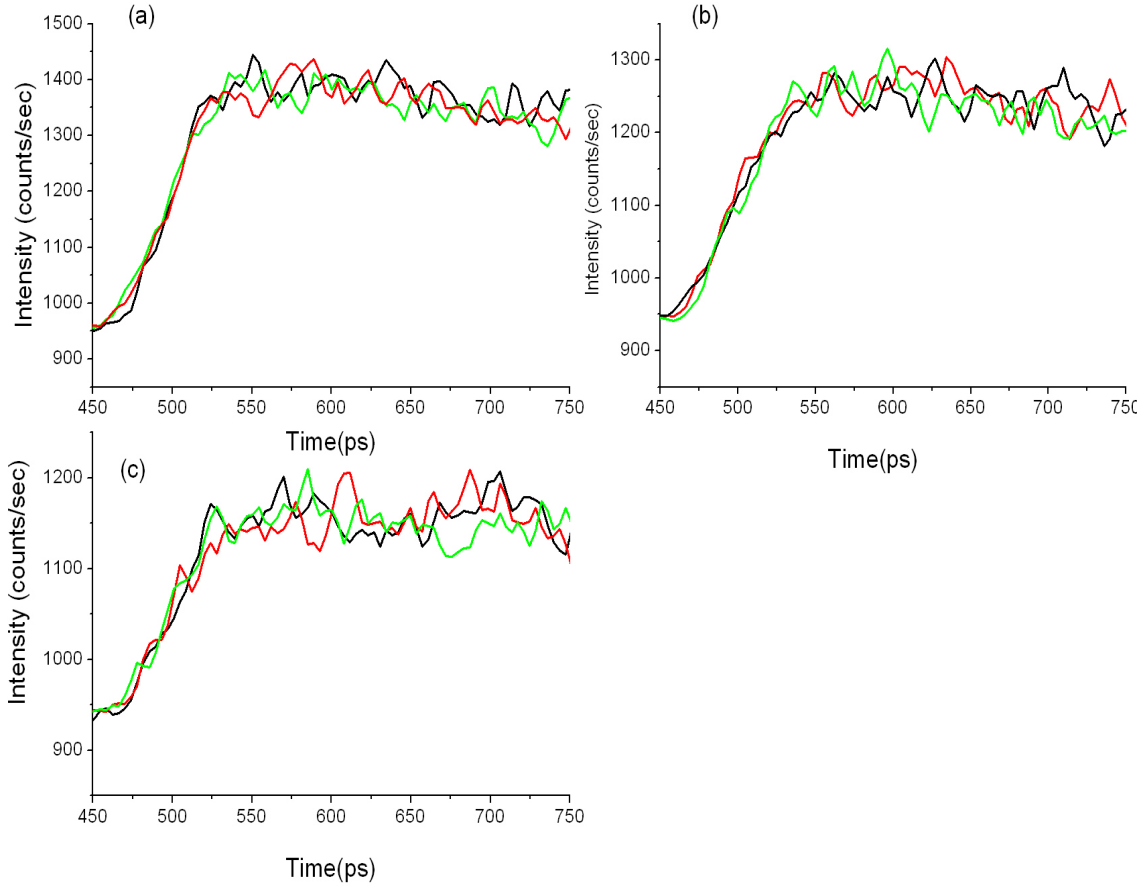

Figure 8.19: PL measurements taken for pump energies of (a) 27 μJ/cm^2, (b) 19 μJ/cm^2 and (c) 13.6 μJ/cm^2. The plots show measurements taken after 5 seconds (*red line*), 20 seconds (*black line*) and 50 seconds (*green line*).

Chapter 9

Waveguide amplifier

Conjugated polymers have been shown to be attractive gain media for optoelectronic devices due to their high gain over broad bandwidths [40, 61–66, 161], simple processing techniques and potential to be electrically pumped [62, 70, 71]. In this thesis, much of the amplifier work had been conducted with a grating based amplifier [43, 69]. For real world applications however, a compact structure would be more suitable, where coupling angle is not an issue. The structures were ridge waveguides etched into an inorganic layer which was 2.2 cm long. They were supplied by Cambridge University, who had them commercially manufactured. The waveguides were designed in Cambridge and tested at Imperial College London. Tests showed 26 dB amplification in a 1.2 cm long device using a polymer blend of PMMA doped with the laser dye, Rhodamine 6G [73]. Apart from compact device structure, it allows to test the conjugated polymer performance with longer waveguides which would be desirable.

9.1 Waveguide structure

The waveguides consisted of a layer of silica doped with germanium (n = 1.4556) on top of a layer of silica (n = 1.4456) both of which were evaporated onto a silicon

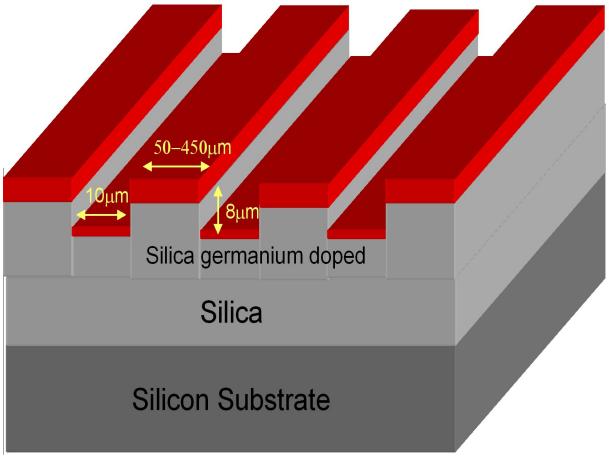

Figure 9.1: Schematic of waveguides. A layer of germanium doped silica on a silicon substrate. The waveguides of varying widths were etched onto the top layer. The red layer on the diagram is the polymer spin coated on top of the structure.

substrate which was 2.2 cm long and 0.5 cm wide. Figure 9.1 shows a schematic of the waveguides, which were etched into the doped silica by reactive ion etching. Waveguides were etched to a depth of 8 μm with varying widths; 50 μm to 450 μm.

Figures 9.2, 9.3 and 9.4 show images taken with scanning electron microscopy (SEM) of the polymer spin coated on the waveguide. The polymer was spun at 5000 and 2500 rpm. The images show that there is deposition of the polymer on the ridge and in the trough of the waveguides. Clearer images were not possible as the waveguide was conductive and the substrate was charging, making it harder to distinguish between polymer and substrate. Even at high spin speeds of 5000 rpm, the troughs had filled up with a layer of polymer. This indicated that for ridge waveguiding of thick polymer films, there is no guarantee that light coupled into the ridge does not spread into the polymer layer in the trough.

The light was end coupled into the polymer. End coupling into polymers is problematic because the facets have to be smooth and this is not possible with polymers. At the facet end polymers tend to form a bead which could scatter light back instead of allowing transmission through. Figure 9.5 shows this bead formation, taken by SEM. The waveguide structure avoids this problem due to the doped layer of silica. Light is coupled into the doped silica and is waveguided down the length of the guide. The evanescent wave of the light in the waveguide would couple into the higher refractive index polymer which was spin coated on top of the waveguide. The polymer

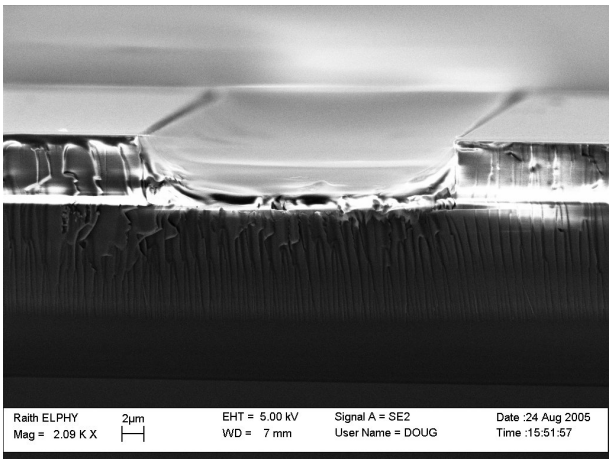

Figure 9.2: SEM image of polymer spin coated on top of the waveguides. The image shows the polymer in the trough.

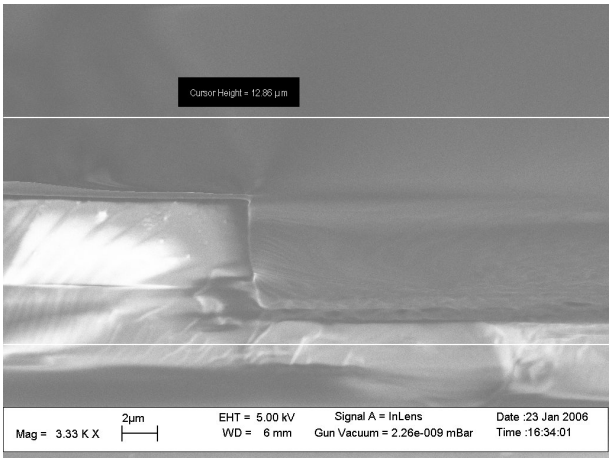

Figure 9.3: SEM image of polymer spin coated on top of the waveguides. The image shows a layer of the polymer on the top of the ridge.

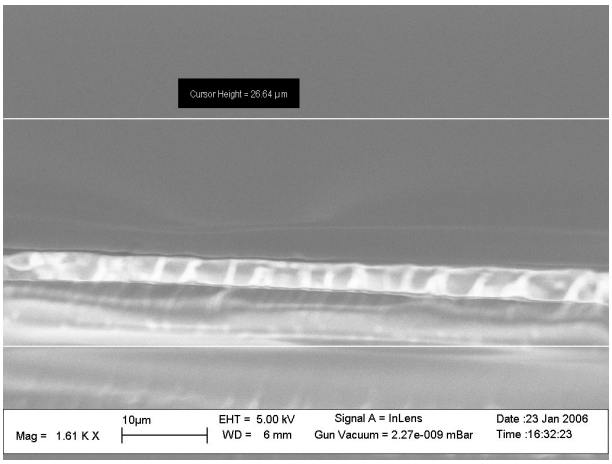

Figure 9.4: SEM image of polymer spin coated on top of the waveguides. The image is zoomed in on the ridge of the waveguide. It shows a layer of polymer spin coated on the ridge.

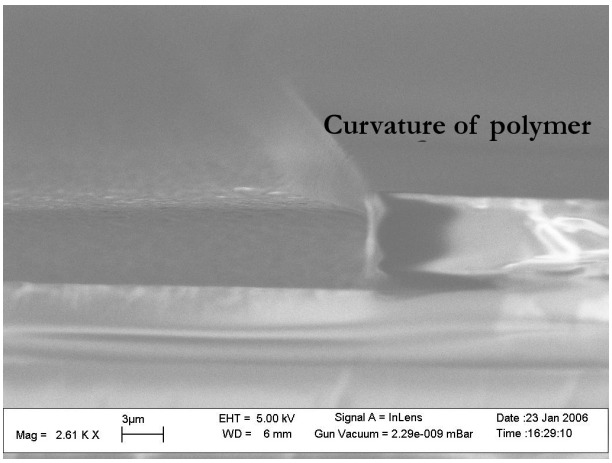

Figure 9.5: SEM image showing polymer on waveguide. On the left hand side of the image is the trough with polymer deposited. In the image, one can see that the polymer at the edge is not flat but shows a 'bump.'

is optically pumped from the surface.

9.2 Materials

The materials used were the conjugated polymers MEH-PPV (n = 1.755 at 630 nm) and F8BT (n = 1.9 at 580 nm). The MEH-PPV solution was made to a concentration of 6 mg/ml in chlorobenzene. This was spin coated on to the waveguide at 1250 rpm for 40 seconds which formed a film thickness of 100 nm. The F8BT solution was made in toulene. The film thicknesses of F8BT were varied to 600, 490, 250 and 160 nm using a combination of different concentrations and spin speeds all for 40 seconds and is summarised in the table below.

Film thickness (nm)	concentration (mg/ml)	spin speeds (rpm)
600	50	1000
490	50	2500
250	30	1000
160	30	2500

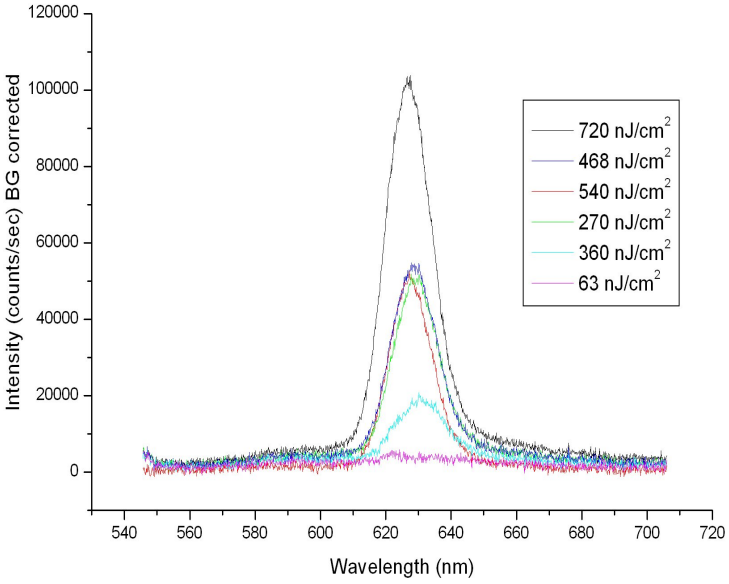

Figure 9.6: PL and ASE spectra of 100 nm thick film of MEH-PPV spin coated on waveguides.

9.3 ASE in waveguides

Figure 9.6 shows ASE spectra for varying pump energy densities of MEH-PPV spin coated on the waveguide structure. The ASE and PL peaks form at 630 and 626 nm respectively. A film thickness of 100 nm was used as it was a suitable thickness for waveguiding and demonstrated good amplification.

9.4 Experimental setup

The input was from the OPA which was seeded by the 'Hurricane' regenerative 5 kHz amplifier. The output from the OPA contained two different wavelengths; one for pump and one for probe. They were inter-connected in the OPA such that tuning one would tune the other. The pump was sent to a delay stage and through a chopper, chopping at 2.5 kHz. The set up was built to couple the probe from the end facet. The probe was coupled into the waveguide with a 20x microscope objective and coupled out using either a 8x or 3.75x microscope objective as shown in Figure 9.7. The microscope objectives had short working distances of < 2 cm. This required

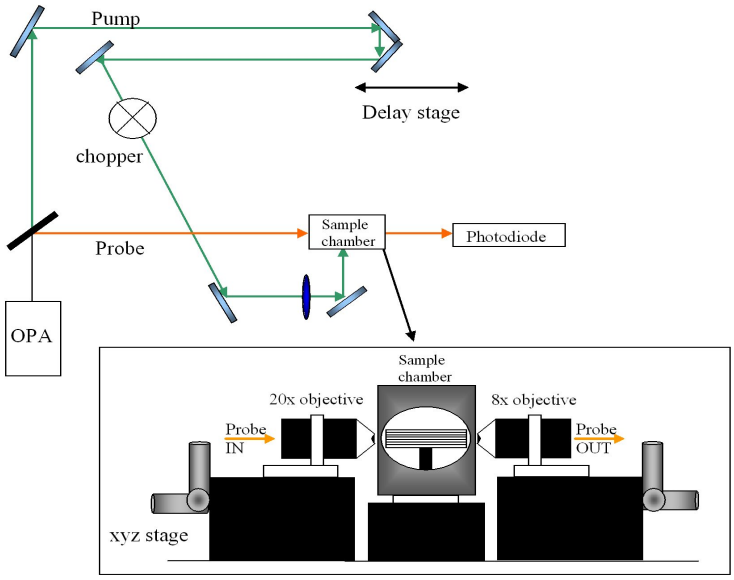

Figure 9.7: Schematic of experimental setup for wave guide and an enlargement of the optics to couple into and out of the waveguide.

the end facets of the waveguide to be close to the microscope objective.

Excitation of the polymer was from the side window. The double windowed, sample chamber had to be modified as three windows were required. The output was recorded using lock-in amplifiers via a photodiode. Once time zero was calculated approximately, the exact time zero was searched by scanning the delay stage and measuring the traces for amplification.

9.4.1 Transmission cross-section

Optical transmission measurements were conducted on the waveguide spin coated with MEH-PPV and rhodamine 101 (shown in Figures 9.8 and 9.9) and F8BT (Figure 9.10). This experiment showed that there was a peak transmission point within the guide and also the maximum transmission possible. Light was coupled into one facet with a 20x microscope and coupled out with an 8x microscope for MEH-PPV and 3.7x with F8BT. The power was recorded at the other end of the waveguide with a power meter via photodiode. Power output measurements were taken for different positions of the input beam on the side facet. These positions were determined in

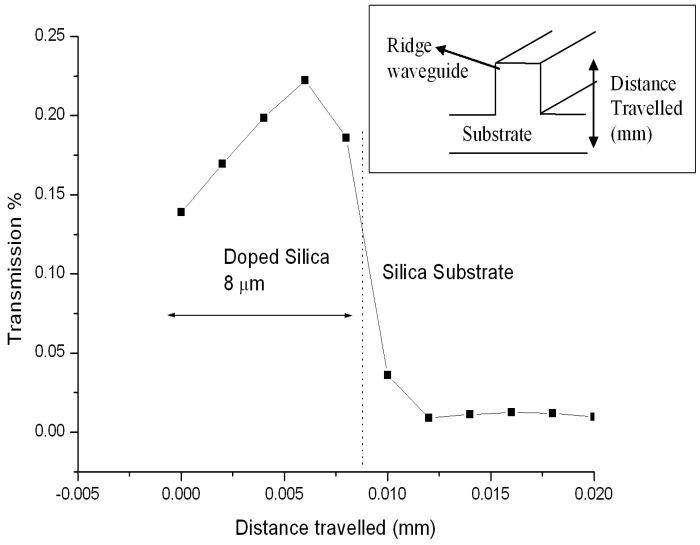

Figure 9.8: Transmission of light through waveguide spin coated with a layer of MEH-PPV and 20 % rhodamine 101. The inset shows the ridge waveguide.

relation to the readings on the micrometer on the xyz stage on which the microscope was placed. The laser used was a He-Ne at 633 nm. With MEH-PPV a maximum transmission percentage of 0.25 to 0.8 % was obtained. With F8BT, this was lower: 0.098 %. For both materials, the transmission wavelength, 633 nm, was within the PL spectra.

9.5 Experiment

The experiments were conducted with MEH-PPV, MEH-PPV blended with Rhodamine 101 and F8BT. Initial experiments were conducted with MEH-PPV, this was moved onto a blended film of MEH-PPV with Rhodamine 101 because results from neat MEH-PPV films were poor, and then onto F8BT.

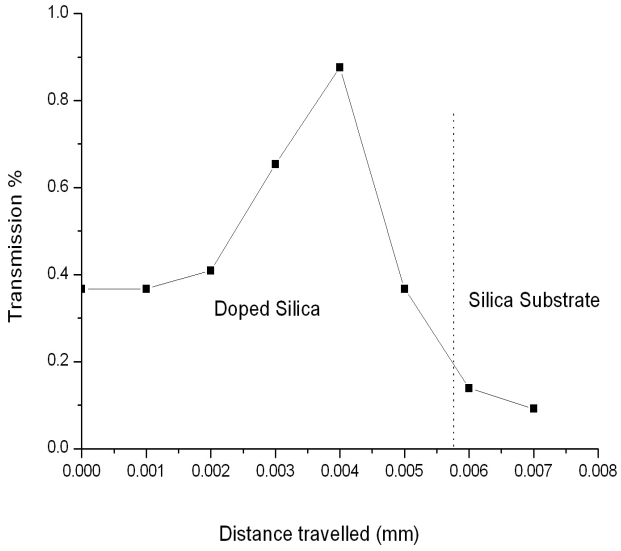

Figure 9.9: Transmission of light through waveguide spin coated with a layer of MEH-PPV and 20 % rhodamine 101.

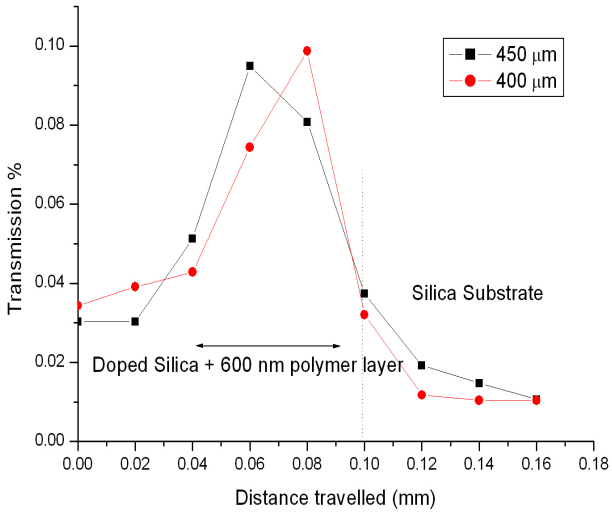

Figure 9.10: Transmission of light through waveguide spin coated with a layer of F8BT.

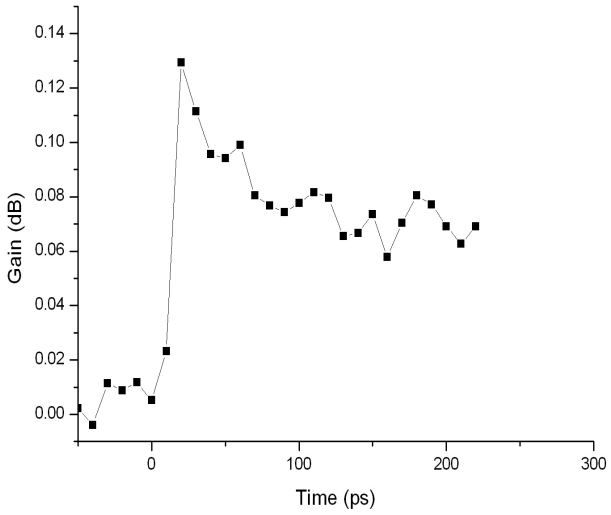

Figure 9.11: Time dynamics of MEH-PPV spin coated on waveguide. A pump energy of 0.31 μJ/cm^2 was used with a probe energy of 0.8 nJ. Gain of 0.13 dB.

9.5.1 MEH-PPV

The material was excited at 500 nm. Figures 9.11 and 9.12 show the gain obtained from neat MEH-PPV spin coated on the waveguide. The waveguide width was not recorded for this measurement. It was a difficult task to find the probe output due to the strong scatter in the same direction as the probe and any increase in the probe power to search for this signal, would mean that the gain would be weaker. This was a problem because I would not be able to see a rise in output during scans to find time zero. Any gain obtained was very low with the highest value being 0.13 dB.

The solution to this problem was to blend the neat conjugated polymer with a dye. The reasons for blending were because:

1). The gain lifetime at high pump density of MEH-PPV is shorter than the time taken to travel along the waveguide. Time taken to travel the 2.2 cm is 129 ps. The gain lifetime of MEH-PPV at high gain is 48 ps, so it is probable that the light would only be amplified in part of the waveguide.

2). Blending would reduce any re-absorption effects as it would move the emission

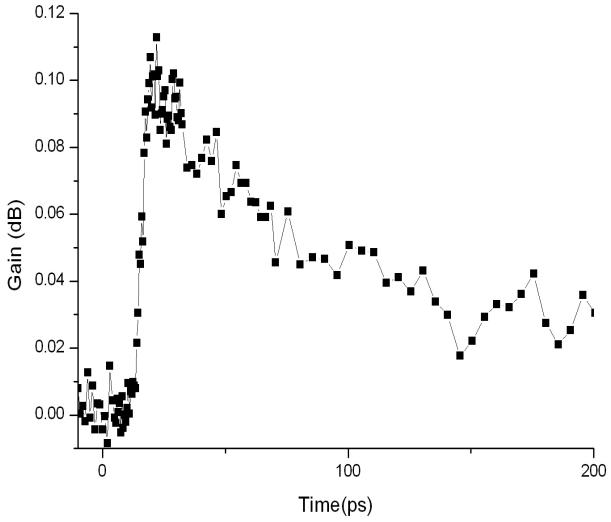

Figure 9.12: Time dynamics of MEH-PPV spin coated on waveguide. A pump energy density of 0.31 μJ/cm^2 was used with a probe energy of 4 nJ. Gain of 0.10 dB was obtained.

wavelength further from the excitation region.

3). The longer waveguide would have lower annihilation, because pumping a larger area would allow for high pumping energies to be used without annihilation effects as the chromophores are further apart but blending would further reduce any annihilation effects as it will space the chromophores further.

Figure 9.13 shows the absorption and emission spectra of MEH-PPV and MEH-PPV blended with different concentrations of Rhodamine 101. The rate of energy transfer to the dye increased with the increase in the dye concentration, and is shown by change in PL lifetime from 18 ps to 4 ps, shown in Figure 9.14. However measurements showed no improvement to the gain. F8BT was used later on because it was known to be a high gain conjugated polymer with less overlap of the absorption edge on the emission spectrum and has a longer gain lifetime at higher pump energy densities.

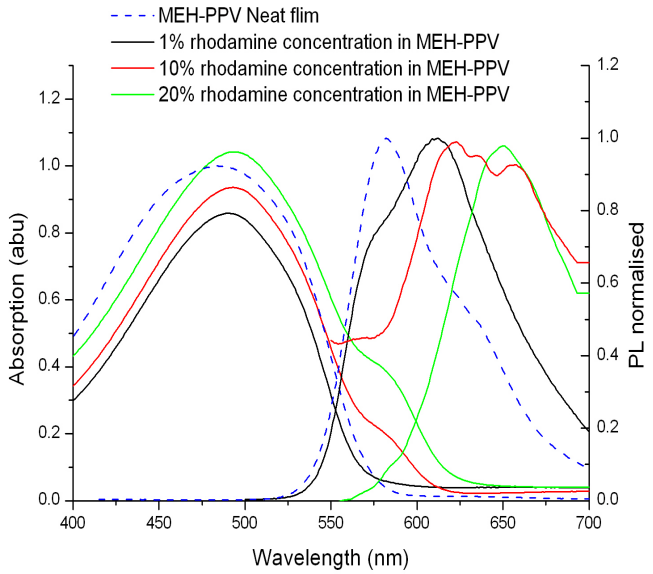

Figure 9.13: Absorption and emission spectra of MEH-PPV neat film and blended with different concentrations of Rhodamine 101.

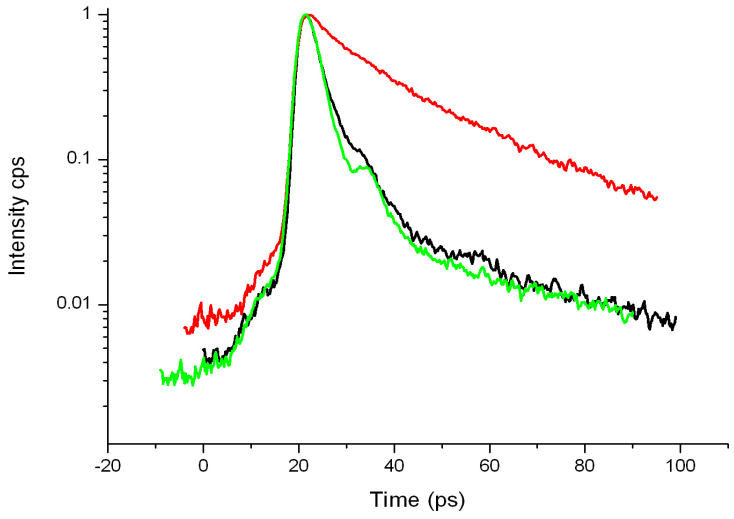

Figure 9.14: Lifetime of emission of MEH-PPV blended with concentrations of rhodamine 101 at 1, 10 and 20 %, represented by the *red*, *black* and *green line*. Excitation was at 500 nm and detection wavelength was at 580 nm.

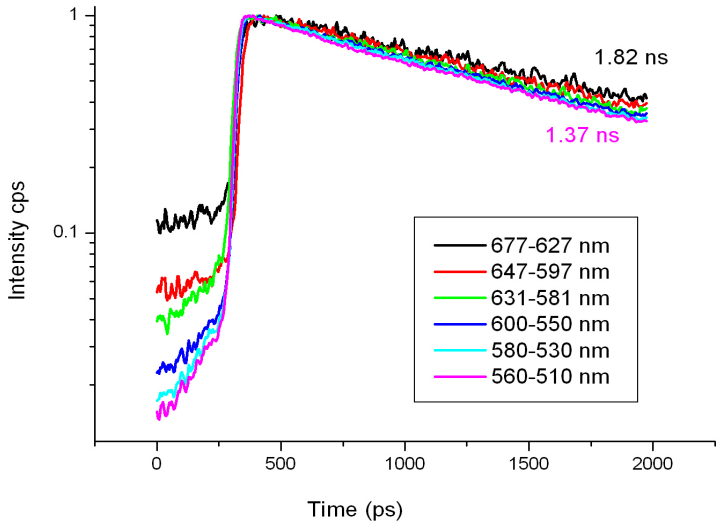

Figure 9.15: Time resolved fluorescence of F8BT in a spectral window of 510 nm to 677 nm. A minimum and maximum lifetime of 1.37 and 1.82 ns respectively were recorded and is labeled in the plot.

9.5.2 F8BT

F8BT had been demonstrated as a good gain material in previous chapters and was tested with the waveguide structure. The PL lifetime of F8BT was measured with the streak camera with concentrations of 50 mg/ml, spun at 1000 rpm to form a 600 nm thick layer. Figure 9.15 shows the PL lifetime measurements taken using the streak camera. PL lifetimes of 1.5 to 1.8 ns were measured in a spectral window of 510 to 677 nm.

Gain dynamics were measured for three probe wavelengths; 580 , 650 and 690 nm. Some of the traces are shown in Figures 9.16, 9.17 and 9.18. Figure 9.19 shows the range of pump powers used for a probe and pump wavelength of 650 and 497 nm respectively. The pump wavelength varied slightly with the probe wavelength because the beams were taken from the OPA system in which both pump and probe beams were interlinked.

It was problematic to obtain good waveguiding with the thick, 600 nm, polymer. The film quality was not uniform and the probe light would scatter as it attempted to propagate down the waveguide. A large thickness of 600 nm was chosen because

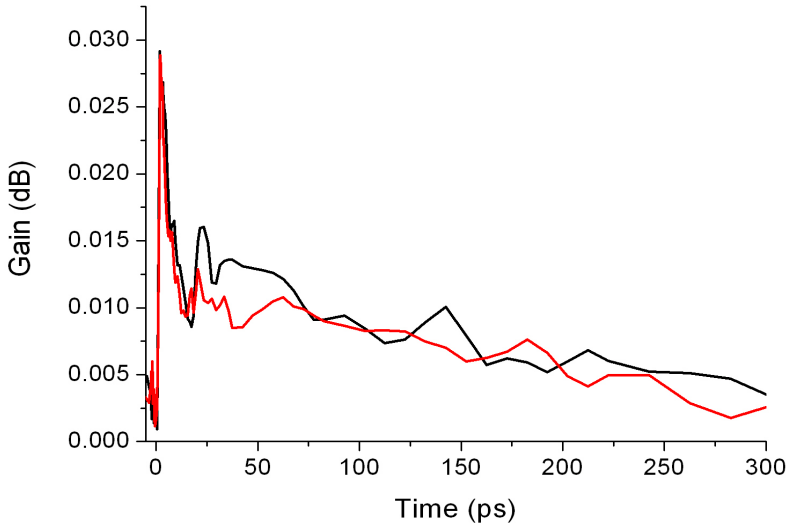

Figure 9.16: Time dynamics of the gain in F8BT with a thickness of 600 nm, pumped at 507 nm and probed at 690 nm. Pump energy density of 1.23 μJ/cm^2.

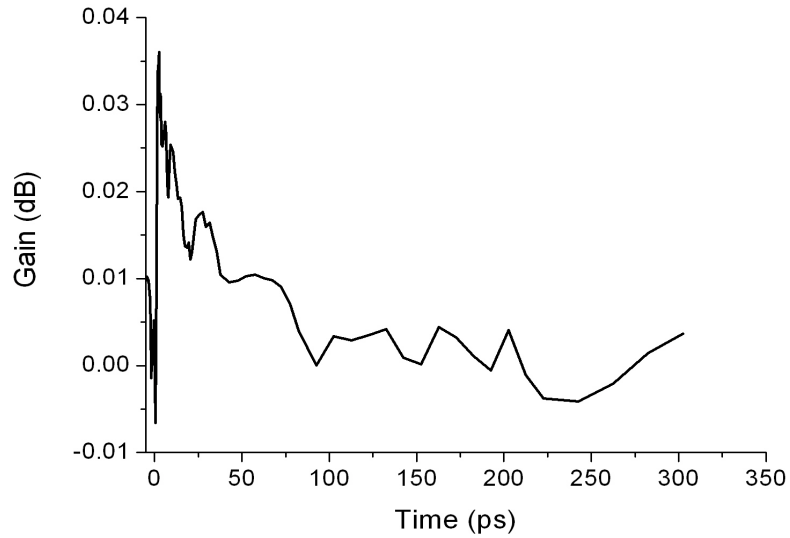

Figure 9.17: Time dynamics of the gain in F8BT with a thickness of 600 nm, pumped at 497 nm and probed at 650 nm. Pump energy density of 0.544 μJ/cm^2 and probe energy of 8 nJ.

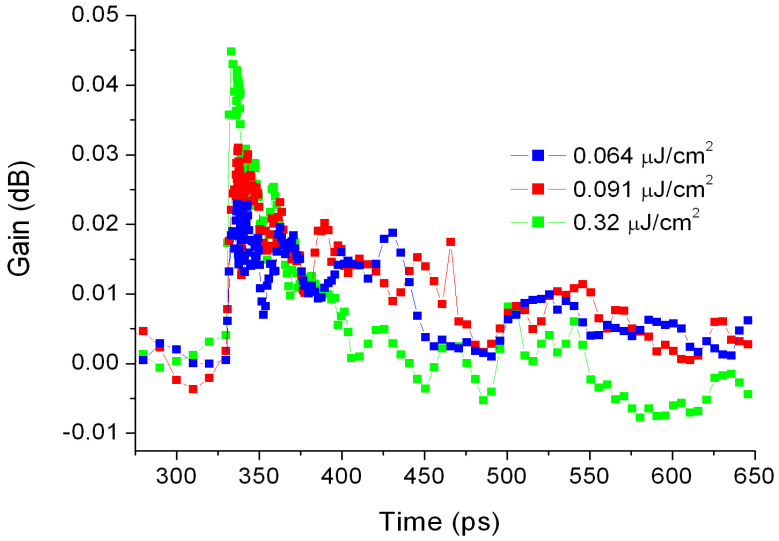

Figure 9.18: Time dynamics of the gain in F8BT with a thickness of 600 nm, pumped at 475 nm and probed at 580 nm. Probe energy of 5 nJ.

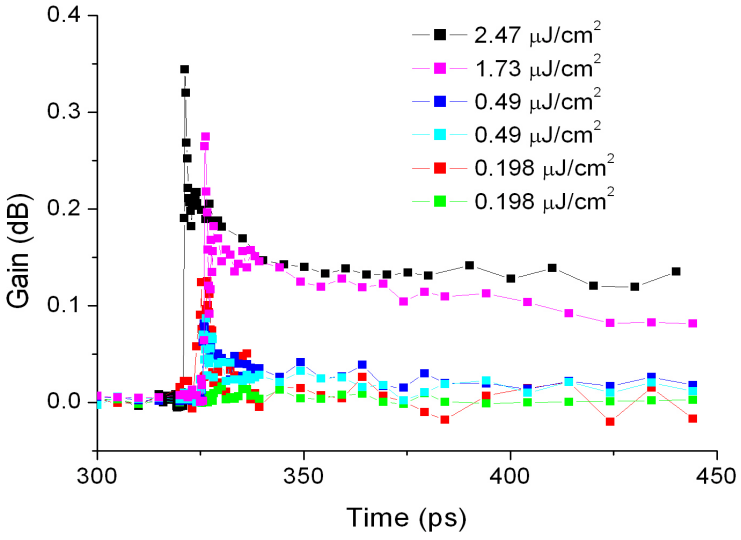

Figure 9.19: Time dynamics of the gain in F8BT with a thickness of 600 nm, pumped at 497 nm and probed at 650 nm for different pump energy densities displayed in the legend. Probe energy was 4 nJ.

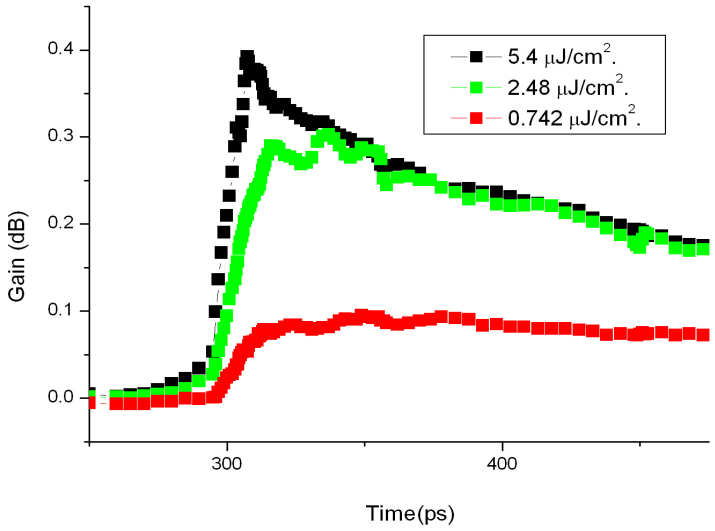

Figure 9.20: Time dynamics of the gain in F8BT pumped at different pump powers. Thickness of film was 490 nm. Pump and probe wavelengths were 485 and 600 nm respectively. The width of this waveguide was 50 μm. Probe energy was 0.8 nJ. The pump energy densities are displayed in the legend.

work carried out by Imperial College used a large thickness of 1 μm. The thickness was gradually reduced from 600 nm to 490, 250 and 160 nm to have a compromise between having a suitable thickness for amplification and uniformity. Figure 9.20 shows the gain dynamics in F8BT for a thickness of 490 nm. These measurements were taken with a waveguide width of 50 μm. Although the measurements do not show a wide variety of pump powers, they were taken to establish whether the thickness and probe/pump wavelengths were apt to give gain. The maximum gain achieved was 0.4 dB, which is not high at all, but is higher than that obtained with MEH-PPV in the waveguides. This was a promising step in the desired direction. The gain obtained in waveguides of different width was also observed and compared.

Figure 9.21 shows the gain variation for waveguide widths of 50 μm and 450 μm for the same probe energy of 0.8 nJ. At a higher probe energy of 1 nJ, the wider waveguide gave the same maximum gain as the narrower waveguide of 0.4 dB. Figure 9.22 shows this result. For a probe energy of 0.8 nJ, the gain obtained in a 450 μm waveguide was slightly lower, however on increasing the probe power for the same width (Figure 9.22) the same gain was obtained. The stronger signal gave a gain higher by 0.05 dB, which would be attributed to better film quality. The results

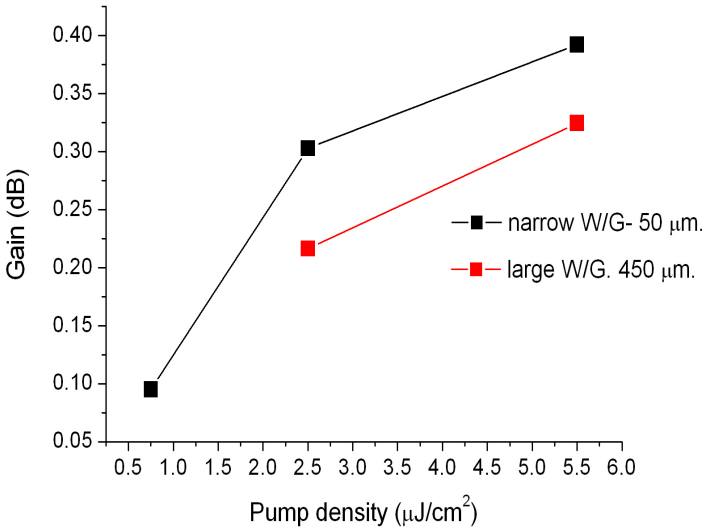

Figure 9.21: Gain for the respective pump energy densities. Film thickness was 490 nm and it was pumped at 484 nm and probed at 600 nm. Probe energy was 0.8 nJ.

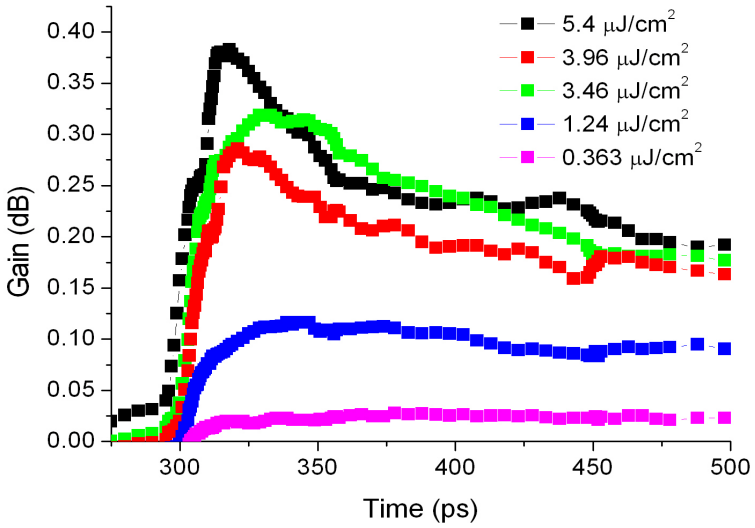

Figure 9.22: Gain dynamics for the respective pump energy densities shown in the legend. Film thickness was 490 nm and pumped at 485 nm and probed at 600 nm. The width of the waveguide was 450 μm. Probe energy was 1 nJ.

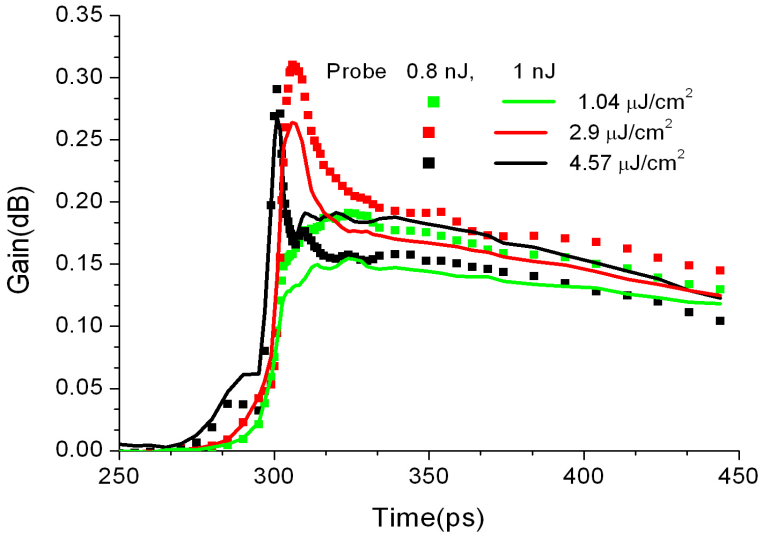

Figure 9.23: Gain dynamics for a film thickness of 160 nm. The *symbols* show the gain dynamics with a probe energy of 0.8 nJ and the *lines* show the gain dynamics for a stronger probe energy of 1 nJ. The drop in the gain at the pump energy density of 4.6 μJ/cm^2 with a probe energy of 0.8 nJ is because the gain has gone past the saturation point and depleted. A pump and probe wavelength of 485 and 600 nm was used. The pump energy densities are given in the legend.

showed that the amount of gain obtained did not depend on the width of the waveguide. This was possibly because gain was obtained from polymer in the trough as well as in the ridge. The pump energy density remained the same for the different waveguide widths because it was focussed to the focal point of the lens, $\sim$ 1 mm, to obtain a stripe which was narrow enough to overlap with the waveguides. The probe would have spread into the polymer in the troughs, hence allowing for the same amount of gain to be obtained even though the probe was coupled into different waveguides.

A further reduction of the film thickness was carried out. The thinner film had a uniform coating, showed less scattering of light, had better beam guiding and the penetration depth would be through the whole film and not the first few nanometers. Figure 9.23 shows gain dynamics for a film thickness of 160 nm. Figure 9.24 shows the gain dynamics for probe powers of 0.52, 0.8, 1 and 4 nJ. They show that the gain increased with a reduction in the probe power, except for a probe power of 13 μJ. The same waveguide was used to keep consistency, hence the drop in gain on the weakest probe was due to degradation of the polymer. The line narrowing effect seen indicates that the pump energy density is past ASE threshold. However, there was still

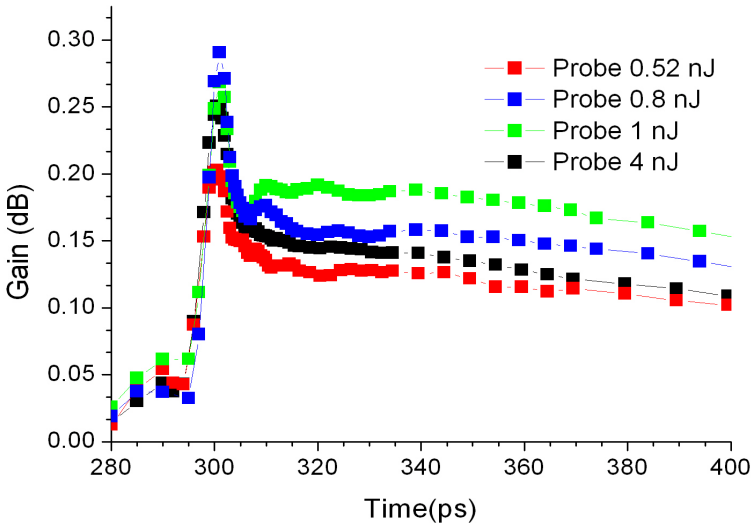

Figure 9.24: Gain dynamics for different probe powers (shown in the legend) on a 50 μm wide waveguide. Pump energy density of 4.57 μJ/cm^2. Film thickness of 160 nm.

no high gain. The highest obtained so far was with F8BT at 0.39 dB. Line narrowing indicated that there is sufficient power to provide gain. However there was still no amplification due to the strong probe energy. In order to reduce the probe energy, the propagation losses need to be reduced. The probe energy should not be increased because it would deplete the population inversion, leading to fast gain saturation and a low maximum gain value.

To try to solve this mode simulations were conducted. They showed that in a thick film of 1 μm, the TE_0 mode would be more confined in the film than in a thinner film. However the mode was positioned in the centre of the film and not close to the substrate or surface, resulting in a low probability of overlap with the pumped region. Moreover the thicker films showed more scattering of the probe light.

The thinner film would have a higher probability of overlap between the propagating mode and the excited region. Moreover the propagation in the waveguide was an evanescent wave through the substrate. This meant that the mode would be closer to the substrate due to the design of the waveguide structure. As pumping could only be done through the surface, a thin film would allow better overlap of the pumped region and the propagating mode. The mode position of a film of 160 nm and 1 μm

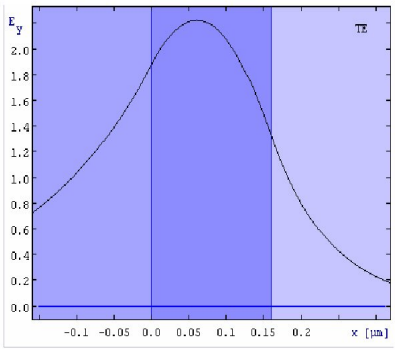

Polymer thickness of 160 nm with a refractive index of 1.8
Substrate refractive index of 1.4556.
The centre of the fundamental mode is closer
to the substrate.

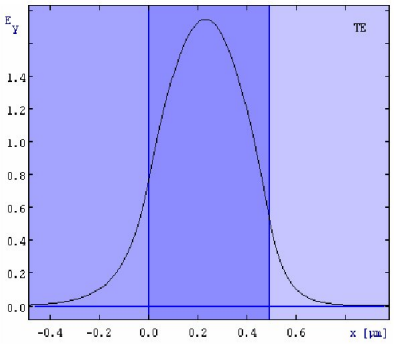

Polymer thickness of 490 nm with a refractive index of 1.8
Substrate refractive index of 1.4556

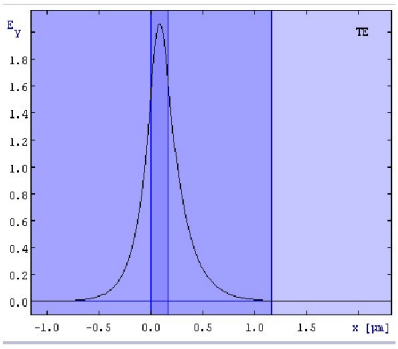

1 μm of PMMA on top of polymer
Polymer thickness of 160 nm with a refractive index of 1.8
Substrate refractive index of 1.4556

Figure 9.25: Top Left: Fundamental TE_0 mode for F8BT thickness of 160 nm Top Right: F8BT thickness of 490 nm. Bottom: Fundamental mode with 1 μm layer of PMMA on top of 160 nm film of F8BT.

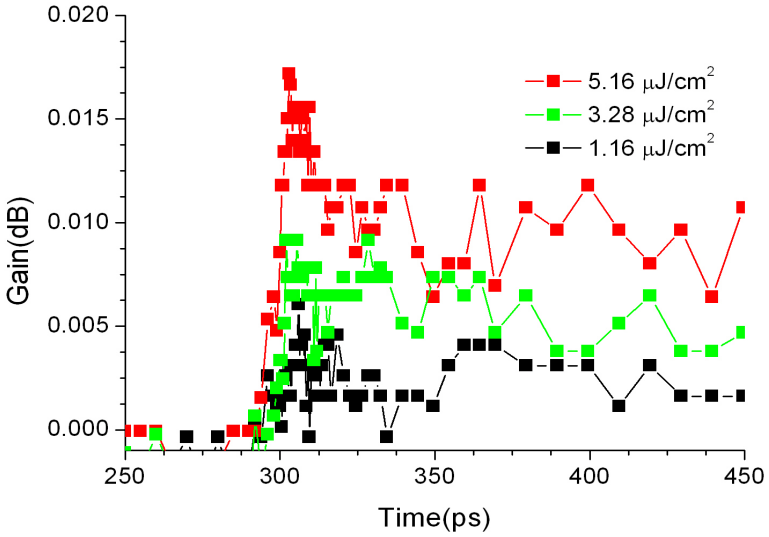

Figure 9.26: Gain dynamics with PMMA spin coated on a layer of F8BT. The waveguide width was 50 μm. The F8BT was 250 nm thick.

thicknesses are shown in the top left and right of Figure 9.25 respectively. Moreover if a layer of PMMA, which has a lower refractive index than the polymer, was used, the light scattered from the polymer surface can be reflected back into the polymer through total internal reflection and reduce the amount of light lost. The TE_0 mode for this configuration is shown in the bottom of Figure 9.25. A layer of PMMA, thickness of 1 μm, was spin coated on a 250 nm thick layer of F8BT. This experiments gave gains < 0.4 dB, shown in Figures 9.26 and 9.27.

9.6 Conclusion

Line narrowing of the amplified signal was observed, and was an indication of ASE. The maximum available pump energy density was $\sim 5\ \mu J/cm^2$, which was within the amplification regime of the polymer as shown in Figure 5.11, another indication that there was sufficient pump energy for amplification. However, before ASE appeared the amplification was low, less than 1 dB in MEH-PPV. The low gain obtained from MEH-PPV led research work into other suitable polymer devices with longer gain lifetimes at high pump densities and onto the waveguide structure and hence the

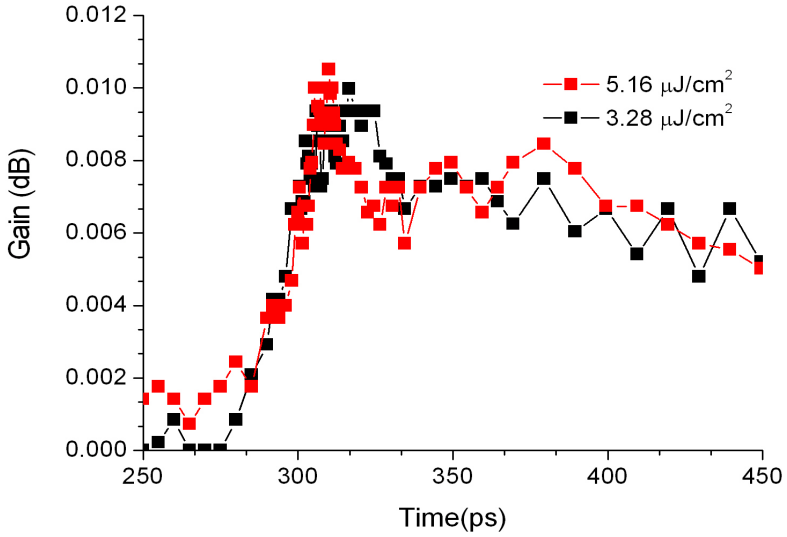

Figure 9.27: Gain dynamics with PMMA spin coated on a layer of F8BT. The waveguide width was 450 μm. The pump and probe wavelengths were 485 and 600 nm.

waveguiding modes. F8BT was used as it had also demonstrated high gain properties. With a combination of a long gain lifetime and analysis of the waveguiding modes, twice the gain was obtained. This was an indication that the work was progressing in the correct direction, however the gains obtained were still extremely small.

The waveguide appeared not to work with the conjugated polymers. The transmission measurements showed that the transmission efficiency of the probe was very low, < 1 %. The low transmission would result in a weak probe beam propagating down the waveguide. The amplified probe beam would be strongly *attenuated* through the waveguide, resulting in the weak amplification value obtained. In order for this experiment to be successful, less lossy waveguide structures would need to be designed.

Chapter 10

Conclusion

This thesis has investigated the potential of conjugated polymers as optical polymer amplifiers, suitable to operate in the visible regime for POF networks. POF networks would require devices to amplify the optical signals to compensate for transmission and splitting losses in the network, similar to the role of SOAs and EDFAs in the silica fiber networks. Polymer optical fibers have been experimentally developed for several years and have shown bandwidths of up to 2.5 Gb/s over 500 m [25] with high attenuation losses of up to 50 dB/km. Many projects have also been undertaken to demonstrate POF operation in real world applications. For example, Keio University have been successfully running a 1 Gb/s POF network for about 7 years [162], connecting four buildings on campus. In June 2007, Siemens announced that they had developed and tested a POF cable transmitting data to a television set [163]. The cable was 100 m in length and had a bandwidth of 1 Gb/s. The optical signal was modulated similar to a Digital Subscriber Line (DSL) and was successfully transmitted to the television set without error or screen flickering. Such demonstrations have shown POF to be a capable transmission medium for short haul applications with high bandwidth at low cost.

The work presented in this thesis was performed as part of the Ultrafast Photonics Collaboration (UPC). The aim of the UPC was to investigate physics and materials for ultrafast data communications. The UPC focussed on quantum dots, photonic

crystals, inorganic and organic lasers, organic amplifiers and the characterisation and development of inorganic and organic materials. Prior to the UPC there was no work conducted on conjugated polymer optical amplifiers. During the course of the UPC, work had been conducted in solution based conjugated polymer amplifiers [67, 72], which lead onto solid state organic amplifiers [43, 68, 69] as they were more inconvenient to integrate. Prior to commencement of this work, work had been conducted on conjugated polymer based solid state lasers [161] and solution based amplifiers [67, 72]. A project had been conducted in a collaboration with Imperial College London on a solid state conjugated polymer amplifier based on the material Red-F. From this a gain of 18 dB in a 300 μm waveguide was obtained [68].

In the present work, further investigation into organic amplifiers progressed to demonstrate conjugated polymer amplifiers in longer waveguides. Amplification was demonstrated in a waveguide 700 μm longer. A gain of 21 dB was obtained with MEH-PPV [43] in a 1 mm waveguide. The annihilation rate of MEH-PPV was calculated to be 3 x 10^{-9} cm^3/s and the gain cross-section was calculated to be 4 x 10^{-17} cm^2. Similar experiments were also conducted with F8BT and a gain of 17 dB was obtained with a 1 mm long device.

As data is not a single pulse, but streams of pulses, the potential to amplify multiple pulses was explored. The data sequence was created optically by splitting the probe beam, which produced multiple probe beams representing a burst of data pulses. The amplification of each probe pulse needed to be uniform, the success of this depended on the gain lifetime of the material. MEH-PPV was a high gain conjugated polymer, it however showed fast decay at fairly high pump energy densities. This was an issue as it would heavily reduce the uniformity of the amplification. F8BT was found to give a suitably longer gain lifetime at similar pump energy densities and high gain. Amplification of 23 dB (peak 1) was obtained in a 1 mm long waveguide. The number of pulses in the sequence was limited to three, to produce uniform amplification, however the experimental arrangement could produce up to seven pulses. The amplification of the longer pulse sequence was uneven.

This work progressed onto switching of the amplification in the pulse sequence. Switching was not effective with F8BT, a maximum of 50 % reduction on the amplified pulse was possible. This was possibly because there was energy transfer of the switch pulse to defective sites, which reduced the effect of the switch pulse on the

amplified signal. This problem was avoided by using a co-polymer. The F8BT chromophores would be excited, leaving the PFO molecules to act as spacers to reduce any quenching. This allowed switching up to 70 % of the signal and had an ultrafast recovery of 2 ps indicating the absence of long lived species.

Switching was also obtained in a laser of the conjugated polymer Red-F [131]. Lasing wavelengths used were 498 nm and 1.3 μm, 492 nm and 1.28 μm which had lasing wavelength and thresholds of 675 nm, 18 nJ/pulse and 692nm, 25 nJ/pulse respectively. Switching was successful for weak switch and high pump energies of 50 and 200 nJ respectively using a pump wavelength of 492 nm. Switching was also obtained with switch and pump energies at 2 μJ and 40 nJ respectively for the same pump wavelength of 492 nm. Re-timing to the laser output was possible by controlling the temporal position of the switch pulse. At switch and pump wavelengths of 1.3 μm and 498 nm respectively, the switch was timed to arrive a few pico-seconds after the pump pulse. There was sufficient temporal overlap of the switch and pump pulse to induce a reduction in the laser output, up to 35 % and a shift of the temporal position of the laser output by 3 ps relative to the control pulse position. *Lanzani et al.* obtained 90 % laser switching with F8BT [130]. However their switched laser did not fully recover for 8 ps due to formation of charge pairs.

Amplifier operation at a higher repetition rate of 50 kHz was possible, as was shown in MEH-PPV and F8BT. However device lifetime was a problem as it was experiencing the same number of pulses in a shorter space of time. The co-polymers: ADS233YE and GP1302, did not produce similar high amplification as the behaviour of the material required more pump energy density for higher gain. This resulted in amplification of 5 dB in ADS233YE and 2 dB in GP1302. The difference in amplification between the two material was possibly due ESA effect from the PFO chromophores and the ratio of PFO to F8BT. The co-polymer with a larger PFO concentration (GP1302) gave smaller amplification.

Amplification using the waveguide structure was not successful, resulting in an extremely weak amplification. With consideration to the gain lifetime, and hence the polymer material, and the waveguide modes, the amplification was improved by 24 times in F8BT.

With regards to future work, the work in this thesis has shown amplification in

conjugated polymers to be higher than that obtained in dye doped fibre amplifiers and can be used to produce switching devices operating over the visible range. Much more work has yet to be conducted:

1. Design and amplification of light in a smaller waveguide structure. The ridge waveguide, although unsuccessful, has the advantage of being independent of the precise coupling angle requirement in the gratings amplifier. In the grating amplifier, the coupling angle changed minutely with different wavelengths. End coupling of the probe signal into the waveguide structure does not suffer from changes made to the probing wavelength.

2. Encapsulation of the amplifier. Encapsulation of a polymer laser has been shown to increase the lifetime by a factor of 2500 over that of a device operating in air [164]. It would be fruitful to test the operation of an encapsulated amplifier device as practical applications would require it to be exposed to water vapour and air.

3. Fiber amplifiers with conjugated polymers. A convenient amplifier structure which can be used with POF would be fiber amplifiers. Current fiber amplifiers that exist are produced with rare earth ions in an inert polymer or laser dyes. This work would require producing fibers doped with the inert polymer PMMA and the required conjugated polymers.

4. Switching of high gain optical amplifier devices in the range of > 10 dB. Work conducted on switching amplified light using MEH-PPV demonstrated that high gain signal can be turned off, however the switching effect was unreliable and insufficient. Further investigation into switching of highly amplified signals would be desirable.

References

[1] Oxford english dictionary, .

[2] Oxford english dictionary, . URL http://dictionary.oed.com/cgi/entry/50056792?single=1&query_type=word&queryword=cynicalness&first=1&max_to_show=10.

[3] A. J. Heeger. Semiconducting and metallic polymers: The fourth generation of polymeric materials. *Reviews of Modern Physics*, 78:681, 2001.

[4] A. G. MacDiarmid. Synthetic metals: A novel role for organic polymers. *Reviews of Modern Physics*, 78:681, 2001.

[5] H. Shirakawa. The discovery of polyacetylene film-the dawning of an era of conducting polymers. *Reviews of Modern Physics*, 78:681, 2001.

[6] http://nobelprize.org/nobel-prizes/chemistry/laureates/2000/index.html. URL http://nobelprize.org/nobel_prizes/chemistry/laureates/2000/index.html.

[7] J. H. Burroughes, D. D. C. Bradley, A. R. Brown, R. N. Marks, K. Mackay, R. H. Friend, P. L. Burns, and A. B. Holmes. Light-emitting diodes based on conjugated polymers. *Nature*, 347:539, 1990.

[8] http://www.plasticlogic.com/index.php. URL http://www.plasticlogic.com/index.php.

[9] http://www.oled-display.net/sony-xel-1-oled-tv. URL http://www.oled-display.net/sony-xel-1-oled-tv.

[10] N. Serdar Sariciftci. Polymeric photovoltaic materials. *Current Opinion in Solid State and Materials Science*, 4:373, 1999.

[11] J. H. Burroughes, C. A. Jones, and R. H. Friend. New semiconductor device physics in polymer diodes and transistors. *Nature*, 335:137, 1988.

[12] G. Yu, J. Wang, J. McElvain, and A. J. Heeger. Large-area, full-color image sensors made with semiconducting polymers. *Advanced Materials*, 10:1431, 1998.

[13] A. E. Vasdekis, G. A. Turnbull, I. D. W. Samuel, P. Andrew, and W. L. Barnes. Low threshold edge emitting polymer distributed feedback laser based on a square lattice. *Applied Physics Letters*, 86:161102, 2005.

[14] A. E. Vasdekis, G. Tsiminis, J.-C. Ribierre, Liam O' Faolain, T. F. Krauss, G. A. Turnbull, and I. D. W. Samuel. Diode pumped distributed bragg reflector lasers based on a dye-to-polymer energy transfer blend. *Optics Express*, 14:9211, 2006.

[15] D. Moses. High quantum efficiency luminescence from a conducting polymer in solution: A novel polymer laser dye. *Applied Physics Letters*, 60:3215, 1992.

[16] I. D. W. Samuel and G. A. Turnbull. *Materials today*, 28, 2004.

[17] T. Riedl, T. Rabe, H.-H. Johannes, W. Kowalsky, J. Wang, T. Weimann, P. Hinze, B. Nehls, T. Farrell, and U. Scherf. Tunable organic thin-film laser pumped by an inorganic violet diode laser. *Applied Physics Letters*, 88:241116, 2006.

[18] M. Salerno, G. Gigli, M. Zavelani-Rossi, S. Perissinotto, and G. Lanzani. Effects of morphology and optical contrast in organic distributed feedback lasers. *Applied Physics Letters*, 90:111110, 2007.

[19] M. Zavelani-Rossi, S. Perissinotto, G. Lanzani, M. Salerno, and G. Gigli. Laser dynamics in organic distributed feedback lasers. *Applied Physics Letters*, 89: 181105, 2006.

[20] R. Xia, G. Heliotis, P. N. Stavrinou, and D. D. C. Bradley. Polyfluorene distributed feedback lasers operating in the green-yellow spectral region. *Applied Physics Letters*, 87:031104, 2005.

[21] M. D. McGehee, M. A. Diaz-Garcia, F. Hide, R. Gupta, E. K. Miller, D. Moses, and A. J. Heeger. Semiconducting polymer distributed feedback lasers. *Applied Physics Letters*, 72:1536, 1998.

[22] C. W. Tang and S. A. VanSlyke. Organic electroluminescent diodes. *Applied Physics Letters*, 51:913, 1987.

[23] http://www.lascomm.com/articles/fib-art1.htm. URL `http://www.lascomm.com/articles/fib-art1.htm`.

[24] BBC. Uk 'slow' on ultra-fast internet. http://news.bbc.co.uk/2/hi/technology/7112373.stm, November 2007. URL `http://news.bbc.co.uk/2/hi/technology/7112373.stm`.

[25] I. T. Monroy, H.P.A. vd Boom, A.M.J. Koonen, G.D. Khoe, Y. Watanabe, Y. Koike, and T. Ishigure. Data transmission over polymer optical fibers. *Optical Fiber Technology*, 9:159–171, 2003.

[26] Y. Koike, T. Ishigure, M. Satoh, and E. Nihei. High-speed photonics polymer and its application. *Pure Applied Optics*, 7:201, 1998.

[27] FibreSystems Europe. Plastic optical fiber tackles automotive requirements. www.mostcooperation.com, May 2004.

[28] M. Pope and C. E. Swenberg. *Electronic Processes in Organic Crystals and Polymers.* Oxford University Press, USA., 1999.

[29] P. Wood. *Conformational disorder and the degree of conjugation in conjugated polymers.* PhD thesis, University of St Andrews, 2002.

[30] M. Karplus and R. N. Porter. *Atoms and molecules: an introduction for students of physical chemistry.* 1970.

[31] J. F. Rabek. *Mechanisms of photphysicsal processes and photochemical reactions in polymers.* Ann Arbor, Mich., 1995.

[32] http://catalogs.mhhe.com/mhhe/home.do. URL `http://www.mhhe.com/physsci/chemistry/animations/chang_7e_esp/bom5s2_6.swf`.

[33] http://www.chemguide.co.uk/basicorg/bonding/benzene2.html.

[34] P. W. Atkins. *Molecular quantum mechanics Part III.* Clarendon Press, 1970.

[35] Larry Luer, Cristian Manzoni, Giulio Cerullo, Guglielmo Lanzani, and Zeev. V. Vardeny. Intra-chain exciton generation by charge recombination in substituted polyacetylenes. *Chemical Physics Letters*, 444:61, 2007.

[36] D. A. Eastham. *Atomic physics of lasers.* Taylor and Francis, 1985.

[37] J. R. Lakowicz. *Principles of fluorescence spectroscopy.* Kluwer Academic/Plenum Publishers, 1999.

[38] M. Goossens. *Ultrafast Organic Lasers And Solid-State Amplifiers.* PhD thesis, University of St Andrews, 2007.

[39] G. R. Hayes, I. D. W. Samuel, and R. T Phillips. Exciton dynamics in electroluminescent polymers studied by femotsecond time-resolved photoluminescence spectroscopy. *Physical Review B*, 52:11569, 1995.

[40] U. Scherf, S. Riechel, U. Lemmer, and R. F. Mahrt. Conjugated polymers: lasing and stimulated emission. *Current Opinion in Solid State and Materials Science*, 5:143, 2001.

[41] B. Schweitzer, G. Wegmann, H. Giessen, D. Hertel, H. Bassler, R. F. Mahrt, U. Scherf, and K. Mullen. The optical gain mechanism in solid conjugated polymers. *Applied Physics Letters*, 72:2933, 1998.

[42] M. D. McGehee and A. J. Heeger. Semiconducting (conjugated) polymers as materials for solid-state lasers. *Advanced Materials.*, 12:1655, 2000.

[43] D. Amarasinghe, A. Ruseckas, A. E. Vasdekis, M. Goossens, G. A. Turnbull, and I. D. W. Samuel. Broadband solid state optical amplifier based on a semiconducting polymer. *Applied Physics Letters*, 89:201119, 2006.

[44] T. Virgili, D. Marinotto, C. Manzoni, G. Cerullo, and G. Lanzani. Ultrafast intrachain photoexcitation of polymeric semiconductors. *Physical Review Letters*, 94:117402, 2005.

[45] B. Ranby and J. F. Rabek. *Photodegradation, photo-oxidation and photostabilization of polymers.* London Wiley-Interscience, 1975.

[46] M. Yan, L. J. Rothberg, F. Papadimitrakopoulos, M. E. Galvin, and T. M. Miller. Defect quenching of conjugated polymer luminescence. *Physical review letters*, 73:744, 1994.

[47] http://micro.magnet.fsu.edu/primer/java/lasers/tsunami/index.html.

[48] Spectra-Physics. *Mai Tai; Diode-Pumped, Mode-Locked Ti:sapphire Laser Manual*, .

[49] A. E. Siegman. *Lasers*.

[50] University of St Andrews; Ultra-short pulse laser group. Self modelocking. URL `http://www.st-andrews.ac.uk/%7Ewsquad/`.

[51] D. E. Spence, P. N. Kean, and W. Sibbett. 60-fsec pulse generation from a self-mode-locked ti:sapphire laser. *Optics Letters*, 42:16, 1991.

[52] D. Strickland and G. Mourou. Compression of amplified chirped optical pulses. *OPTICS COMMUNICATIONS*, 56:219–221, 1985.

[53] Spectr-Physics. *Spectra-Physics Lasers: Spitfire Manual*.

[54] Spectra-Physics. *Spectra-Physics Lasers: Hurricane Manual*, .

[55] Spectra-Physics. Ultrafast optical parametric amplifier manual, .

[56] *Topas-white*. Light conversion.

[57] *Guide to Streak Cameras*. Hamamatsu.

[58] C. L. Tang and D. E. Spence. Ultrashort-pulse phenomena.

[59] J. R. Lawrence. *Organic semiconductors: Optical Amplification, Lasing and Soft Lithography*. PhD thesis, University of St Andrews, 2003.

[60] P. Wang, C.J. Collison, and L.J. Rothberg. Origins of aggregation quenching in luminescent phenylenevinylene polymers. *Journal of Photochemistry and Photobiology A*, 144:63, 2001.

[61] R. Xia, G. Heliotis, Y. Hou, and D. D.C. Bradley. Fluorene-based conjugated polymer optical gain media. *Organic Electronics 4*, page 165, 2003.

[62] N. Tessler. Lasers based on semiconducting organic materials. *Advanced Materials*, 11:363, 1999.

[63] B. J. Schwartz, F. Hide, M. R. Andersson, and A. Heeger. Ultrafast studies of stimulated emission and gain in solid films of conjugated polymers. *Chemical Physics Letters*, 327, 1997.

[64] A. K. Sheridan, G. A. Turnbull, A. N. Safonov, and I. D. W. Samuel. Tuneability of amplified spontaneous emission through control of the waveguide-mode structure in conjugated polymer films. *Physical Review B*, 62, 2000.

[65] M. Yan, L. J. Rothberg, F. Papadimitrakopoulos, M. E. Galvin, and T. M. Miller. Spatially indirect excitons as primary photoexcitations in conjugated polymers. *Physical review letters*, 72:1104, 1994.

[66] R. Xia, G. Heliotis, and D. D.C. Bradley. Semiconducting polyfluorenes as materials for solid-state polymer lasers across the visible spectrum. *Synthetic Metals*, 140:117, 2004.

[67] J. R. Lawrence, G. A. Turnbull, and I. D. W. Samuel. Broadband optical amplifier based on a conjugated polymer. *Applied Physics Letters.*, 80:3036, 2002.

[68] *Organic Light-Emitting Materials and Devices*, volume 28-36, 2005. M. Goossens, G. Heliotis, G. A. Turnbull, A. Ruseckas, J. R. Lawrence, R. Xia, D. D. C. Bradley and I. D. W. Samuel, Proc. SPIE. page 5937.

[69] D. Amarasinghe, A. Ruseckas, A. E. Vasdekis, G. A. Turnbull, and I. D. W. Samuel. Amplification of optical pulse sequences at a high repetition rate in a polymer slab waveguide. *Applied Physics Letters*, 91:011105, 2007.

[70] E. M. Calzado, J. M. Villalvilla, P. G. Boj, J. A. Quintana, and M. A. Diaz-Garcia. Concentration dependence of amplified spontaneous emission in organic-based waveguides. *Organic Electronics*, 7:319, 2006.

[71] C. Pflumm, C. Karnutsch, M. Gerken, and U. Lemmer. Parametric study of modal gain and threshold power density in electrically pumped single-layer organic optical amplifier and laser diode structures. *IEEE Journal of Quantum Electronics.*, 41:316, 2005.

[72] G. Heliotis, D. D. C. Bradley, M. Goossens, S. Richardson, G. A. Turnbull, and I. D. W. Samuel. Operating characteristics of a traveling-wave semiconducting polymer optical amplifier. *Applied Physics Letters*, 85:6122, 2004.

[73] M. A. Reilly, C. Marinelli, C. N. Morgan, R. V. Penty, I. H. White, M. Ramon, M. Ariu, R. Xia, and D. D. C. Bradley. Rib waveguide dye-doped polymer amplifier with up to 26 db optical gain at 625 nm. *Applied Physics Letters.*, 85: 5137, 2004.

[74] M. A. Reilly, B. Coleman, E. Y. B. Pun, R. V. Penty, I. H. White, M. Ramon, R. Xia, and D. D. C. Bradley. Optical gain at 650 nm from a polymer waveguide with dye-doped cladding. *Applied Physics Letters*, 87:231116, 2005.

[75] G. J. Denton, N. Tessler, N. T. Harrison, and R. H. Friend. Factors influencing stimulated emission from poly(p-phenylenevinylene). *Physical Review Letters*, 78:733, 1997.

[76] A. Ruseckas, M. Theander, L. Valkunas, M. R. Andersson, O. Inganas, and V. Sundstrom. Energy transfer in conjugated polymer with reduced interchain coupling. *Journal of Luminescence*, 76 & 77:474, 1998.

[77] T. Nguyen, V. Doan, and B. J. Schwartz. Conjugated polymer aggregates in solution: Control of interchain interactions. *Journal of Chemical Physics*, 110: 4068, 1999.

[78] A. K. Sheridan, G. A. Turnbull, A. N. Safonov, and I. D. W. Samuel. Tuneability of amplified spontaneous emission through control of the waveguide-mode structure in conjugated polymer films. *Physical Review B*, 62:11929, 2000.

[79] R. G. Kepler, V. S. Valencia, S. J. Jacobs, and J. J. McNamara. Exciton-exciton annihilation in poly(p-phenylenevinylene) films. *Synthetic Metals*, 78: 227, 1996.

[80] T. Nguyen, I. B. Martini, J. Liu, and B. J. Schwartz. Controlling interchain interactions in conjugated polymers: The effects of chain morphology on exciton-exciton annihilation and aggregation in meh-ppv films. *Journal of Physical Chemistry B*, 104:237, 2000.

[81] A.J. Lewis, A. Ruseckas, O.P.M. Gaudin, G.R. Webster, P.L. Burn, and I.D.W. Samuel. Singlet exciton diffusion in meh-ppv films studied by exciton exciton annihilation. *Organic Electronics*, 7:452, 2006.

[82] T. K. Koch, L. C. Chiu, and A. Yariv. Analysis and performance of a picosecond dye laser amplifier chain. *Journal of Applied physics.*, 53:6047, 1982.

[83] Dr. Rüdiger Paschotta. Encyclopedia of laser physics and technology. Technical report, RP Photonics Consulting GmbH; http://www.rp-photonics.com/encyclopedia.html. URL `http://www.rp-photonics.com/encyclopedia.html`.

[84] G. Heliotis, R. Xia, D. D. C. Bradley, G. A. Turnbull, I. D. W. Samuel, P. Andrew, and W. L. Barnes. Two-dimensional distributed feedback lasers using a broadband, red polyfluorene gain medium. *Journal of Applied Physics*, 96:6959, 2004.

[85] G.Heliotis, M. Goossens, A. Ruseckas, R. xia, Y. Hou, J. R. Lawrence, G. A. turnbull, I.D.W.Samuel, and D.D.C.Bradley. Unpublished. A high gain solid-state conjugated polyer optical amplifier.

[86] R. Xia, G. Heliotis, and D.D. C. Bradley. Fluorene-based polymer gain media for solid-state laser emission across the full visible spectrum. *Applied Physics Letters*, 82:3599, 2003.

[87] A. Tagaya, S. Teramoto, E. Nihei, K. Sasaki, and Y. Koike. High-power and high-gain organic dye-doped polymer optical fiber amplifiers: novel techniques for preparation and spectral investigation. *Applied Optics*, 36:572, 1997.

[88] A. Tagaya, Y. Koike, E. Nihei, S. Teramoto, K. Fujii, T. Yamamoto, and K. Sasak. Basic performance of an organic dye-doped polymer optical fiber amplifier. *Applied Optics*, 34:988, 1995.

[89] M. Karimi, N. Granpayeh, and M. K. Morraveg Farshi. Analysis and design of a dye-doped polymer optical fiber amplifier. *Applied Physics B*, 78:387, 2004.

[90] M. Rajesh, M. Sheeba, K. Geetha, C. P. G. Vallaban, P. Radhakrishnan, and V. P. N. Nampoori. Fabrication and characterization of dye-doped polymer optical fiber as a light amplifier. *Applied Optics*, 46:106, 2007.

[91] G. Karve, B. Bihari, and R. T. Chen. Demonstration of optical gain at 1.06 mm in a neodymium-doped polyimide waveguide. *Applied Physics Letters*, 77: 1253, 2000.

[92] A. Q. Quang, R. Hierle, J. Zyss, I. Ledouxa, G. Cusmai, R. Costa, A. Barberis, and S. M. Pietralungab. Demonstration of net gain at 1550 nm in an erbium-doped polymer single mode rib waveguide. *Applied Physics Letters*, 89:141124, 2006.

[93] W. H. Wong, E. Y. B. Pun, and K. S. Chan. Er3-yb3 codoped polymeric optical waveguide amplifiers. *Applied Physics Letter*, 84:176, 2004.

[94] A. Q. Quang and. G. Truong, A.-M. Jurdyc, B. Jacquier, J. Zyss, and I. Ledoux. Gain properties of an er3+ complex in a polymethylmethacrylate matrix for 1540 nm broadband optical amplification. *Applied Physics Letters*, 101:023110, 2007.

[95] S. K. Park, J. Oh, C. Hwang, J. Lee, Y. S. Yang, H. Y. Chu, and K. Kang. Ultra thin film encapsulation of organic light emitting diode on a plastic substrate. *ETRI Journal*, 27:545–550, 2005.

[96] N. T. Harrison, G. R. Hayes, R. T. Phillips, and R. H. Friend. Singlet intrachain exciton generation and decay in poly(p-phenylenevinylene). *Physical Review Letters*, 77:1881, 1996.

[97] T. Virgili, D. Marinotto, G. Lanzani, and D. D.C. Bradley. Ultrafast resonant optical switching in isolated polyfluorenes chains. *Applied Physics Letters*, 86: 091113, 2005.

[98] S. V. Frolov, M. Liess, P. A. Lane, W. Gellermann, Z. V. Vardeny, M. Ozaki, and K. Yoshino. Exciton dynamics in soluble poly(p-phenylene-vinylene): Towards an ultrafast excitonic switch. *Physical Review Letters*, 78:4285, 1997.

[99] B. Chen, M. Wang, Y. Wu, and H. Tian. Reversible near-infrared fluorescence switch by novel photochromic unsymmetrical-phthalocyanine hybrids based on bisthienylethene. *The Royal Society of Chemistry*, page 1060, 2002.

[100] R. A. Illos, E. Harlev, and S. Bittner. A novel all-organic chemical and electrochemical fluorescent switch. *Tetrahedron Letters*, 46:8427, 2005.

[101] X. Sheng, A. Peng, H. Fu, Y. Liu, Y. Zhao, Y. Ma, and J. Yao. Modulation of a fluorescence switch based on photochromic spirooxazine in composite organic nanoparticles. *Nanotechnology*, 18:145707, 2007.

[102] S. Lim, J. Seo, and S. Y. Park. Photochromic switching of excited-state intramolecular proton-transfer (esipt) fluorescence: A unique route to high-contrast memory switching and nondestructive readout. *Jounal of the American chemical society*, 128:14542, 2006.

[103] A. J. Myles and N. R. Branda. 1,2-dithienylethene photochromes and non-destructive erasable memory. *Advanced Functional Materials*, 12:167, 2002.

[104] P. D. Townsend, J. L. Jackel, G. L. Baker, J. A. Shelburn, and S. Etemad. Observation of nonlinear optical transmission and switching phenomena in polydiacetylene-based directional couplers. *Applied Physics Letters*, 55:1829, 1989.

[105] I. Ledoux and J. Zyss. Nonlinear organic molecules and materials. *Journal of nonlinear optical physics and materials*, 3:287, 1994.

[106] F. Yoshino, S. Polyakov, and G. I. Stegeman. All-optical multiphoton absorption figures of merit: Polydiacetylene poly (bis para-toluene sulfonate) of 2,4-hexadiyne-1,6 diol. *Applied Physics Letters*, 84:5362, 2004.

[107] B. L. Lawrence, M. Cha, W. E. Torruellas, G. I. Stegeman, S. Etemad, G. Baker, and F. Kajzar. Measurement of the complex nonlinear refractive index of single crystal p-toulene sulfonate at 1064 nm. *Applied Physics Letters*, 64:2773, 1994.

[108] B. I. Greene, J. Orenstein, and S. Schmitt-Rink. All-optical nonlinearities in organics. *Science*, 247:679, 1990.

[109] K.W.delong and G. I.Stegeman. Two-photon absorption as a limitation to all-optical waveguide switching in semiconductors. *Applied Physics Letters*, 57: 2063, 1990.

[110] S. Nakamura, Y. Ueno, and K. Tajima. Femtosecond switching with semiconductor-optical-amplifier-based symmetric mach-zehnder-type all-optical switch. *Applied Physics Letters*, 78:3929, 2001.

[111] A. Gomez-Iglesias. *Dynamical Optical Nonlinearities in semiconductor optical amplifiers and quantum cascae lasers.* PhD thesis, University of St Andrews, 2005.

[112] D. T. Reid. Nonlinear optics and modulators module. 2003.

[113] J. G. Fenn. *Ultrafast dynamics in semiconductor optical amplifiers,*. PhD thesis, University of St Andrews, 2003.

[114] A. Gomez-Iglesias, J. G. Fenn, M. Mazilu, R. J. Manning, and A. Miller. Carrier heating in semiconductor optical amplifier-based sagnac-type all-optical switches. *Semiconductor Science Technology*, 21:1703, 2006.

[115] H. Ju, S. Zhang, D. Lenstra, H. de Waardt, E. Tangdiongga, and G. D. Khoe. Soa-based all-optical switch with subpicosecond full recovery. *Optics Express*, 13:942, 2005.

[116] P. Borri, W. Langbein, J. M. Hvam, F. Heinrichsdorff, M. H. Mao, and D. Bimberg. Spectral hole-burning and carrier-heating dynamics in quantum-dot amplifiers: Comparison with bulk amplifiers. *phys. stat. sol.*, 224:419, 2001.

[117] T. Akiyama, H. Kuwatsuka, T. Simoyama, Y.i Nakata, K. Mukai, M. Sugawara, and O. Wada. Nonlinear gain dynamics in quantum-dot optical amplifiers and its application to optical communication devices. *IEEE Journal of Quantum Electronics*, 37:1059, 2001.

[118] K. Tajima, S. Nakamura, and Y. Sugimoto. Ultrafast polarization-discriminating mach-zehnder all-optical switch. *Applied Physics Letters*, 67: 3709, 1995.

[119] X. Yang, A. K. Mishra, D. Lenstra, F. M. Huijskens, H. de Waardt, G. D. Khoe, and H. J. S. Dorren. Sub-picosecond all-optical switch using a multi-quantum-well semiconductor optical amplifier. *Optics Communications*, 236: 329, 2004.

[120] H. Nakamura, Y. Sugimoto, K. Kanamoto, N. Ikeda, Y. Tanaka, Y. Nakamura, S. Ohkouchi, Y.i Watanabe, K. Inoue, H. Ishikawa, and K.i Asakawa. Ultra-fast photonic crystal/quantum dot alloptical switch for future photonic networks. *Optics Express*, 12:6606, 2004.

[121] D. A. Mazurenko, R. Kerst, J. I. Dijkhuis, A.V. Akimov, V.G. Golubev, D. A. Kurdyukov, A. B. Pevtsov, and A.V. Sel'kin. Ultrafast optical switching in three-dimensional photonic crystals. *Physics Review Letters*, 2003:213903, 91.

[122] A. Hache and M. Bourgeois. Ultrafast all-optical switching in a silicon-based photonic crystal. *Applied Physics Letters*, 77:4089, 2000.

[123] X. Hu, P. Jiang, C. Ding, H. Yang, and Q. Gong. Picosecond and low-power all-optical switching based on an organic photonicbandgap microcavity. *Nature*, 2008.

[124] D. Yeo and S. Shin. Polymer-silica hybrid 1 x 2 thermooptic switch with low crosstalk. *Optics Communications*, 267:388, 2006.

[125] X. Wang, B. Howley, M. Y. Chen, and R. T. Chen. Phase error corrected 4-bit true time delay module using a cascaded 2 x 2 polymer waveguide switch array. *Applied Optics*, 37946:379, 2007.

[126] D. Beggs, T. White, L. O'Faolain, and T. Krauss. Ultracompact and low power optical switch based on silicon photonic crystals. *Optics Letters*, 33:147, 2008.

[127] X. Hu, Y. Liu, J. Tian, B. Cheng, and D. Zhang. Ultrafast all-optical switching in two-dimensional organic photonic crystal. *Applied Physics Letters*, 86:121102, 2005.

[128] D. Amarasinghe, A. Ruseckas, A. E. Vasdekis, G. A. Turnbull, and I. D. W. Samuel. Picosecond gain switching of an organic semiconductor optical amplifier. *Applied Physics Letters*, 92:083305, 2008.

[129] M. A. Stevens, C. Silva, D. M. Russell, and R. H. Friend. Exciton dissociation mechanisms in the polymeric semiconductors poly9,9-dioctylfluorene and poly9,9-dioctylfluorene-co-benzothiadiazole. *Physical Review B*, 63:165213, 2001.

[130] S. Perissinotto, G. Lanzani, M. Zavelani-Rossi, M. Salerno, and G. Gigli. Ultrafast optical switching in distributed feedback polymer laser. *Applied physics Letters*, 91:291108, 2007.

[131] R. Xia, C. Cheung, A. Ruseckas, D. Amarasinghe, I. D. W. Samuel, and D. D. C. Bradley. Wavelength conversion from silica to polymer optical fibre communicationwavelengths via ultrafast optical gain switching in a distributed feedback polymer laser. *Advanced Materials*, 19:4054, 2007.

[132] K. Tajima, S. Nakamura, Y. Ueno, J. Sasaki, T. Sugimoto, T. Kato, T. Shimoda, M. Itoh, H. Hatakeyama, T. Tamanuki, and T. Sasaki. Hybrid integrated symmetric mach-zehnder all-optical switch with ultrafast, high extinction switching. *Electronic Letters*, 1999:2030, 35.

[133] A. Lagatsky, C.G. Leburn, C.T.A. Brown, W. Sibbett, A.M. Malyarevich, V.G. Savitski, K.V. Yumashev, E.L. Raaben, and A.A. Zhilin. Passive mode locking of a cr4+:yag laser by pbs quantum-dot-doped glass saturable absorber. *Optics Communications*, 241:449, 2004.

[134] A. Lagatsky, C. Brown, and W. Sibbett. Highly efficient and low threshold diode-pumped kerr-lens mode-locked yb:kyw laser. *Optics Express*, 12:3928, 2004.

[135] E. Riedle, M. Beutter, S. Lochbrunner, J. Piel, S. Schenkl, and W. Zinth S. Sprlein. Generation of 10 to 50 fs pulses tunable through all of the visible and the nir. *Applied Physics B*, 71:457, 2000.

[136] I. D. Jung, F. X. Kartner, N. Matuschek, D. H. Sutter, F. Morier-Genoud, G. Zhang, U. Keller, V. Scheuer, M. Tilsch, and T. Tschudi. Self-starting 6.5-fs pulses from a ti:sapphire laser. *Optics Letters, Vol. 22, Issue 13, pp. 1009-1011*, 22:1009, 1997.

[137] G. J. Crofts, X. Banti, and M. J. Damzen. Tunable phase conjugation in a ti:sapphire amplifier. *Optics Letters*, 20:1634, 1995.

[138] T. W. Boyd. *Nonlinear Optics*. Academic Press Inc.

[139] B. B. Laud. *Lasers and non-linear optics*. John Wiley and sons.

[140] Hecht E. *Optics*. Addison-Wesley Publishing Company.

[141] H. E. Bates. Noncollinear phase-matching effects in lithium niobate. *Journal of the optical society of America*, 61:904, 1971.

[142] H. E. Bates. Analysis of noncollinear phase-matching effects in uniaxial crystals. *Journal of the optical society of America*, 63:146, 1973.

[143] T. Wilhelm, J. Piel, and E. Riedle. Sub-20-fs pulses tunable across the visible from a blue-pumped single-pass noncollinear parametric converter. *Optics Letters*, 22:1494, 1997.

[144] G. M. Gale, M. Cavallari, T. J. Driscoll, and F. Hache. Sub-20-fs tunable pulses in the visible from an 82-mhz optical parametric oscillator. *Optics Letters*, 20: 1562, 1995.

[145] A. Baltuska and T. Kobayashi. Adaptive shaping of two-cycle visible pulses using a flexible mirror. *Applied Physics B*, 75:427, 2002.

[146] A. Shirakawa and T. Kobayashi. Noncollinearly phase-matched femtosecond optical parametric amplification with a 2000 cm21 bandwidth. *Applied Physics Letters*, 72:147–149, 1998.

[147] P. Wasylczyk, I. A. Walmsley, W. Wasilewski, and C. Radzewicz. Broadband noncollinear optical parametric amplifier using a single crystal. *Optics Letters*, 30:1704, 2005.

[148] P. Baum, S. Lochbrunner, and E. Riedle. Tunable sub-10-fs ultraviolet pulses generated by achromatic frequency doubling. *Optics letters*, 29:1686, 2004.

[149] C. Lee, J. Zhang, J. Y. Huang, and C. Pan. Generation of femtosecond laser pulses tunable from 380 nm to 465 nm via cascaded nonlinear optical mixing in a noncollinear optical parametric amplifier with a type-i phase matched bbo crystal. *Optics Express*, 11:1702, 2003.

[150] R. Ernstorfer, L. Gundlach, C. Zimmermann, F. Willig, R. Eichberger, and E. Riedle. Generation of sub 20-fs tunable visible pulses from a 100 khz nopa for measuring ultrafast heterogeneous electron transfer. *Ultrafast Optics IV*, page 389, 2004.

[151] R. L. Fork, 0. E. Martinez, and J. P. Gordonn. Negative dispersion using pairs of prisms. *Optics letters*, 9:150, 1984.

[152] Wilson Sibbet. Ultrafast photonics lectures. msc; photonics and optoelectronic devices., 2003.

[153] A. Yariv. *Optical electronics in modern communications*. 1997.

[154] T. Kobayashi and A. Baltuska. Sub-5 fs pulse generation from a noncollinear optical parametric amplifier. *Meas. Sci. Technol.*, 13:1671, 2002.

[155] J. Piel, M. Beutter, and E. Riedle. 20 to 50-fs pulses tunable across the near infrared from a blue-pumped noncollinear parametric amplifier. *Optics Letters*, 25:180, 2000.

[156] BBC. Uk homes to get super-fast fibre. http://news.bbc.co.uk/2/hi/technology/7202396.stm, January 2008. URL `http://news.bbc.co.uk/2/hi/technology/7202396.stm`.

[157] T. Kobayashi, M. Djiango, G. Jordan, M. Rüther, W. J. Blau, Y. Suzuki, and T. Kaino. Laser emission at 0.8 um from photopumped luminescent polymer microresonators. *Applied Physics Letters*, 88:181119, 2006.

[158] G. Heliotis, R. Xia, G. A. Turnbull, P. Andrew, W. L. Barnes, I. D. W. Samuel, and D. D. C. Bradley. Emission characteristics and performance comparison of polyflourene lasers with one-, two- dimensional distributed feedback. *Advanced Functional Materials*, 14:91, 2004.

[159] T. Rabe, K. Gerlach, T. Riedl, H.-H. Johannes, W. Kowalsky, J. Niederhofer, W. Gries, J. Wang, T. Weimann, P. Hinze, F. Galbrecht, and U. Scherf. Quasi-continuous-wave operation of an organic thin-film distributed feedback laser. *Applied Physics Letters*, 89:081115, 2006.

[160] M. Yan, L. J. Rothberg, E. W. Kwock, and T. M. Miller. Interchain excitations in conjugated polymers. *Physical Review Letters*, 75:1992, 1995.

[161] I. D. W. Samuel and G. A. Turnbull. Organic semiconductor lasers. *Chemical Reviews*, 107:1272–1295, 2007.

[162] London Metropolitan University Dr. Demetri Kalymnios. Report on the 11th international pof conference 2002, sept.18-20, tokyo. http://www.lancs.ac.uk/depts/spc/research/Plastic-Optical-Fibre-Consortium/pof-02-report.doc, September 2002. URL `http://www.lancs.ac.uk/depts/spc/research/Plastic-Optical-Fibre-Consortium/pof-02-report.doc`.

[163] Techworld reporters. Siemens shows 1gbit/s over polymer optical fibre. http://www.computerworlduk.com/technology/networking/lan-wan/news/index.cfm?newsid=3353, June 2007. URL `http://www.computerworlduk.com/technology/networking/lan-wan/news/index.cfm?newsid=3353`.

[164] S. Richardson, O. P. M. Gaudin, G. A. Turnbull, and I. D. W. Samuel. Improved operational lifetime of semiconducting polymer lasers by encapsulation. *Applied Physics Letters*, 91:261104, 2007.

Appendex A:

Publications arising from this work

1. D. Amarasinghe, A. Ruseckas, A. E. Vasdekis, M. Goossens, G. A. Turnbull and I. D. W. Samuel, 'Broadband solid state optical amplifier based on a semiconducting polymer.' *Applied Physics Letters*, **89**, 201119 (2006).

2. D. Amarasinghe, A. Ruseckas, A. E. Vasdekis, G. A. Turnbull and I. D. W. Samuel, 'Amplification of optical pulse sequences at a high repetition rate in a polymer slab waveguide.' *Applied Physics Letters*, **91**, 011105 (2007).

3. R. Xia, C. Cheung, A. Ruseckas, D. Amarasinghe, I. D. W. Samuel and D. D. C. Bradley, 'Wavelength Conversion from Silica to Polymer Optical Fibre CommunicationWavelengths via Ultrafast Optical Gain Switching in a Distributed Feedback Polymer Laser.' *Advanced Materials*, **19**, 4054 (2007).

4. D. Amarasinghe, A. Ruseckas, A. E. Vasdekis, G. A. Turnbull and I. D. W. Samuel, 'Picosecond Gain Switching of an Organic Semiconductor Optical Amplifier.' *Applied Physics Letters*, **92**, 083305 (2008).